VERTICES

Duke's Undergraduate Research Journal

FALL 2023
Vol. 2 | Iss. 2

Investigating Serotonin Dynamics and Simulating Effects of Antidepressants Using Variation in Enzyme Expression

Evaluating SLAM Performance with Synthesized Datasets from Unreal-Based Emulators

An Examination of Competing Interpretations of Quantum Mechanics with a Critique of the Kochen-Specker Theorem

Effects on Status Striving: How Self-Perceived Value, Self-Esteem, and Personality Traits Impace Prefered Status

Table of Contents

Letter from the Editor

Dear Reader,

Welcome to the fourth issue of Vertices: Duke's Undergraduate Research Journal. This semester's issue is marked by a record number of new peer reviewers who worked hard to ensure that the research we present to you is held to rigorous standards of scientific quality. With the Academic Editing branch being the largest it has ever been, we were able to host more exchanges of ideas between our reviewers, Duke's faculty and graduate students, and our collaborators at Georgetown University. We are therefore excited to present this collaborative issue, and we are proud of the academic community that has contributed to its final form.

Within this multidisciplinary issue, there is something for readers with interests varying from quantum mechanics to neurobiology. Our first article discusses the role of self-esteem and self-perceived value in group dynamics, which have implications for assessing how social factors may contribute to the idea of status. Second, we present an article that discusses multiple hypotheses regarding the randomness of variables within quantum mechanics, providing a unique perspective that blends quantum physics with philosophy. We next present a biochemistry article that models the effect of varying expression levels of transporters involved in serotonin reuptake (e.g. SERT) on extracellular serotonin concentrations, highlighting potential explanations for heterogeneous responses to serotonin reuptake inhibition as a treatment for depression. Last, we present an article that discusses and tests simultaneous localization and mapping (SLAM): a computer vision technique that uses algorithms to generate first-person visual simulations.

With that introduction, I invite you to continue into our fourth issue and explore these examples of rigorous science, wonderful communication, and fascinating research.

Sincerely,

Kaeden Hill, Co-Academic Editor in Chief

Investigating Serotonin Dynamics and Simulating Effects of Antidepressants Using Variation in Enzyme Expression

Alexander Diefes

Volume 2, Issue 2

Article Synopsis

Depression is often treated with selective serotonin reuptake inhibitors (SSRIs), but some patients do not show improvements in their symptoms while taking them. Using a mathematical model of serotonin, we simulate the effects of various antidepressants and predict which factors may influence SSRI success.

Graphic by Erin Heyeck

Investigating Serotonin Dynamics and Simulating Effects of Antidepressants Using Variation in Enzyme Expression

Alexander Diefes

Duke University
https://doi.org/10.55894/dv2.21

Abstract

Serotonin plays a crucial role in the symptoms of depression, and understanding its dynamics in the brain is of the utmost importance in determining how to mitigate the effects of depression. We investigate a mathematical model presented by Best et al. (2020) that examines serotonin dynamics in the substantia nigra pars reticulata. By incorporating experimental data and a stochastic systems population model, several biological mechanisms and observations are further understood. A populations model is utilized to account for enzymatic expression level variation from 75% to 125% of their base values. When generating the population model, uniform distributions are assumed when simulating maximum velocity values, which correspond to enzyme expression levels. We investigate this assumption and show that it is reasonably insensitive; that is, changes in the distributions used to generate these values do not significantly change the results of the model. We also use the model to simulate the effects of monoamine oxidase inhibitors (MAOIs), one of the first treatments discovered for depression. We then use similar methods to simulate the effects of selective serotonin reuptake inhibitors (SSRIs), the most common antidepressant used today. We demonstrate that low enzyme expression levels of tryptophan hydroxylase and neutral amino acid transporter are most associated with low extracellular serotonin values at the steady state, indicating that these two enzymes may play key roles in predicting which patients may or may not respond to SSRI treatment.

Keywords: major depressive disorder, selective serotonin reuptake inhibitors, monoamine oxidase inhibitors, stochastic systems population model, tryptophan hydroxylase, neutral amino acid transporter

1. Background

Major Depressive Disorder (MDD), commonly known as depression, can affect all aspects of daily life, causing loss of interest in normal activities, sleep and appetite disturbances, and general hopelessness about the present and the future **[1]**. Episodes of depression vary in frequency and duration, with depression sometimes requiring treatment that may last from months to years **[1]**. Symptoms may also lead to a diverse array of behavioral dispositions including outbursts of irritability or frustration, difficulty remembering and concentrating on cognitive tasks, and physical symptoms, such as headaches or back pain **[1]**. In extreme cases, MDD can also lead to suicide; several studies find that the proportion of patients with MDD that take their own lives can as high as 15% or 16.6% **[2][3]**. The severity of MDD is further highlighted by recent global health statistics, which cite that as of 2020, suicide was the third leading cause of death for ages 15-24 and the second leading cause of death for ages 25-34 in the United States **[4]**. Thus, understanding the causes and potential treatment mechanisms of MDD are evidently urgent for public health.

Environmental factors, such as parental abuse or neglect, bullying, social nonconformity, and other traumatic experiences, play a pivotal role in the onset of depressive symptoms **[5]**. Depression may also result from the progression of other diseases

and disorders, such as cancer, schizophrenia, diabetes, and other chronic illnesses **[5]**. While these external factors are important to consider in a comprehensive model of depression, we focus primarily on biochemical pathways in the brain. Specifically, we investigate the dynamics of serotonin in the brain. Serotonin is a neurotransmitter that is known to be closely tied to body weight regulation, alcoholism, and anxiety disorders, amongst other behaviors **[6]**. There is a known, strong correlation between serotonin and symptoms of depression **[7]**, and we aim to elucidate the mechanisms behind this relationship.

2. The Model

This study evaluates the use of a deterministic model of serotonin metabolism presented by Best et al. (2020). This model integrates computationally simulated outcomes with experimental data to explain several biological mechanisms, including features of autoreceptor function, tryptophan input, and two separate reuptake mechanisms **[6]**.

The experimental data was produced in the lab of Parastoo Hashemi, who measured extracellular serotonin and histamine levels in mice. In these experiments, the medial forebrain bundle of the mouse is stimulated for two seconds, which causes antidromic spikes to excite the dorsal raphe nucleus. Bursts of action potentials then fire to various projection regions in the brain, such as the substantia nigra pars reticulata, the prefrontal cortex, and the hippocampus. Extracellular serotonin and histamine levels are then measured in these projection regions, which serve as the primary locations of focus in this paper. Specifically, we focused on the results in the CA2 region of the murine hippocampus, which was the region studied *in vivo* **[6]**.

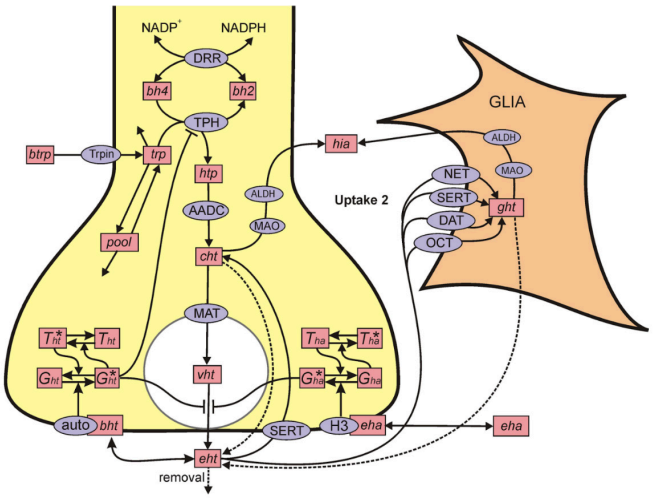

Figure 1: Schematic representation of the model. Names of enzymes and transporters are as follows: Trpin, neutral amino acid transporter; DRR, dihydrobiopterin reductase; TPH, tryptophan hydroxylase; AADC, aromatic amino acid decarboxylase; MAT, vesicular monoamine transporter; SERT, 5-HT reuptake transporter; auto, 5-HT autoreceptors; MAO, monoamine oxidase; ALDH, aldehyde dehydrogenase; NET, norepinepherine transporter; DAT, dopamine transporter; OCT, organic cation transporter. Taken from Best et al. (2020).

The schematic in Figure 1 is the basis for this deterministic mathematical model. The yellow structure is known as an axonal varicosity, a structure that is vital for the synaptic transmission of neurotransmitters **[8]**. Action potentials fired down axons to various projection regions in the brain stimulate these axonal varicosities to release neurotransmitters **[9]**. Thus, changes in biochemistry can essentially be projected across different regions of the brain, adding to the complexity of modeling serotonin dynamics and other neurobiological topics **[9]**. Each blue oval represents an enzyme within the varicosity, which facilitates one or multiple biochemical reactions as the substrates in red boxes increase or decrease in concentration. The red box labeled *eht*, located below the axonal varicosity in Figure 1, represents the concentration of serotonin in the extracellular space, which is used as a metric for depressive symptoms **[6]**.

The orange structure is known as a glial cell, a class of cell that is known to be involved in a myriad of

distinct functions **[10]**, including modulating nerve signal propagation and aiding neural development **[11]**. In our model system, glial cells are involved in one of the reuptake mechanisms for extracellular serotonin. When serotonin is released into the extracellular space, it is transported back into the varicosity as cellular serotonin via the 5-HT reuptake transporter enzyme (SERT in the schematic) or through an alternative pathway, Uptake 2, when the extracellular serotonin reaches a certain critical concentration **[6]**. The presence of two separate uptake mechanisms has been confirmed experimentally *in vivo* **[12]**. Since the Uptake 2 mechanism relies on glial cells, it is expected that the value associated with the kinetics of its biochemical pathways varies with respect to glial cells near the electrode taking the readings **[6]**. Thus, this value will sometimes be higher than the value used in the model **[6]**.

In this model, maximum velocity (V_{max}) values capture the maximum rates at which an enzyme-catalyzed reaction can occur. It is directly proportional to enzyme concentration, and therefore varies based on enzyme expression **[6]**. Since enzyme expression levels are known to vary across individuals, V_{max} values vary as well **[6]**. This variation is the subject of this paper.

The various enzymatically driven biochemical reactions at the axonal varicosity can be modeled as standard Michaelis-Menten kinetics, as governed by the Michaelis-Menten equation,

$$V_0 = \frac{V_{max} \cdot [S]}{K_m + [S]}$$

where [S] represents the substrate concentration over time, V_0 represents the velocity of the reaction at a given time, V_{max} represents the maximum possible rate of the enzymatic reaction, and K_m represents the substrate concentration at which $V_0 = ½\ V_{max}$.

However, not all reactions follow this simplified curve. The kinetics of the tryptophan hydroxylase (TPH) enzyme, an enzyme responsible for converting tryptophan into 5-hydroxytryptophan, which is a precursor to serotonin, show a deviation from traditional Michaelis-Menten kinetics. A phenomenon known as substrate inhibition is observed, as outlined in Figure 1 by G_{ht}*, the activated form of the signaling G-protein unit, inhibiting TPH. When G_{ht}* is above its equilibrium value, this results in a reduction of V_{TPH}, and the converse is observed when G_{ht}* is below its equilibrium value. This relationship can instead be modeled by the Hill kinetics equation,

$$V_0 = \frac{V_{max} \cdot [S]^n}{K_{0.5}^n + [S]^n}$$

where *n* represents the Hill coefficient, quantifying degrees of cooperativity in binding. As the long range dynamics of TPH inhibition are unknown, the Hill coefficient is assumed to be constant with change in time **[6]**.

The $5HT_{1B}$ autoreceptor is in the family of G protein-coupled receptors, and their relationships are shown in the bottom left of Figure 1 near the blue *auto* oval. The system is responsible for regulating G_{ht}*, and thus, V_{max} **[6]**. G_{ht} represents the inactive concentration of the G-protein subunit, the counterpart to the signaling G-protein unit denoted G_{ht}* **[6]**. Their relative amounts change via the equilibrium arrows, and these kinetics are represented in the differential equations of the model. The G-protein network is regulated by regulators of G-protein signaling (RGS), shown in the schematic as the T substrates **[6]**. Analogously, T_{ht} represents the inactive RGS protein, and T_{ht}* represents the active RGS protein. As described by Figure 1, bound extracellular serotonin (*bht*) stimulates the conversion of G_{ht} to its active form, G_{ht}* **[6]**. Following the network, G_{ht}* stimulates conversion of T_{ht} to its active form, T_{ht}*, and in turn, T_{ht}* stimulates the deactivation of G_{ht}* **[6]**. These interactions form the basis for the regulatory system, as it is also involved in V_{TPH}, a vital step in producing extracellular serotonin that can then be bound to the autoreceptor. The iteration of this process leads to the overall equilibrium of the system; the increase of extracellular serotonin concentration inhibits the synthesis and release of vesicular serotonin, and the decrease of extracellular serotonin concentration facilitates it **[6]**. However, these kinetics are likely

to differ across varicosities and projection regions, depending on the expression level of $5HT_{1B}$ autoreceptors **[6]**. In the model, it is assumed that total autoreceptors, total G protein, and total RGS protein are constants **[6]**. A similar system is evident in the histamine (H3) pathway in Figure 1.

Histamine regulates several physiological processes including gastric acid secretion, inflammation, and vasodilation regulation **[13][14]**. It has also been determined that histamine plays an important role in serotonin dynamics **[15][16]**. In a study involving male and female mice injected with acute systemic lipopolysaccharide to induce inflammation, consequent decreases in extracellular serotonin were exhibited in the murine hippocampus **[16]**. Increased histamine activity was caused by inflammation, which acted on inhibitory histamine H3 heteroreceptors on serotonin terminals **[16]**. This experimentally confirmed homeostasis between serotonin and histamine presents an important dynamic in serotonin-based treatments for depression **[16]**.

The model describes system changes through a system of differential equations. Equilibrium states, represented by twin arrows in Figure 1, exist in the autoreceptor (auto) and histamine (H3) pathways. As described above, this allows for concentrations of G proteins and RGS proteins to balance each other. An inhibition arrow is shown from G_{ht}* to TPH, and this long-range kinetic process is accounted for in the system of differential equations. The full set of sixteen differential equations is shown below:

$$\frac{d[bh2]}{dt} = V_{TPH}(trp, bh4, G_{ht}^*) - V_{DRR}(bh2, NADPH, bh4, NADP)$$

$$\frac{d[bh4]}{dt} = V_{DRR}(bh2, NADPH, bh4, NADP) - V_{TPH}(trp, bh4, G_{ht}^*)$$

$$\frac{d[trp]}{dt} = V_{trpin}(btrp) - V_{TPH}(trp, bh4, G_{ht}^*) - V_{pool}(trp, pool) - k_{trp}^{catab} \cdot trp$$

$$\frac{d[htp]}{dt} = V_{TPH}(trp, bh4, G_{ht}^*) - V_{AADC}(htp)$$

$$\frac{d[cht]}{dt} = V_{AADC}(htp) - V_{MAT}(cht, vht) + V_{SERT}(eht) - V_{CATAB}(cht) - k_{cht}^{leak} \cdot cht$$

$$\frac{d[vht]}{dt} = V_{MAT}(cht, vht) - inhib_{ht}(G_{ht}^*) \cdot inhib_{ha}(G_{ha}^*) \cdot fire(t) \cdot vht$$

$$\frac{d[eht]}{dt} = inhib_{ht}(G_{ht}^*) \cdot inhib_{ha}(G_{ha}^*) \cdot fire(t) \cdot vht - V_{SERT}(eht) - V_{U2}(eht) - k_{eht}^{rem} \cdot eht + k_{ght}^{leak} \cdot ght \cdot k_{cht}^{leak} \cdot cht - k_5 \cdot eht \cdot (B_{ht}^{tot} - B_{ht}) + k_6 \cdot B_{ht}$$

$$\frac{d[hiaa]}{dt} = V_{CATAB}(cht) + V_{CATAB}(ght) - k_{hiaa}^{catab} \cdot hia$$

$$\frac{d[pool]}{dt} = V_{pool}(trp, pool) - k_{pool}^{catab} \cdot pool$$

$$\frac{d[G_{ht}^*]}{dt} = \beta_1[k_1 \cdot B_{ht}^2 \cdot (G_{ht}^{tot} - G_{ht}^*) - k_2 \cdot T_{ht}^* G_{ht}^*]$$

$$\frac{d[T_{ht}^*]}{dt} = \beta_2[k_3 \cdot (G_{ht}^*)^2 \cdot (T_{ht}^{tot} - T_{ht}^*) - k_4 \cdot T_{ht}^*]$$

$$\frac{d[B_{ht}]}{dt} = \beta_3[k_5 \cdot eht \cdot (B_{ht}^{tot} - B_{ht}) - k_6 \cdot B_{ht}]$$

$$\frac{d[ght]}{dt} = V_{U2}(eht) - V_{CATAB}(ght) - k_{ght}^{leak} \cdot ght$$

$$\frac{d[G_{ha}^*]}{dt} = k_7 \cdot B_{ha}^2 \cdot (G_{ha}^{tot} - G_{ha}^*) - k_8 \cdot T_{ha}^* G_{ha}^*$$

$$\frac{d[T_{ha}^*]}{dt} = k_9 \cdot (G_{ha}^*)^2 \cdot (T_{ha}^{tot} - T_{ha}^*) - k_{10} \cdot T_{ha}^*$$

$$\frac{d[B_{ha}]}{dt} = k_{11} \cdot eha \cdot (B_{ht}^{tot} - B_{ha}) - k_{12} \cdot B_{ha}$$

The maximum velocity of a given enzyme may depend on the concentrations of several different substrates. For example, V_{TPH} depends on *trp*, *bh4*, and G_{ht}*, shown in parentheses in the first differential equation.

Using the differential equations, K_m values were determined from the literature, and V_{max} values were chosen such that the concentrations were correct assuming Michaelis-Menten kinetics **[6]**. The model was solved until it reached a steady state in which substrate concentrations remained constant. V_{max} values essentially represent the expression level of a particular enzyme. It is known that enzyme expression levels vary from approximately 75% to 125% of their base values in each projection region of the brain **[6]**. In order to appropriately account for this variation, Best et al. (2020) created a stochastic systems population model, in which V_{max} values were randomized from 75% to 125% of their base values. Each set of randomized values represented a single computer-generated individual, and then a population of individuals was created using this methodology. Thus, extracellular serotonin distributions of a simulated population could be visualized, and various simulations could be performed on that population. For example, three such populations of 1000 were generated, and their extracellular serotonin levels (nanomolar concentration) were graphed below, as

shown in Figure 2.

Extracellular serotonin concentration at the steady state was graphed on the x-axes, and the number of individuals in a given population of 1000 for a given range of *eht* values was graphed on each y-axis. While there were some visible differences between the three populations, the distribution of extracellular serotonin at the steady state was roughly the same, with an approximately bell-curved shape with maximum frequencies near 60 nM. It should be noted well that the numerical values of extracellular serotonin concentration are not as important, since again, the steady state values and enzyme expression levels are known to differ across different projection regions **[6]**. While we focused on the CA2 region of the hippocampus in these simulations, the steady state values of extracellular serotonin could very well be distributed around 40 nM or 80 nM in other regions of the brain.

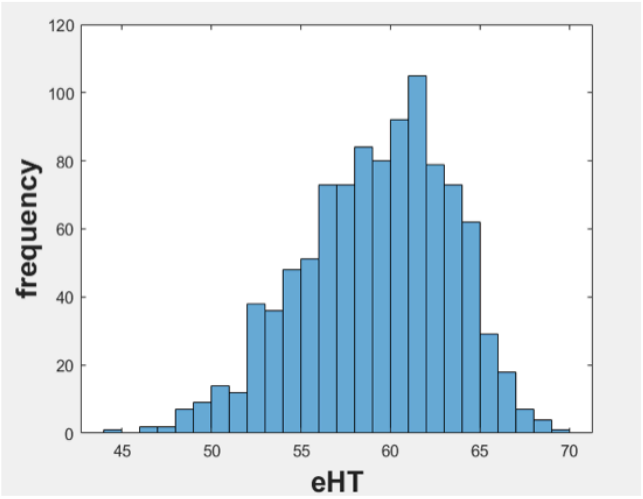

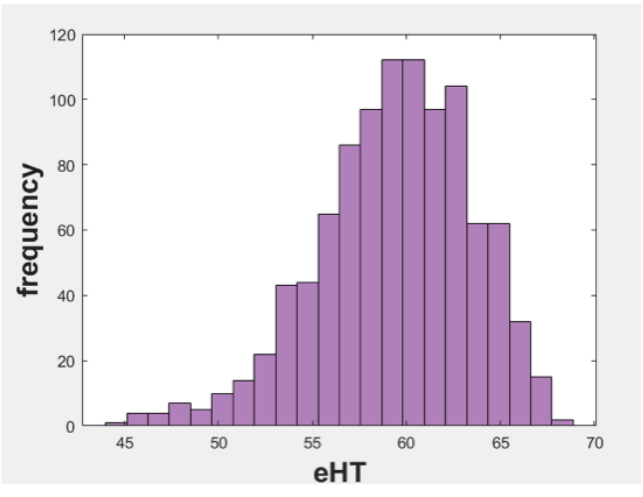

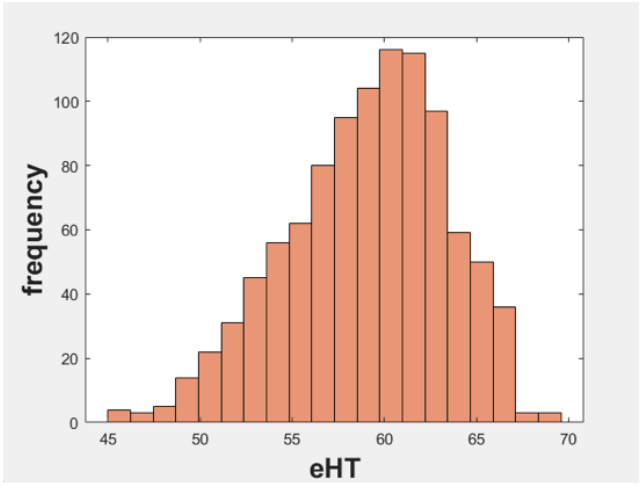

Figure 2: Sample populations generated using uniform distributions for maximum velocity values. Frequency represents the number of simulated individuals, and eHT is represented in units of nM.

3. Distribution Simulations

In the model created by Best et al. (2020), it was assumed that the enzyme expression levels were uniformly distributed from 75% to 125% of their base values. We investigated the sensitivity of this assumption by changing uniform distributions to other distributions and evaluating the similarity of the results. Our goal was to show how the general shape of the distributions either fluctuate or remain the same based on different distributions used to generate these initial enzyme expression levels. The enzyme expression levels themselves were not randomized; rather, multipliers are used in the code instead. This allows for the same methodology to be applied to other projections in the brain, in which absolute maximum velocity values may be different.

3.1 V_{TPH} simulations

We began by changing the distribution of V_{TPH}, the maximum velocity of TPH **[6]**. The first distribution we substituted was a normal distribution. All other V_{max} values were kept distributed according to uniform distributions, and a new set of random values were generated for a new population of 1000. For V_{TPH} values, a normal distribution of multipliers was

set with mean 1 and standard deviation 0.125, so two standard deviations in either direction of the mean captured the interval from 0.75 to 1.25. Thus, roughly 95% of values generated were kept within this range, which is consistent with determinations for enzyme expression levels in the literature **[6]**. The results are shown in Figure 3.

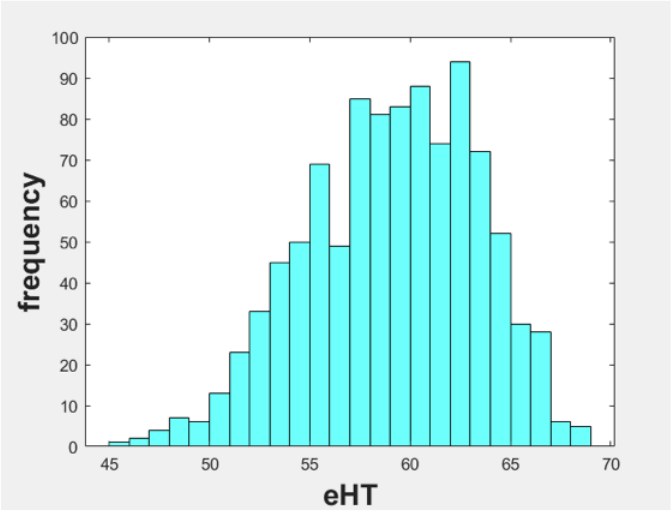

Figure 3: Extracellular serotonin distribution according to a normal V_{TPH} distribution. Frequency represents the number of simulated individuals, and eHT is represented in units of nM.

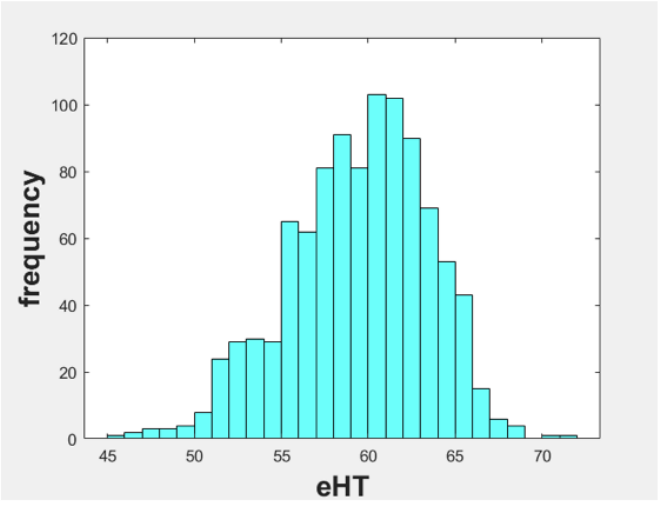

Figure 4: Extracellular serotonin distribution according to a bimodal V_{TPH} distribution. Frequency represents the number of simulated individuals, and eHT is represented in units of nM.

The results from this simulation can be compared with the control populations in Figure 2, in which all enzyme expression levels were varied according to uniform distributions. The general shape of the normally distributed V_{TPH} values was roughly the same as the control populations, and the mean of the newly simulated distribution showed no significant difference from the blue control population, $t(1998) = -1.3$, $p > 0.1$. Thus, changing the distribution of V_{TPH} from uniform to normal does not have a significant effect on the results. We further investigated their similarities later in this section.

A similar investigation with a bimodal distribution was also conducted. This distribution consisted of two normal distributions for the multipliers: one centered at 0.85 and the other centered at 1.15. This captured the possibility of a genetic predisposition toward a higher or lower TPH expression level, for example. Standard deviations for both normal distributions were chosen as 0.05, so the interval between two standard deviations below the lower distribution and two standard deviations above the higher distribution were from 0.75 to 1.25. To generate these randomized values, each individual had a 50% chance of receiving a value according to the lower normal distribution and a 50% chance of receiving a value according to the higher normal distribution. This yielded a roughly bimodal distribution of simulated values. The results of this investigation are shown in Figure 4.

Like the results for the normal V_{TPH} distribution simulation, these distribution means also did not differ significantly from the blue control population in Figure 2, $t(1998) = 0.6$, $p > 0.5$. The peak is still centered around 60 nM and follows an approximate bell-shape. In order to further visualize the relationships between generated V_{TPH} values and extracellular serotonin values at the steady state, scatterplots of population data were created. These results are shown in Figure 5.

These scatterplots provide further evidence that results were not heavily influenced by changing the distribution of generated V_{TPH} values. Each plot shows a relatively weak positive association between extracellular serotonin concentration at the steady state and initially generated V_{TPH} values. Since we

cannot accurately predict extracellular serotonin values from simulated V_{TPH} values, regardless of their distributions, we show that the two variables do not influence each other.

3.2 Further distribution simulations

We showed that varying the distributions of V_{TPH} alone did not have a significant effect on steady state results. We further tested the sensitivity of the uniform distribution assumption by changing the distributions of *all* related enzyme expression levels. By deviating further from this assumption, we challenged the bounds to which results will remain relatively unaffected. We varied the distributions of nine different multipliers in this simulation, instead of just a singular multiplier as in the V_{TPH} simulations. Although there are more than nine different enzymes in the schematic in Figure 1, some of the enzymes were grouped together as a single expression level; for example, the Uptake 2 mechanism was varied as a whole, as opposed to varying individual multipliers for norepinephrine transporter (NET), 5-HT reuptake transporter (SERT, in the Uptake 2 mechanism), dopamine transporter (DAT), and organic cation transporter (OCT). Two more populations of 1000 computer-simulated individuals were generated, using the same specifications for the normal and bimodal distributions as above for each multiplier. The results of this simulation are shown in the two histograms in Figure 6.

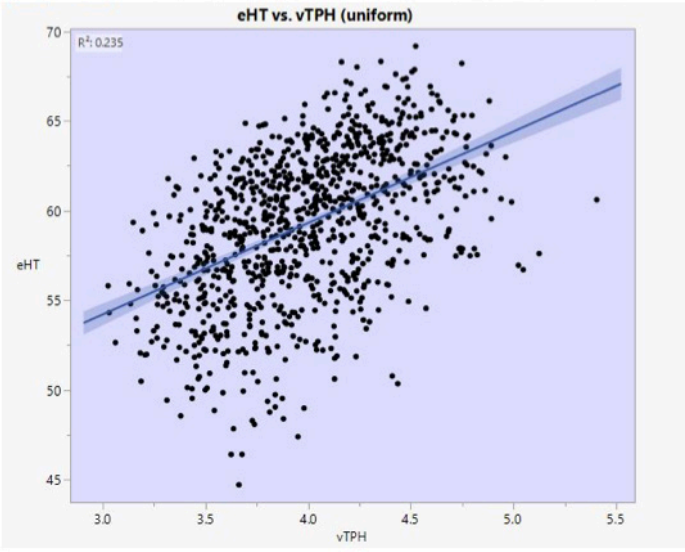

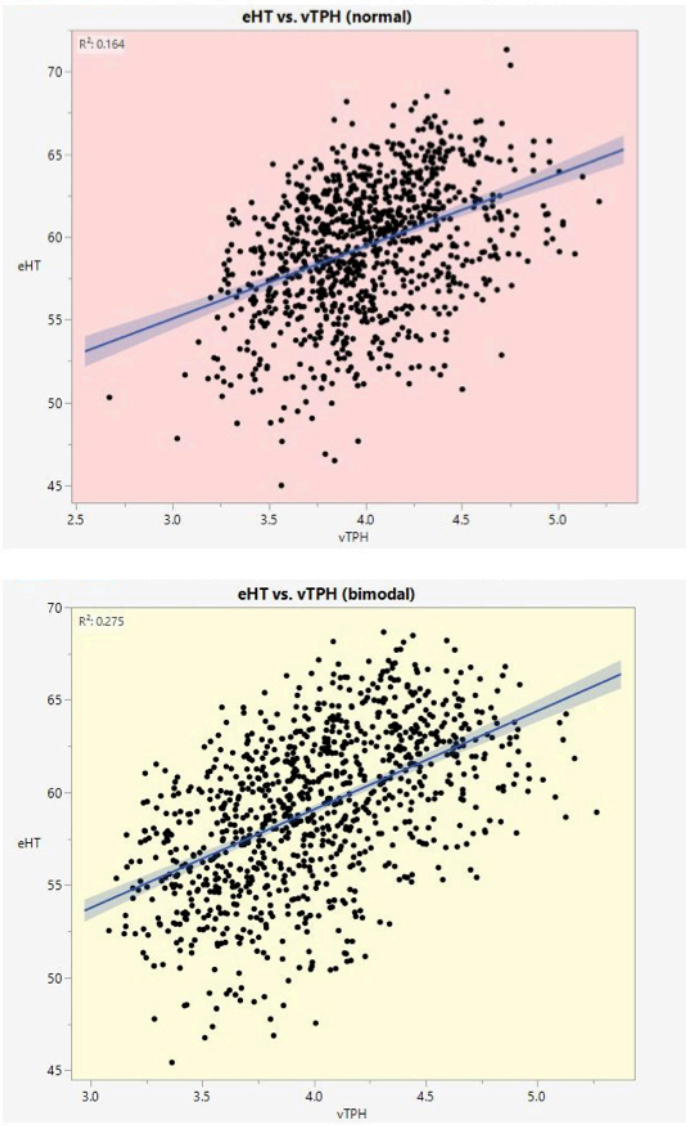

Figure 5: Extracellular serotonin concentration vs. V_{TPH} in populations generated according to uniform (blue), normal (red), and bimodal (yellow) distributions for V_{TPH}.

These distributions can be compared to the control populations using uniform distributions for each multiplier in Figure 2. Once again, their distributions follow the familiar quasi-bell-shaped curve and peaks in frequency near 60 nM. When comparing the means from the normally distributed parameters (red) to the blue control population in Figure 2, there was no significant difference, $t(1998) = -0.5, p > 0.5$; the bimodally distributed parameter distribution (green) also showed no significant difference in means, $t(1998) = 0.67, p > 0.1$.

These simulations show that the assumption that enzyme expression levels are uniformly distributed from 75% to 125% is not particularly sensitive. Knowledge of the biological mechanisms driving these distributions is somewhat limited **[17][18][19]**, but any new discoveries of non-uniform distributions may not significantly impact the results of this model. Reasonable distributions were chosen for these simulations; distributions resembling delta functions or distributions strongly skewed toward 75% or 125% were not tested. However, if a function similar to a delta function were the most biologically appropriate distribution, we would not observe the variability in enzyme expression level from 75% to 125%. Additionally, if a strongly skewed distribution toward either 75% or 125% were more biologically appropriate than a uniform distribution, the literature values for maximum velocities would have reflected this. Thus, changes to the uniform distributions of the enzyme expression levels, within reason, do not significantly impact resulting extracellular serotonin distributions, as shown above. We can be much more confident in using the assumption that maximum velocities are distributed according to uniform distributions, because even if this is not truly representative of the neurobiological reasoning behind it, the results are left relatively unchanged. Therefore, we used the uniform distribution assumption for subsequent simulations.

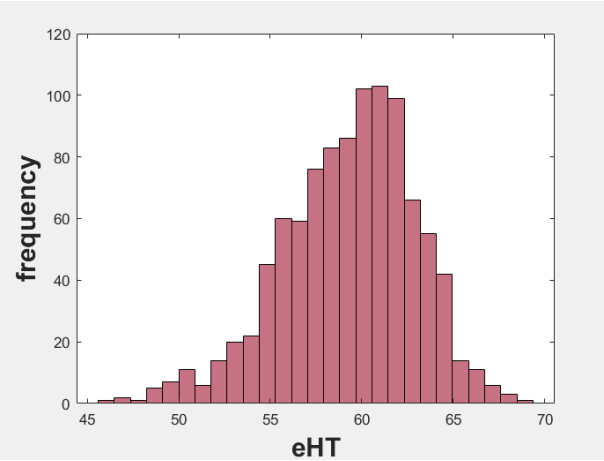

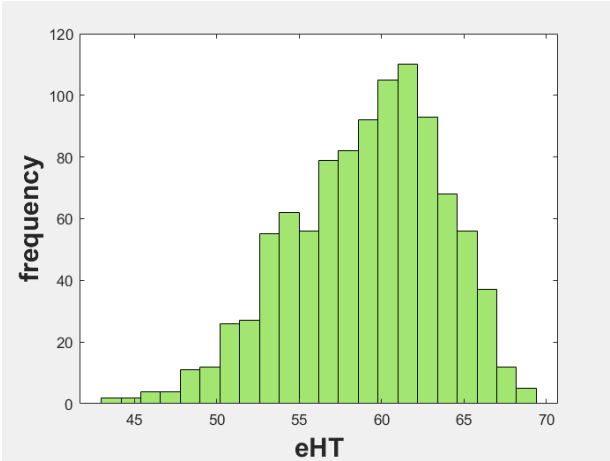

Figure 6: Extracellular serotonin distributions according to normal (red) and bimodal (green) distributions. Frequency represents the number of simulated individuals, and eHT is represented in units of nM.

4. Effects of MAOIs

Monoamine oxidase inhibitors (MAOIs) were the first treatments developed to combat depressive symptoms **[20]**. Examples of MAOIs include isocarboxazid, phenelzine, selegiline, and tranylcypromine, and they are usually taken orally **[20]**. They work by restricting the activity of the enzyme monoamine oxidase **[20]**, which is essentially the equivalent of lowering the enzyme expression level of monoamine oxidase (MAO) in the model. By inspecting the schematic in Figure 1, one can see that cytosolic serotonin (*cht*) undergoes two pathways: one to vesicular serotonin (*vht*) via the vesicular monoamine transporter enzyme (MAT), and the other to 5-hydroxyindoleacetic acid (*hia*) via the MAO enzyme and the aldehyde dehydrogenase (ALDH) enzyme. By restricting the activity of MAO, one would expect more cytosolic serotonin to be routed toward vesicular serotonin, which then becomes extracellular serotonin, according to the schematic **[6]**. To simulate the effects of MAOIs, we generated another population with V_{MAO} values distributed according to a uniform distribution between 75% and 125% of the base value and then multiplied by one half. A comparison of this new population with a control population is shown in Figure 7.

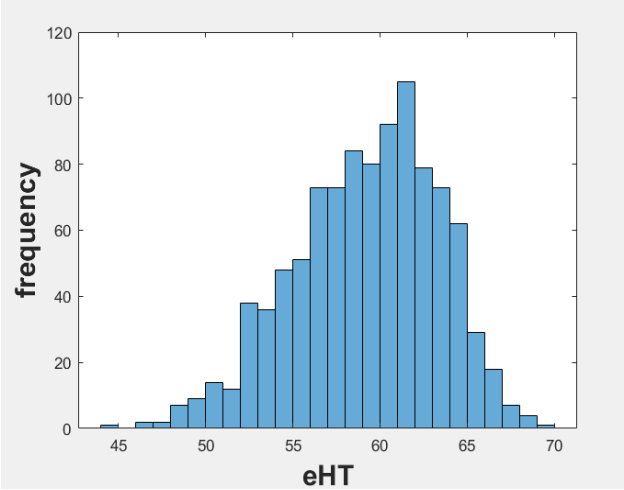

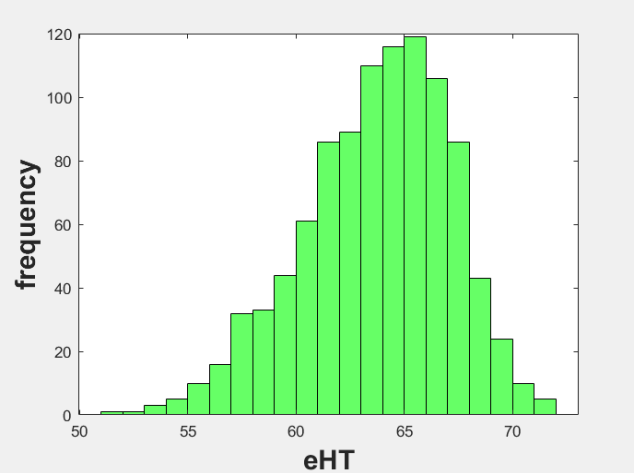

Figure 7: Extracellular serotonin distributions of a control population (blue) and a population with halved V_{MAO} (green). Frequency represents the number of simulated individuals, and eHT is represented in units of nM.

The general shapes of the two distributions are similar, but the peak of the halved V_{MAO} distribution is approximately 5 nM higher than the control population. Their means show a statistically significant difference, $t(1998) = -26.6$, $p < 0.001$. As expected, MAOIs cause an increase in extracellular serotonin *in silico*, and we use this as a barometer for depressive symptoms. It is important to note that the choice to multiply V_{MAO} values by one half is arbitrary. It is not known exactly how MAOI treatment quantitatively impacts the analogous enzyme expression level used in the model. As a result, the fact that the peak of the halved V_{MAO} population is 5 nM higher than the control is also arbitrary; the true difference may be higher or lower, and this difference likely varies in different projection regions of the brain. The takeaway is that the extracellular serotonin distribution as a whole was shifted to the right upon simulated treatment with MAOIs.

Unfortunately, MAOIs are known to cause many side effects, including dry mouth, nausea, headache, drowsiness, and insomnia, among others **[20]**. More serious side effects include involuntary muscle movement, weight gain, low blood pressure, and issues with the urinary and reproductive systems **[20]**. MAOI use also typically requires dietary restrictions and monitoring intake of other medications, as certain foods and medications can cause dangerously high blood pressure when taken with MAOIs **[20]**. Furthermore, when taken with other drugs that raise extracellular serotonin levels, patients may experience serotonin syndrome **[20]**, a condition characterized by dangerously high levels of serotonin that can lead to major changes in blood pressure and rapid heart rate and even death if left untreated **[21]**. Serotonin syndrome may be difficult to predict, as certain pain or headache medications and herbal supplements are known to induce serotonin syndrome when taken with MAOIs **[20][21]**. Other antidepressants are favored in modern practice since they are safer and cause fewer side effects **[20]**. We examined another class of antidepressant in the following simulations.

5. Effects of SSRIs

Selective serotonin reuptake inhibitors (SSRIs) are currently the most commonly prescribed antidepressants **[22]**. They can ease depressive symptoms in moderate to severe cases while typically causing fewer side effects than other classes of antidepressants **[22]**. Examples of SSRIs include citalopram, escitalopram, fluoxetine, paroxetine, and sertraline, which are commonly known by their brand-names as Celexa, Lexapro, Prozac, Paxil or Pexeva, and Zoloft, respectively **[22]**. Side effects are similar to those caused by MAOIs, but they are less common and less severe **[22]**. In the model, the pathway associated with SSRIs is carried out by the SERT enzyme directly connected to the varicosity in Figure 1. This enzyme removes serotonin from the extracellular space and converts it into cytosolic

serotonin **[6]**. SSRIs hinder the enzymatic activity of SERT, leading to a higher concentration of serotonin left in the extracellular space, which is thought to ease the symptoms of depression **[6]**. SERT is also involved in the Uptake 2 mechanism, but this second form of extracellular serotonin uptake is only active once a certain concentration of extracellular serotonin is reached, as predicted by the model and verified by experimental results **[6]**. In these simulations, we primarily focused on individuals with low extracellular serotonin levels at the steady state, so SERT is the primary mechanism that transports extracellular serotonin back into the varicosity.

We utilized the same methodology from the MAOI simulations; a new population of 1000 was generated using a uniform distribution for SERT expression, and then these values were subsequently multiplied by one half. This simulated the function of SSRIs by inhibiting the ability of SERT to convert serotonin from its extracellular to cytosolic form. We once again juxtaposed a control population with this new population with halved V_{SERT} values in Figure 8.

The results from this simulation are similar to the results obtained from the halved V_{MAO} simulation; the general shape of the extracellular serotonin distribution remains unchanged, but values are shifted toward higher extracellular serotonin levels at the steady state. The means show a statistically significant difference, $t(1998) = -31.0, p < 0.001$. Just as in the V_{MAO} simulations, the choice for multiplying the V_{SERT} multiplier by one half was arbitrary, so the exact difference between frequency peaks does not carry any confirmed biological significance.

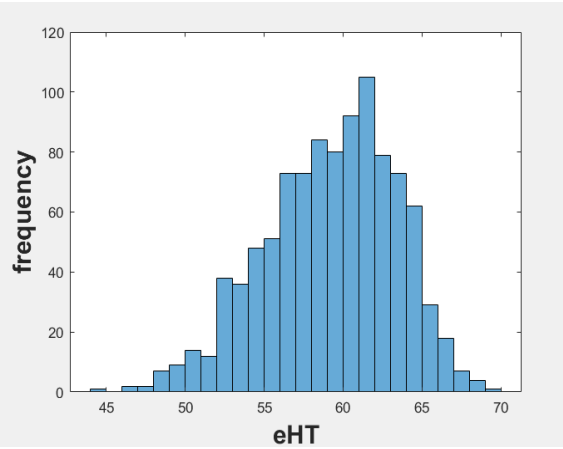

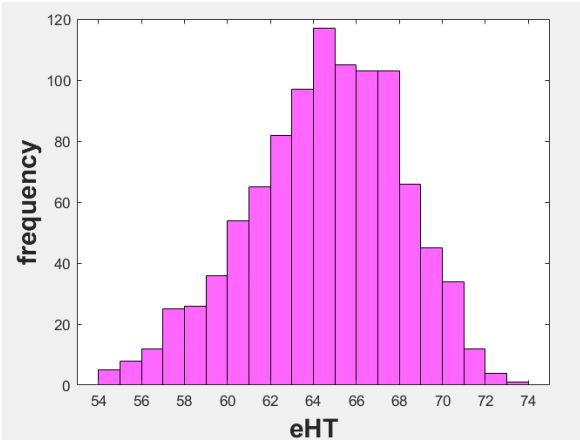

Figure 8: Extracellular serotonin distributions of a control population (blue) and a population with halved V_{SERT} (purple). Frequency represents the number of simulated individuals, and eHT is represented in units of nM.

While SSRIs tend to be the preferred treatment for MDD in modern medicine, there are still a multitude of obstacles in finding a personalized treatment. People may react differently to the same SSRI, so certain medications may be more effective for some than others **[22]**. Different SSRIs exhibit different kinetics **[23]**, which are likely influenced by genetic factors. In a clinical setting, the responses of family members to SSRIs may provide insight on the optimal SSRI for a patient **[22]**. However, many patients do not have family members who have not responded successfully to an SSRI, so it can take time to test different medications. Another nuance is introduced by dosage, since dosage alterations may be necessary to alleviate symptoms and avoid side effects **[22]**. A particular antidepressant at a particular dose may require several weeks of testing to get through initial side effects and determine the efficacy of the treatment **[22]**. Since untreated patients with depression are at a high suicide risk **[2][3]**, this method of trial and error is increasingly dangerous the longer it takes. Furthermore, roughly 30% of patients with major depression do not show responses to SSRIs of any form **[24]**, so efforts to experiment with different drugs and doses may not lead to any productive treatment. Patients then must turn to other solutions, which takes more time that a patient may not have. The issue of drug identity is beyond the scope of the model, since molecular biochemistry and

kinetics are not accounted for in the schematic. The dosage issue is also unexplored in this paper, since more work would have to be done in determining how changing dosages of a given SSRI quantitatively impacts the V_{max} of SERT. However, we sought to provide insight into the third issue mentioned above and investigated why certain patients may not respond to SSRIs in general.

We assumed that there was some overlap between people with low levels of extracellular serotonin in the halved V_{SERT} population and people that do not respond to SSRIs, because we used serotonin as a barometer for symptoms of depression. While depressive symptoms are influenced by external factors **[5]**, which cannot all be captured in the model, there is a strong association between low extracellular serotonin levels and depressive symptoms **[25]**. We isolated the computer-simulated population with steady state extracellular serotonin values below 60 nM from the halved V_{SERT} distribution shown in Figure 8. Again, this numerical choice of serotonin concentration was arbitrary, as we were trying to capture the people on the lower end of this distribution. Individuals with steady state extracellular serotonin values lower than 60 nM totaled 112 of 1000. Then, for each multiplier, the value of the randomly generated multiplier was graphed on the x-axis, and a histogram was created from the count of people falling within each interval of multiplier values. This was done with hopes of finding which characteristics were common among people with low steady state extracellular serotonin concentrations. The results are displayed in Figure 9.

The first seven graphs did not show a strong inclination toward extreme values, but the last two graphs showed high counts of people with low simulated expression levels of TPH and neutral amino acid transporter; the vast majority of randomly generated multiplier values fell below 1.0 for these two enzymes. Thus, low expression levels of these two enzymes were most correlated to low extracellular serotonin values at the steady state. These two enzymes may be the key in predicting whether patients will respond to SSRI treatment.

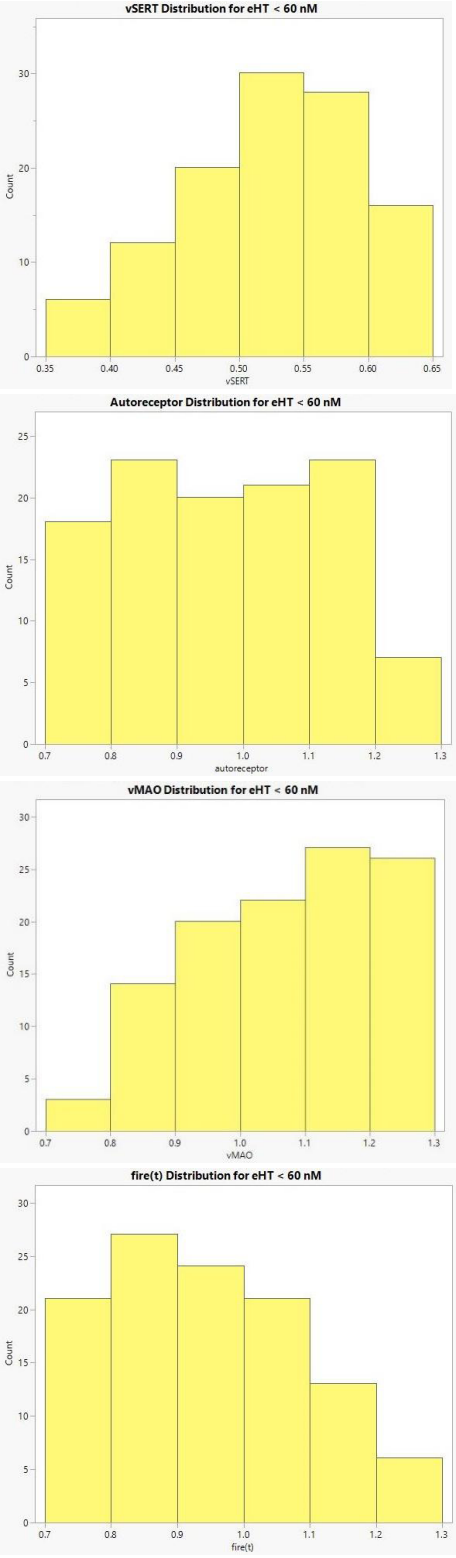

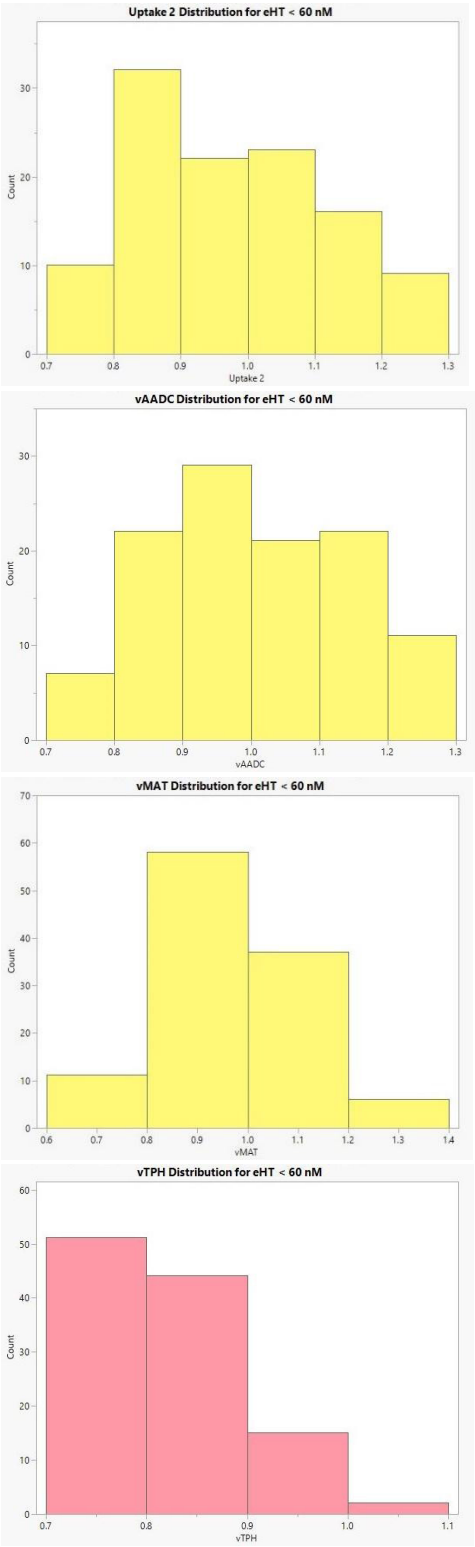

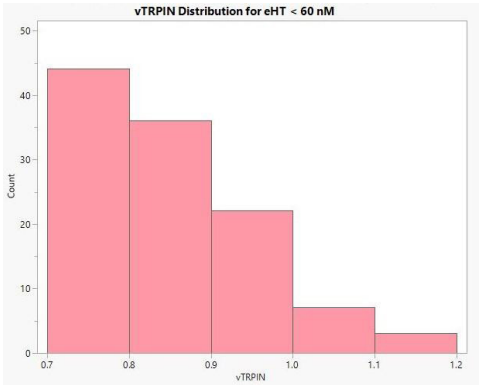

Figure 9: Counts of people with low steady state extracellular serotonin concentrations vs. randomly generated multiplier values of enzymes or groups of enzymes. The order of multiplier distributions displayed are as follows: 5-HT reuptake transporter (V_{SERT}), 5-HT autoreceptors (autoreceptor), monoamine oxidase (V_{MAO}), *fire(t)*, Uptake 2, aromatic amino acid decarboxylase (V_{AADC}), vesicular monoamine transporter (V_{MAT}), tryptophan hydroxylase (V_{TPH}), and neutral amino acid transporter (V_{trpin}).

6. Discussion

Mathematical modeling cannot replace *in vivo* experimentation. There exists a balance between the two; mathematical modeling may drive motivation for certain experiments, and these results may confirm what the model predicts or reveal a flaw in the model's design or our current understanding of the biological problem at hand. Problems in neurobiological topics pose a greater challenge, since it can be difficult to measure or determine needed parameters or concentrations *in vivo*. In serotonin dynamics, it can be challenging to measure enzyme expression levels, so confirming the results from the SSRI simulations may require advancement in experimental techniques. It may also be difficult to utilize the results from the simulations, since with current capabilities, it may not be possible or practical to determine enzyme expression levels of specific patients and determine personalized treatments. The development of a system to determine the most effective SSRIs or other medications for treating depression in individual patients may offer substantial benefits. However, it is important to recognize that

patients with limited access to healthcare are unlikely to reap these benefits until access to such a system is expanded.

Further research should account for differences in SSRI doses. Reducing the time it takes for patients to discover their correct personalized treatment for depressive symptoms is crucial, so any insights in shortening any part of this process deserve to be extensively studied, both *in vivo* and *in silico*. If quantitative relationships are determined between a certain SSRI dosage and its enzyme expression reduction equivalent, simulations of people with low steady state extracellular serotonin can be analyzed for future insights. These observations should be confirmed or refuted with *in vivo* experimentation; however, this comes with limitations. The assumption that low serotonin levels are associated with depressive symptoms may not hold for every patient, so it is possible that the isolated patients with low serotonin levels may not actually be the ones displaying these symptoms. *In vivo* experimentation in this field is typically performed on rodents, so depressive symptoms cannot necessarily be extrapolated to humans; only extracellular serotonin values can be measured. Overall, we hope these findings provide motivation for further *in vivo* experimentation.

Acknowledgements

This work was completed under the direction of Michael Reed, Duke University. Figures were constructed using MATLAB and JMP Pro 17. Statistical analyses were performed using Python.

References

1. Mayo Clinic Staff. (2022, October 14). *Depression (major depressive disorder)*. Mayo Clinic. Retrieved April 13, 2023, from https://www.mayoclinic.org/diseases-conditions/depression/symptoms-causes/syc-20356007

2. Sokero, T. P., Leskela, U. S., Rytsala, H. J., Lestela-Mielonen, P. S., Melartin, T. K., & Isometsa, E. T. (2002). Risk factors for suicidal ideation and attempts among psychiatric patients with major depressive disorder. *European Psychiatry*, *17*, 204. https://doi.org/10.1016/s0924-9338(02)80873-2

3. Kumar, R., & Srivastava, A. S. (2005). Suicidal ideation and attempts in patients with major depression: Sociodemographic and clinical variables. *Indian Journal of Psychiatry*, *47*(4), 225. https://doi.org/10.4103/0019-5545.43059

4. U.S. Department of Health and Human Services. (2020). *Suicide*. National Institute of Mental Health. Retrieved April 18, 2023, from https://www.nimh.nih.gov/health/statistics/suicide

5. Nabeshima, T., & Kim, H.-C. (2013). Involvement of genetic and environmental factors in the onset of depression. *Experimental Neurobiology*, *22*(4), 235–243. https://doi.org/10.5607/en.2013.22.4.235

6. Best, J., Duncan, W., Sadre-Marandi, F., Hashemi, P., Nijhout, H. F., & Reed, M. (2020). Autoreceptor control of serotonin dynamics. *BMC Neuroscience*, *21*(1). https://doi.org/10.1186/s12868-020-00587-z

7. Meltzer, H. Y. (1990). Role of serotonin in depression. *Annals of the New York Academy of Sciences*, *600*(1 The Neurophar), 486–499. https://doi.org/10.1111/j.1749-6632.1990.tb16904.x

8. Gu, C. (2021). Rapid and reversible development of axonal varicosities: A new form of neural plasticity. *Frontiers in Molecular Neuroscience*, *14*. https://doi.org/10.3389/fnmol.2021.610857

9. Best, J., Marie Buchanan, A., Frederik Nijhout, H., Hashemi, P., & C. Reed, M. (2022). Mathematical models of serotonin, histamine, and depression. *Serotonin and the CNS - New Developments in Pharmacology and Therapeutics*. https://doi.org/10.5772/intechopen.96990

10. Jäkel, S., & Dimou, L. (2017). Glial cells and their function in the Adult Brain: A journey through the history of their ablation. *Frontiers in Cellular Neuroscience*, *11*. https://doi.

org/10.3389/fncel.2017.00024

11. Purves D., Augustine G.J., Fitzpatrick D., et al., editors. Neuroscience. 2nd edition. Sunderland (MA): Sinauer Associates; 2001. Neuroglial Cells. Available from: https://www.ncbi.nlm.nih.gov/books/NBK10869/

12. Wood, K. M., Zeqja, A., Nijhout, H. F., Reed, M. C., Best, J., & Hashemi, P. (2014). Voltammetric and mathematical evidence for dual transport mediation of serotonin clearance in vivo. *Journal of Neurochemistry*, *130*(3), 351–359. https://doi.org/10.1111/jnc.12733

13. Barnes, P. J. (1991). Histamine receptors in the lung. New Perspectives in Histamine Research, 103–122. https://doi.org/10.1007/978-3-0348-7309-3_9

14. Hill, S. J. (1992). Multiple histamine receptors: Properties and functional characteristics. Biochemical Society Transactions, 20(1), 122–125. https://doi.org/10.1042/bst0200122

15. Best, J., Nijhout, H. F., Samaranayake, S., Hashemi, P., & Reed, M. (2017). A mathematical model for histamine synthesis, release, and control in Varicosities. *Theoretical Biology and Medical Modelling*, *14*(1). https://doi.org/10.1186/s12976-017-0070-9

16. Hersey, M., Samaranayake, S., Berger, S. N., Tavakoli, N., Mena, S., Nijhout, H. F., Reed, M. C., Best, J., Blakely, R. D., Reagan, L. P., & Hashemi, P. (2021). Inflammation-induced histamine impairs the capacity of escitalopram to increase hippocampal extracellular serotonin. *The Journal of Neuroscience*, *41*(30), 6564–6577. https://doi.org/10.1523/jneurosci.2618-20.2021

17. Boeuf, S., Keijer, J., Franssen-Van Hal, N. L., & Klaus, S. (2002). Individual variation of adipose gene expression and identification of covariated genes by cdna microarrays. *Physiological Genomics*, *11*(1), 31–36. https://doi.org/10.1152/physiolgenomics.00051.2002

18. Oleksiak, M. F., Churchill, G. A., & Crawford, D. L. (2002). Variation in gene expression within and among natural populations. *Nature Genetics*, *32*(2), 261–266. https://doi.org/10.1038/ng983

19. Sigal, A., Milo, R., Cohen, A., Geva-Zatorsky, N., Klein, Y., Liron, Y., Rosenfeld, N., Danon, T., Perzov, N., & Alon, U. (2006). Variability and memory of protein levels in human cells. *Nature*, *444*(7119), 643–646. https://doi.org/10.1038/nature05316

20. Mayo Foundation for Medical Education and Research. (2019, September 12). *Monoamine oxidase inhibitors (MAOIs)*. Mayo Clinic. Retrieved April 20, 2023, from https://www.mayoclinic.org/diseases-conditions/depression/in-depth/maois/art-20043992

21. Mayo Foundation for Medical Education and Research. (2022, January 22). *Serotonin syndrome*. Mayo Clinic. Retrieved April 20, 2023, from https://www.mayoclinic.org/diseases-conditions/serotonin-syndrome/symptoms-causes/syc-20354758#:~:text=Serotonin%20is%20a%20chemical%20that,cause%20death%20if%20not%20treated.

22. Mayo Foundation for Medical Education and Research. (2019, September 17). *Selective serotonin reuptake inhibitors (SSRIs)*. Mayo Clinic. Retrieved April 20, 2023, from https://www.mayoclinic.org/diseases-conditions/depression/in-depth/ssris/art-20044825

23. Marken, P. A., & Munro, J. S. (2000). Selecting a selective serotonin reuptake inhibitor. *The Primary Care Companion For CNS Disorders*, *2*(6). https://doi.org/10.4088/pcc.v02n0602

24. Al-Harbi, K. S. (2012). Treatment-resistant depression: Therapeutic trends, challenges, and Future Directions. Patient Preference and Adherence, 369. https://doi.org/10.2147/ppa.s29716

25. Nautiyal, K. M., & Hen, R. (2017). Serotonin receptors in depression: From A to B.

F1000Research, *6*, 123. https://doi.org/10.12688/f1000research.9736.1

Evaluating SLAM Performance with Synthesized Datasets from Unreal-Based Emulators

Muchang Bahng

Volume 2, Issue 2

Article Synopsis

This study investigates how to better map and navigate inside buildings using advanced computer simulations and video game technology. The research delves into various camera settings and virtual environments to improve the accuracy of these mapping systems. Key findings demonstrate significant enhancements in indoor navigation, especially in complex and dynamic spaces. These advancements are crucial for developing more efficient and reliable indoor mapping technologies, which have wide-ranging applications in robotics and augmented reality.

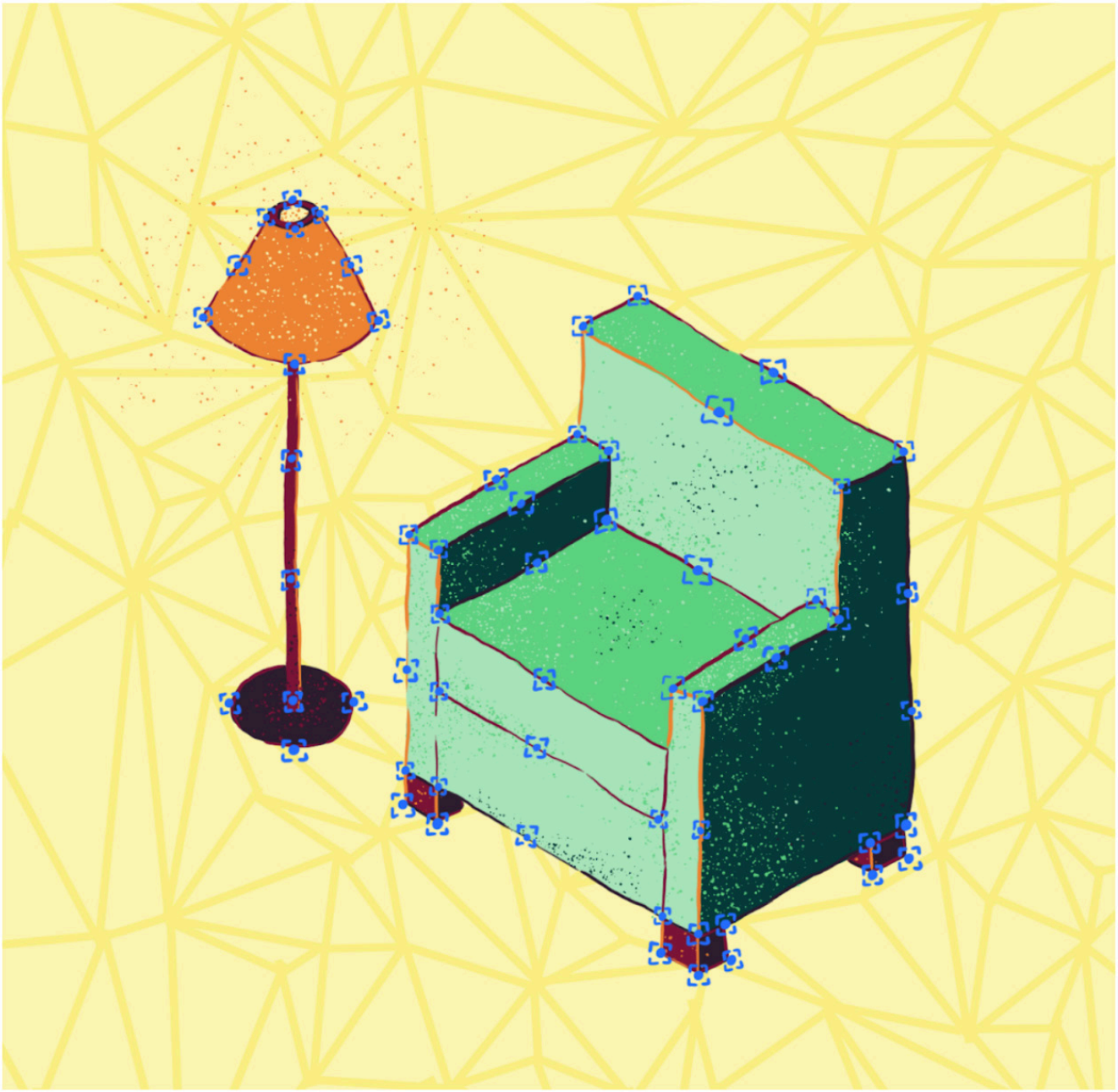

Graphic by Gaby Dunn

Evaluating SLAM Performance with Synthesized Datasets from Unreal-Based Emulators

Muchang Bahng

Duke University
https://doi.org/10.55894/dv2.22

Abstract

The rapid advancement in visual-inertial simultaneous localization and mapping (SLAM) has opened numerous applications in computer vision. However, the scarcity of high quality, publicly accessible datasets hampers the evaluation of SLAM performance in varied and tailored environments. In this study, I employed the AirSim simulator and the Unreal Engine 4 to generate a trajectory resembling that of the TUM VI Room 1 ground truth dataset within the ArchViz indoor environment representing a well-lit, furnished room. I further modified the environment and trajectory through various expansions, addition of features, and data smoothing to ensure a more stable sequence of input frames into the SLAM architecture. I then examined the efficiency of visual ORB-SLAM3 by inputting images of resolution 256×144 and 512×288 at 30 frames per second (FPS), while also adjusting the feature threshold - the maximum number of feature points that ORB-SLAM3 tracks per frame. This investigation of the camera parameters within AirSim and ORB-SLAM3 has led to the essential finding that the resolution of the input images must coincide with the dimensions of the film. The subsequent runs under these variables reveal that higher resolution images lead to considerably better tracking, with an optimal feature threshold ranging between 3000~12000 feature points per frame. Moreover, ORB-SLAM3 demonstrated significantly enhanced robustness within dynamic environments containing moving objects when using higher resolution inputs, with a decreased error of close to 0cm compared to 23.19cm for lower resolutions (averaged over three runs). Finally, I conducted qualitative testing using real-life indoor environments recorded with an iPhone Xr camera, which produces results that highlight the challenges faced by ORB-SLAM3 due to factors such as glare and motion blur.

Index Terms—Visual simultaneous localization and mapping, Unreal, AirSim, ORB-SLAM3, Feature threshold

I. INTRODUCTION

Simultaneous localization and mapping (SLAM) is an essential component in robotics and computer vision systems. It involves constructing a three-dimensional map of an unknown environment while simultaneously locating the robot or a camera within that environment. SLAM algorithms typically use a combination of sensor measurements and motion models to estimate the position of the robot or camera at each point in time, and to update the map of the environment based on these estimates. A typical visual SLAM workflow includes the following steps [1], [16]–[18]:

1) Sensor data acquisition: Acquisition and preprocessing of camera images.
2) Visual odometry (VO): Estimation of the camera movement between adjacent frames to estimate the displacement of the observer (ego-motion) and generate a rough local map, also known as the frontend. This tends to generate noisy estimates of the map and accumulates displacement error.
3) Backend filtering and optimization (backend): Generation of a fully optimized trajectory and map from camera pose and time stamp data from the VO and loop closing modules.
4) Loop closing: Loop closing: Determines whether the robot has returned to its previous position to reduce accumulated drift. If a loop is detected, it will provide information to optimize the backend.
5) Reconstruction: Constructs the map based on camera trajectory.

The most direct applications of SLAM are in the fields of autonomous systems and augmented reality. By constructing a map and localizing, SLAM enables vehicles to navigate autonomously in unknown environments and to detect objects, which is essential for identifying and avoiding pedestrians and other obstacles. SLAM also allows robots to navigate through warehouses and hospitals to perform tasks such as inventory management, patient care, and creating accurate maps of complex infrastructure to efficiently detect needed maintenance. In the field of augmented reality, the precision of localization and mapping is essential for creating an immersive experience in realistic virtual environments, which branches out into gaming, training simulations, and remote collaboration.

To reliably test the accuracy of these models, researchers use public, pre-available datasets such as TUM VI [3], KITTI [2], EuRoC [13], and SenseTime [14]. These datasets provide real-world sensor data collected from cameras and more advanced sensors such as laser range finders (LIDAR) mounted on a mobile agent.

Data generation using simulators has become an increasingly popular approach to computer vision research for several reasons. First, simulators provide researchers with greater flexibility to create complex datasets with specific features and characteristics that may not be available in existing datasets. This allows researchers to test their algorithms under a wide range of scenarios, which can improve their performance in real-world applications [4]. Second, simulators provide precise ground truth data, which is the exact location, orientation, and other relevant information of the objects in the scene, without the need to collect it separately through more advanced sensors. This is important for training and evaluating computer vision algorithms since ground truth data provides a reference for accuracy and helps to ensure that the algorithm is performing as intended. Third, generating data using simulators like AirSim can be a cost-effective alternative to collecting real-world data, which can be time-consuming, expensive, and may require specialized equipment and personnel. Using a simulator can be a more affordable and accessible option for researchers.

The key contributions of this study are as follows. First, I generate a trajectory resembling the TUM VI Room 1 ground truth dataset within the ArchViz indoor environment using the AirSim simulator and Unreal game engine, and further modify the environment and trajectory to ensure a more stable sequence of input frames for the SLAM architecture. Second, I perform a comprehensive analysis of the efficiency of visual ORB-SLAM3 by adjusting the input image resolution and feature threshold, leading to essential findings on the optimal settings for improved tracking performance within both static and dynamic environments. Third, I investigate the importance of tuning the camera parameters within AirSim and ORB-SLAM3, highlighting the need for the input image resolution to match the dimensions of the film. Lastly, I conduct qualitative testing using real-life indoor environments recorded with an iPhone Xr camera, providing insights into the challenges faced by ORB-SLAM3 in real-world scenarios with everyday commercial cameras due to factors such as glare and motion blur. Collectively, these contributions aim to enhance the understanding of visual SLAM performance and its practical applications in various indoor environments.

II. RELATED WORKS

A. Feature Extraction

An effective visual odometry system relies not only on the quantity of feature points but also on their quality, which refers to the properties of feature points that influence the performance of feature-based image registration. These properties include repeatability, distinctiveness, efficiency, and locality [1]. Several feature detection algorithms have been developed over the years, aiming to extract distinctive points from images that can be matched across multiple frames. Some of the widely used feature detection algorithms include scale invariant feature transform (SIFT), speeded-up robust features (SURF), features from accelerated segment test (FAST), oriented FAST and rotated BRIEF (ORB), and acceleratedKAZE (AKAZE), which vary in their level of accuracy and computational efficiency.

The applicability of these extraction algorithms depends on their ability to run in real time at 30FPS, or 33ms per iteration. The SIFT and SURF algorithms, which are known for their scale and rotational invariance, suffer from high computational costs that cannot meet the 33ms threshold. The FAST algorithm sacrifices the robustness of SIFT and SURF for faster speed, which may negatively impact its performance in scenarios with significant changes in scale or orientation. ORB, which compromises between efficiency and accuracy, is a combination of the FAST keypoint detector and the BRIEF descriptor, offering an efficient and binary feature detection algorithm. It is more computationally efficient than SIFT and SURF while providing some degree of scale and rotation invariance.

Recent advancements in feature detection algorithms have focused on incorporating machine learning techniques, particularly deep learning, to improve their performance. Convolutional neural networks (CNNs) have been employed to learn feature representations that are more robust and discriminative than traditional hand-crafted features. While these learned features show promising results, they often require significant computational resources, which can limit their applicability in real-time scenarios. Recently, with the advent of edge computing and efficient parallelization, this paradigm of extraction algorithms has been shown to be effective in feature detection.

The SuperPoint algorithm is a learning-based approach for keypoint detection and description, which aims to overcome the limitations of traditional hand-crafted feature detection algorithms such as SIFT and FAST, particularly in challenging conditions like poor lighting or low-texture scenes [2]. SuperPoint is based on a lightweight neural network architecture that is trained on image pairs undergoing known homographic transformations. The algorithm comprises three main steps: MagicPoint detection, homographic adaptation, and descriptor training.

1) MagicPoint is the initial step in the SuperPoint algorithm, which focuses on keypoint detection. It is trained on synthetic data to detect corner points in images.
2) Homographic adaptation is then employed to generate image pairs with known homographic transformations, which are used to train the descriptor network.
3) The final step involves training the descriptor network, which is responsible for providing a descriptor for each keypoint detected by MagicPoint. These descriptors are used for image matching tasks, enabling the algorithm to find correspondences between keypoints in different images.

SuperPoint has demonstrated superior performance compared to traditional hand-crafted algorithms in most benchmarks. It has been found to extract more feature points and perform more stably in low-texture scenes, as well as in poor lighting conditions [2]. The lightweight architecture of the SuperPoint network allows it to maintain relatively low computational requirements while providing improved keypoint detection and description performance, with an empirical runtime of 70FPS on an NVIDIA Titan X ® GPU.

B. Complex Dataset Generation

Simulators have become a valuable tool in robotics and computer vision research, enabling researchers to generate diverse and complex datasets for various applications. One notable example is TartanAir, a synthetic dataset created by researchers at the Robotics Institute at Carnegie Mellon University, which is specifically designed for visual localization, visual odometry, and SLAM research [8].

TartanAir is an extensive dataset comprising photorealistic RGB-D images, depth maps, and camera poses collected from a wide range of indoor and outdoor virtual environments using a custom-designed flying robot. The creators of TartanAir have designed a diverse dataset with dynamic objects, varying lighting conditions, and different types of textures and materials. This level of diversity allows researchers to develop and evaluate algorithms in a more comprehensive and realistic manner,

accounting for many real-world challenges that simpler datasets might overlook.

The TartanAir dataset has been instrumental in advancing the state of the art in visual localization, visual odometry, and SLAM research. Its comprehensive nature enables researchers to identify limitations in existing algorithms and develop novel solutions to overcome these challenges. Furthermore, by providing a standardized dataset, TartanAir facilitates fair and consistent comparison between different detection and tracking algorithms, which is crucial for understanding the strengths and weaknesses of various techniques.

The use of simulators to generate datasets such as TartanAir not only offers a cost-effective and efficient alternative to collecting real-world data but also provides researchers with the flexibility to easily modify and tailor the dataset to specific needs. This adaptability allows for rapid iteration and experimentation, accelerating the development and refinement of algorithms in the field of computer vision.

C. Edge-Assisted SLAM

The integration of SLAM with edge computing has gained significant interest in recent years due to the need for real time processing of localization and mapping data for various applications. Edge computing refers to the processing of data on devices located close to the source of the data, instead of sending it to a centralized cloud server for processing. This approach has several advantages, such as reduced latency, improved data privacy, and reduced network bandwidth consumption [9]. One of the main needs for using SLAM with edge computing is to enable real-time processing (of 30FPS) of data from sensors such as cameras, LIDAR, or inertial measurement units (IMUs). These sensors generate a large amount of data, which must be processed in real-time and may cause computational bottlenecks in a lightweight mobile agent. To overcome this limitation, outsourcing computation to an edge server can improve accuracy and performance [10].

One prominent example of integrating edge computing with SLAM is the Edge-SLAM system, which adapts visual SLAM into an edge computing architecture to enable prolonged operation on mobile devices [9]. Edge-SLAM offloads computation-intensive modules of visual SLAM, such as global map optimization and loop closing, to the edge, reducing resource usage on the mobile device without sacrificing accuracy. That is, Edge-SLAM maintains the tracking computation on the mobile device while moving the rest of the computation to the edge [10], allowing the system to overcome the computational bottlenecks often faced by lightweight mobile agents that need real-time processing. Additionally, edge computing allows the agent to offload tasks without the large latencies seen when offloading to the cloud, saving a considerable portion of time during transmission. This approach may be particularly applicable when using machine learning-based feature extraction algorithms such as the previously mentioned SuperPoint algorithm, which may require significant computational power to process data in real-time. By offloading these tasks to the edge, the mobile device can focus on other critical tasks, and the overall system performance can be improved.

III. METHODOLOGY

A. Environment and Trajectory Initialization and Modification

1) Building Emulators with Unreal and AirSim Plugin: Unreal Engine 4 is a game engine developed by Epic Games that provides developers with a highly customizable editor, a wide range of pre-built templates and advanced rendering capabilities [15].

AirSim is an open-source simulator developed by Microsoft that provides a platform for researchers to simulate and test the performance of autonomous systems, such as drones or cars, which can be controlled through its API supported by C++, Python, and MATLAB. It supports a variety of sensors, such as RGB cameras, depth cameras, LIDAR, and GPS, which allows for efficient data collection that can be streamlined directly into SLAM algorithms. It takes a sequence of pose vectors as inputs and assigns this pose to the agent within the Unreal environment per frame. After the sequence is complete, a directory containing the stream of frames for each pose is generated.

In this study, I used ORB-SLAM3, an open-source simultaneous localization and mapping system developed by the Robotics and Perception Group at the University of Zurich [9]. ORB-SLAM3 uses a combination of feature-based and direct monocular, stereo, and RGB-D visual odometry methods and incorporates advanced features such as semantic segmentation, loop closure detection, and multi-map fusion. I will specifically focus on performance testing of visual ORBSLAM3 with a non-distorted monocular camera at 30FPS.

2) Environment and Trajectory Initialization: In order to investigate the performance of ORB-SLAM3 in a typical indoor setting, I selected a representative environment that closely resembled a standard household

interior. The chosen environment, *ArchViz Interior*, is publicly accessible through the Unreal marketplace. This specific environment offers a unique advantage as the distribution of furniture and objects is non-uniform, and consequently, certain frames within the room will exhibit numerous feature points, while others, such as specific wall sections and the ceiling, will have a sparse feature distribution. This non-uniformity presents a substantial challenge for ORB-SLAM3 during tracking, unlike the TUM VI Room 1 environment, which contains checkerboards, densely packed shelves, and hanging nets that create a grid-like structure, simplifying the tracking process for ORB-SLAM3.

My objective was to identify a trajectory that accurately reflects the movement patterns within an indoor setting, while simultaneously presenting a considerable challenge. The TUM VI Room 1 trajectory proved to be an ideal choice, as it encompasses multiple pans, tilts, and rotations, which together create a complex trajectory for evaluating the performance of ORB-SLAM3.

3) Coordinate Conversion in AirSim: The ground truth data of the TUM VI consists of 16,541 rows in a CSV file, with each row formatted as row

$$r = (T^r, p_x^r, p_y^r, p_z^r, q_w^r, q_x^r, q_y^r, q_z^r)$$

where T^r represents the number of nanoseconds past Unix Epoch, (p_x^r, p_y^r, p_z^r) is the translation component in centimeters, and $(q_w^r, q_x^r, q_y^r, q_z^r)$ is the unit quaternion representation of the $SO(3)$ orthogonal group.

When comparing side-by-side the trajectories of the TUM VI Room 1 image frames and those generated by AirSim in the ArchViz environment, I noticed that the coordinates did not align. It is common for different software to use different coordinate systems, so I needed to incorporate a conversion factor between the Unreal and AirSim bases. For conciseness of notation, let (p, q) represent the timestamp plus the 7D pose in Unreal coordinates, and (p', q') represent the same in AirSim coordinates. The proper conversion has been empirically tested to be

$$p_x \mapsto -p_y' \quad p_y \mapsto -p_x' \quad p_z \mapsto -p_z' \quad q_w \mapsto q_w' \quad q_x \mapsto q_x' \quad q_y \mapsto -q_y' \quad q_z \mapsto -q_z'$$

Therefore, after I extracted the TUM-VI ground truth into a tabular format, I followed the coordinate conversion above before inputting the poses into the AirSim API.

Note that the translational conversion factor may differ depending on the orientation of the entire environment. That is, if the entire Unreal environment was rotated 90 degrees across the XY-plane without any change in the world coordinate system, the x and y components in Unreal and AirSim would align.

4) Environment Expansion: After the conversion, I noticed that the total area covered by the trajectory was greater than the original room. During multiple instances, the camera would get too close to the furniture and walls, sometimes going through them, which was unrealistic and is problematic for tracking. My goal was for there to be approximately 20cm of space between the agent's camera and the walls throughout the entire simulation, since the ground truth video in the TUM VI Room 1 dataset had kept this approximate distance throughout.

Therefore, I manually expanded the room by selecting all objects on one side of the room, translating them out a specific point in the expanded room, and manually added more sections of the walls, floors, and ceiling where needed. It was not as straightforward as simply highlighting all objects and stretching them across the axis using the built-in stretch tool, as there were already too many dependencies between the objects that caused errors. Additionally, stretching the furniture itself would cause noticeable deformations.

The expansion caused a significant decrease in lighting in two corners of the room, so further modifications were made:

1) The windows on the walls on the north end of the blueprint were likewise stretched accordingly to cover the majority of the stretched wall.
2) An extra window along with a directional light source was added on the walls of the south end of the blueprint to allow for more consistent lighting.

B. ORB-SLAM3 and AirSim Parameter Adjustment

1) Timestamp Conversion for ORB-SLAM3 Preprocessing: The frames generated by AirSim are labeled with a timestamp (in nanoseconds after Unix Epoch) representing the time at which the frame was captured in the API. The variance of the time gaps between adjacent frames may be high depending on the hardware in which the simulator is run, the latency of the API calls, the presence of additional functions within the API scripts, and the length of the sleep timer between each API call.

To process this into ORB-SLAM3 at 30FPS, I needed to relabel these timestamps such that the time gap between adjacent poses is 33ms. ORB-SLAM3 also processes timestamp labels in nanoseconds after Unix Epoch, so I

relabeled them by choosing an arbitrary starting point $T_0 = 1.5 \cdot 10^{18}$ and setting the timestamp for frame k to be

$$T_k = T_0 + 33,000,000k$$

where 33,000,000ns represents 33ms.

2) Camera Parameter Adjustment: I had later discovered that the parameters of the AirSim camera must align with the those of ORB-SLAM3. The relevant parameters of ORB-SLAM3 can be found and set in a yaml file, each of which I explain and computed below.

1) The type of camera is always set to "PinHole", since I am working with a monocular camera.
2) (W, H) is the width and height of the image, in pixels.
3) (c_x, c_y) is the central point of the camera.
4) (k_1, k_2, k_3) and (p_1, p_2) describe the radial and tangential distortion parameters, respectively.
5) (f_1, f_2) are the focal lengths for each axis.
6) The FPS will always be set to 30 within this study.

The basic settings of the AirSim camera can be specified in the settings.json file, which should be located at the same directory of the Unreal project executable. By default, it contains one camera, with the "ImageType" set to 0 (to indicate that this is RGB) and the CameraName set to "0". I have specified the resolution $W \times H$ in pixels of the AirSim camera here.

For reasons elaborated in the *Necessity of Resolution Consistency* subsection, I have noticed that the ORB-SLAM3 parameters require that the resolution ratio $W:H$ matches the ratio $W_{sens}:H_{sens}$ of the sensor width and height of the AirSim camera digital film, which can be accessed directly in the API. While the simulator is running in "AirSimGameMode" in Unreal, I can connect to the API with the following commands.

```
client = airsim.VehicleClient()
client.confirmConnection()
```

One the connection has been established, I have called the client.simGetFilmbackSettings("0") method to return the sensor width and height, which is by default $23.76 : 13.365$. I went back to settings.json and modified the resolution to match the sensor ratio (e.g. 512×288 if the ratio is $23.76 : 13.365$). Once the proper resolution $W \times H$ has been set, the central points can be set as simply half the resolution as a float value: $c_x = W/2$ and $c_y = H/2$. The distortion parameters can be found by calling client.getDistortionParams("0"), which in this study was set to all 0's. The focal lengths f_x, f_y are not as straightforward to retrieve since AirSim does not have built in functions that directly provide them, so I calculated them manually. To clarify, the axes focal lengths refer to the f_x, f_y shown below when the 3D diagram in figure 1 is projected in the X and Y axes.

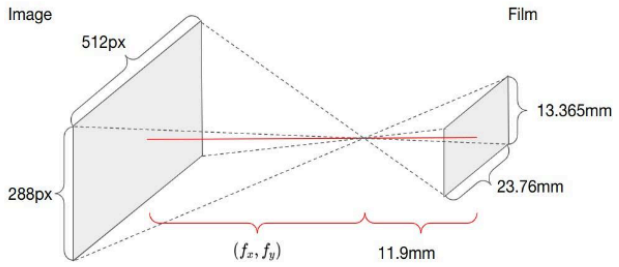

Fig. 1: The diagram representing the projection of the camera image onto the film in the pinhole camera allows us to use geometry to calculate the focal lengths f_x, f_y needed to correctly parameterize ORB-SLAM3.

By calling the client.simGetFocalLength("0") method, I found the focal length to be 11.9cm, and by simple geometry, the axes focal lengths are computed as

$$f_x = \frac{W f}{W_{sens}} = \frac{512 \times 11.9}{23.76} = 256.431px \quad f_y = \frac{H f}{H_{sens}} = \frac{288 \times 11.9}{13.365} = 256.431px$$

While not directly relevant for focal length calculation, I found that simGetCameraInfo could be useful, which returns the pose and the projection matrix of the camera, and simGetLensSettings, which returns additional parameters of the AirSim camera, which may be useful for fine-tuning camera parameterizations.

C. Improving SLAM Stability through Environment Enhancement and Trajectory Smoothing

1) Environment Modification with Feature Addition: Even with the proper unobstructed trajectory and the proper camera parameters, ORB-SLAM3 consistently lost tracking during multiple timestamps, leading to a trajectory error of 87.98cm. This may be due to the lack of features that resulted from the previous environmental expansion. When expanding the room, I did not add any new furniture to it, which subsequently led to large sections of the wall and floor with significantly less

features. It seemed that when ORB-SLAM3 processed frames that turned towards these relatively featureless sections, it lost tracking.

Therefore, I added more features to the environment to reduce the possibility of these sudden feature "dead zones." As seen below in the two diagrams, several pieces of furniture were copied and added, including a new dining table set, the rug underneath, multiple ceiling fans, an extra couch, multiple paintings, and other slight modifications. However, running ORB-SLAM3 within this modified environment led to a marginal improvement from 87.98cm to 80.75cm, which was not significant enough to consider a lack of features to be the issue, especially since there were still several instances of lost tracking.

Fig. 2: After manual feature addition within the environment resulting in the room shown above, ORB-SLAM3 performed marginally better, improving the trajectory error from 87.98cm to 80.75cm.

I hypothesized that the presence of transparent objects such as glass or windows can severely affect the performance of ORB-SLAM3 due to lighting issues like glare. I tested this hypothesis by taking the same trajectory but stopping localization right before the frame turns to look at the windows. Creating this new subtrajectory had required significant cutoff, reducing the number of timesteps from 16,541 to less than 2000, but this led to a great improvement in the error, from 80.75cm to 13.17cm.

However, two pieces of evidence from further testing have shown me that the presence of windows was not the main problem behind lost tracking. First, when I slightly extended the subtrajectory to include the windows for 150 more frames, the error of ORB-SLAM3 still remained at approximately 13cm and did not spike as I had expected. Second, when I initialized the trajectory at a pose that initially included the windows in its frame, there was no considerable effect on the error.

2) Trajectory Jumps and Data Smoothing: Further testing with different initial poses and subtrajectories did not indicate that the main cause of lost tracking was the windows, so I have concluded that it was not at a certain frame that ORB-SLAM3 lost tracking, but it was at a certain *timestamp*. This indicated that the problem might have been the trajectory itself. Upon inspection of the TUM VI Room 1 ground truth data, I noticed that there were several large "jumps" between adjacent poses, where the pose in row R was significantly different

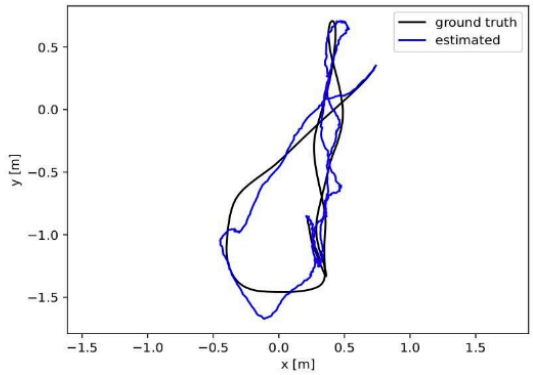

Fig. 3: Upon stopping localization right before the frame turns to look at the first window, the estimated subtrajectory was much closer to the ground truth subtrajectory, reducing the error from 80.75cm to 13.17cm.

from the pose in row $R + 1$. To quantify the magnitude of these differences, I constructed a custom pseudo-metric. To compute the distances between the translational components, I took the Euclidean distance between them. The quaternion component is slightly less straightforward.

Let $P = R^3 \times SO(3)$ be the space of all poses, constructed as the Cartesian product of translations R^3 and rotations $SO(3)$. Let $(H_1, \sim)$ denote the quotient group of unit quaternions representing rotations. It is well known that the natural mapping

$$\rho: H_1 \mapsto SO(3)$$

is 2-to-1. That is, given $q \in H_1$, both q and $-q$ represent the same rotation. Therefore, the distance between q and itself should be 0, but also q and $-q$ should also be 0. In fact, Ravani and Roth recognizes this ambiguity in quaternion representation and constructs the metric for

quaternions q_1 and q_2 as $\{\|q_1 - q_2\|, \|q_1 + q_2\|\}$, where $||\cdot||$ is the Euclidean norm [11]. Therefore, in this study, I will define the *pose metric* of two poses $P_1 = (p_1, q_1), P_2 = (p_2, q_2)$ to be

$$d(P_1, P_2) = \|p_1 - p_2\|_2 + min\{\|q_1 - q_2\|_2, \|q_1 + q_2$$

From graphing the pose metric of each consecutive pair throughout the ground truth trajectory in figure 4, it was evident that there were huge distances between several pairs. While the vast majority of pose metrics remained small (< 0.02), I have observed in several instances that some translational and rotational components vastly exceeded this difference. For example, in rows 11588 and 11589, the difference of just the q_z components was as large as 0.79. In fact, most of the pose metric values came from the difference between quaternion components, rather than the translational ones.

Closer inspection revealed that the time gap between these large pose jumps were also very large, so the ground truth data contained several "time gaps" where the pose was not collected. Some data smoothing was required, but before I

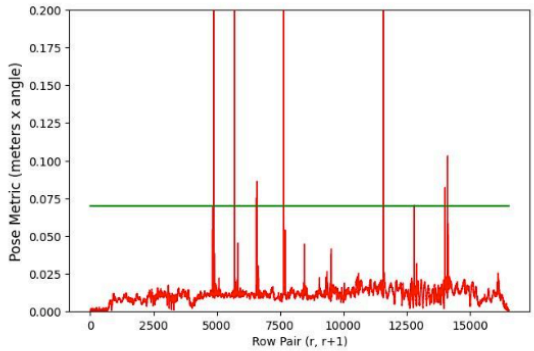

Fig. 4: The graph of the pose metric between adjacent poses in TUM VI Room 1 ground truth trajectory shows several spikes that indicate that there are huge jumps between adjacent frames in our estimated trajectory.

could begin, I also noticed that the ground truth had several instances of where the rotational pose q_r at row r suddenly jumps to $q_{r+1} \approx -q_r$ in the next row. This flip in orientation is not a problem when simulating the trajectory in AirSim since given a rotation quaternion q, both q and $-q$ represent the same rotation in $SO(3)$. This was a problem for data smoothing, so I created a script that parsed through the ground truth file and converted all the quaternions to the correct orientation. Once all quaternions have been oriented, the data smoothing was done in 3 steps:

1) *smooth.py*: I ran a simple moving average of 10 rows (SMA-10) on only the quaternion components of the oriented data, to ensure that the differences in each component of q_r and q_{r+1} was < 0.07, which was a threshold that I've empirically determined to be an acceptable pose metric that did not cause ORB-SLAM3 to lose tracking. This smoothed out most of the data.
2) The greatest pose metric after smoothing had remained at a value of ~ 0.5 and increasing the timesteps of the moving average further may have distorted the rotational data too much, so I cut off the trajectory right before this massive jump.
3) I manually smoothed out any other remaining spikes by inserting rows in between them and linearly interpolating until all pose metrics met the < 0.07 threshold.

D. Resolution and Feature Threshold Adjustment

The two main factors of performance of ORB-SLAM3 are the resolutions of the input images, which dictate how much data is being fed into the algorithm, and the number of features that ORB-SLAM3 is allowed to detect. There is another parameter in the settings yaml file, nFeatures, that sets the maximum number of feature points M that ORB-SLAM3 would detect in a given frame. If L feature points are detected in a frame, then $\{M, L\}$ features would be extracted for visual odometry.

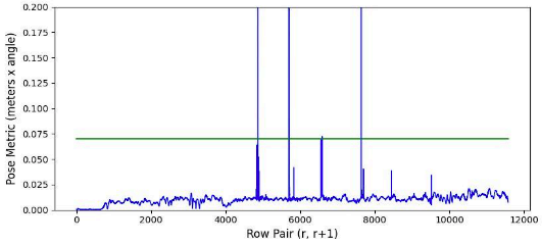

(a) Pose metric between adjacent poses in TUM VI Room 1 groundtruth trajectory after SMA-10 smoothing and cutoff.

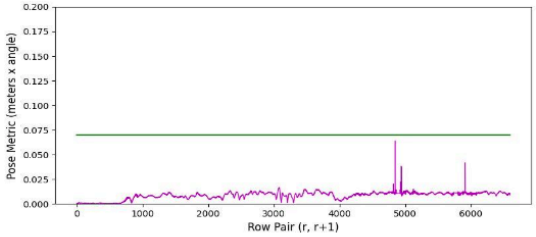

(b) Pose metric between adjacent poses in TUM VI Room 1 groundtruth trajectory after linear interpolation and cutoff.

Fig. 5: After performing both smoothings and cutoffs, there were no more instances of ORB-SLAM3 losing tracking.

Therefore, I have performance tested ORB-SLAM3 with the following datasets and parameters:

1) I work with two different resolutions: 256 × 144 and 512 × 288 pixels.
2) For each resolution, I set the feature threshold to 750, 1500, 3000, 6000, and 12000 points.
3) Due to the stochastic nature of ORB-SLAM3, I run ORB-SLAM3 three times for each resolution and for each feature threshold.

1) Error Evaluation: I computed the error using the *evaluate_ate_scale.py* module, which computes the absolute trajectory error of the estimated trajectory. It first reads in the ground truth trajectory $\{P_k\}_{k=1}^{N} = \{(p_k, q_k)\}_{k=1}^{N}$ and estimated trajectories $\{P_k'\}_{k=1}^{N} = \{(p_k', q_k')\}_{k=1}^{N}$ as two lists of 7D poses, each pose consisting of a timestamp, 3D translation, and 4D quaternion representing the rotation. Then, it aligns the estimated trajectory to the ground truth trajectory using Horn's method, which computes a rotation matrix and a scale factor that best aligns the two trajectories, which I will denote $\{P_k^*\}$ for the ground truth and $\{P_k^{*'}\}$ for the estimated. After alignment, it computes the translational error between the two trajectories by finding the Euclidean distance between the corresponding translation components of each pose. The script then reports the Root Mean Squared Error (RMSE) of the translational error over all poses as the absolute trajectory error.

$$Error = \sqrt{\frac{1}{N}\sum_{k=1}^{N}\left\|p_k^* - p_k^{*'}\right\|^2}$$

In figure 6, we can observe Horn's method aligning the ground truth trajectory within the TUM VI Room 1 environment and ORB-SLAM3's estimated trajectory within the ArchViz Interior environment by seeing that the translational components roughly align if we perform the coordinate conversion $p_x \mapsto p_z$, $p_y \mapsto p_x$, $p_z \mapsto p_y$ which is represented by the rotation matrix

$$\begin{pmatrix} 0 & 1 & 0 \\ 0 & 0 & 1 \\ 1 & 0 & 0 \end{pmatrix}$$

Similarly in figure 7, for the rotational components, we expect Horn's method to align the basis elements of the quaternions with the coordinate conversion $q_w \mapsto q_z$, $q_x \mapsto q_y$, $q_y \mapsto q_w$, $q_z \mapsto q_x$, represented by the rotation matrix

$$\begin{pmatrix} 0 & 0 & 1 & 0 \\ 0 & 0 & 0 & 1 \\ 0 & 1 & 0 & 0 \\ 1 & 0 & 0 & 0 \end{pmatrix}$$

2) Robustness in Dynamic Environments: I further tested the robustness of ORB-SLAM3 by repeating the experiment within a dynamic environment containing moving objects. After identifying a range optimal feature thresholds within the static environment, I analyzed the change in tracking performance of ORB-SLAM3 for both the 256×144 and 512×288 resolutions. The moving objects consisted of three ceiling fans, rotating at fast speed (~1 rotation per 6 frames), and a decorative hanger, rotating relatively slowly (~1 rotation per 45 frames). While this may not seem like a significant difference, the directional lights coming in from the windows had cast large moving shadows as well.

E. Performance Testing in Real-Life Environments

Furthermore, I have tested ORB-SLAM3 within two real world environments in Duke University:

1) the Wilkinson 4th floor graduate lounge, which consisted of glass walls, with multiple tables, chairs, a fridge, a sink, under bright lighting.
2) the Kilgo Quad N common room, consisting of various couches, tables, chairs, a TV, a foosball table, and framed walls.

Both environments represent typical indoor locations with consistent lighting. The main difference between the two is that the graduate lounge consists of glass walls, while the common room has few windows and transparent objects. I believed that having at least a qualitative analysis of how the performance of ORB-SLAM3 is affected by the presence of transparent windows and walls would prove useful in developing assumptions in future works. While the ground truth data was not available, I have qualitatively observed the general accuracy of ORB-SLAM3 by manually comparing the trajectories

taken in the video with the ego-motion computed by the localization module.

An iPhone Xr camera, which has comparable technical specifications with most commercial phones in the United States, was chosen as the performance benchmark. The default resolution for an iPhone Xr camera is 1920 × 1080px, but I compressed and cropped the image frames to be 960×720px for easier processing of the data in real-time. The camera type was also sent to pinhole, the central point was set as (480,360), and the distortion parameters were all set to 0. To compute the axes focal lengths (f_x, f_y), I collected measurements on the focal length and the film dimensions online.

Fig. 8: Corner view of Wilkinson 4th floor graduate lounge.

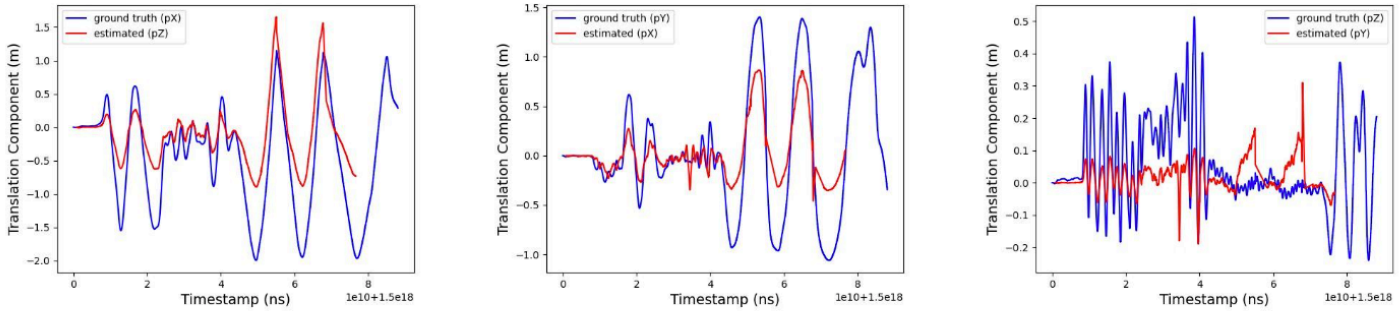

Fig. 6: Rough estimate of how Horn's method would align the translational components of the ground truth and estimated trajectories with a rotational factor.

(a) Ground truth pX aligned with estimated pZ trajectory
(b) Ground truth pY aligned with estimated pX trajectory
(c) Ground truth pZ aligned with estimated pY trajectory

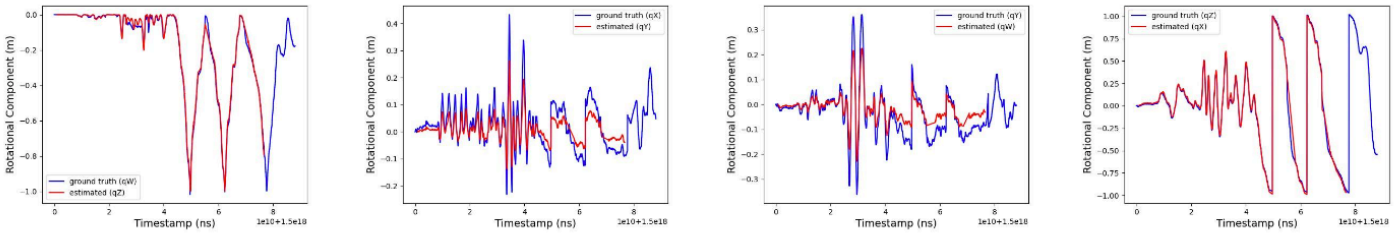

Fig. 7: Rough estimate of how Horn's method would align the rotational components of the ground truth and estimated trajectories with a rotational factor.

(a) Ground truth qW aligned with estimated qZ trajectory
(b) Ground truth qX aligned with estimated qY trajectory
(c) Ground truth qY aligned with estimated qW trajectory
(d) Ground truth qZ aligned with estimated qX trajectory

1) The sensor number is known to be 1/2.55″, which corresponds to a film dimension of 5.33 × 4mm
2) The focal length is 2.45mm (26mm equivalent for digital camera lens)

The axes focal lengths were calculated to be

$$f_x = \frac{960 \times 4.25}{5.33} = 765.478px,\ f_y = \frac{720 \times 4.25}{4} = 765.0px$$

Fig. 9: Corner view of Kilgo N common room.

Once the video was taken, each frame was saved as an image using OpenCV and labeled with the appropriate timestamp as specified previously before inputting the data into ORBSLAM3.

IV. RESULTS

I have collected the AirSim dataset of images and ground truth labels in Unreal Engine 4.27, run on a Dell XPS 9570 with 16GB RAM and 16 CPU cores. I have then ran ORB-SLAM3 on an Ubuntu 20.04 operating system, with 8GB RAM and 8 CPU cores. Within both the static and dynamic environments, the performance of ORB-SLAM3 with 512 × 288 resolution images had significantly outperformed that of 256 × 144 resolution images. Furthermore, ORB-SLAM3 with the higher resolution inputs had been much more robust in dynamic environments, with no noticeable loss in accuracy, while the accuracy had significantly dropped with lower resolution inputs.

A. Impacts of Resolution and Threshold in Static Environment

In the static environment, I observed that the absolute trajectory error was smaller by a factor of 5~12 when utilizing higher resolution inputs compared to lower resolution ones under all threshold levels. Although this may seem obvious, as higher image resolution intuitively leads to improved tracking, it is important to consider the role of feature points in visual odometry for localization. In this case, both the 256 × 144 and 512 × 288 resolution images had their feature threshold limited at the same level, which indicates that ORB-SLAM3 is extracting the same number of features per frame, particularly for lower thresholds.

TABLE I: Absolute trajectory error of estimated trajectory in stationary environment (cm)

		Feature Threshold				
		750	1500	3000	6000	12000
Res.	256×144	65.825 96.676 97.385	64.089 86.998 96.858	42.787 78.844 66.803	31.556 68.121 64.351	77.704 40.119 100.312
	512×288	12.735 6.000 9.963	10.025 9.963 9.384	9.431 9.315 11.959	8.246 6.657 6.652	5.815 4.942 7.763

I have slightly modified ORB-SLAM3 to have it output the number of features detected in each frame, and it was evident that for the runs with the lower thresholds (750 and 1500), the number of features extracted from each frame remained consistently at the maximum threshold for both the higher and lower resolution inputs. This suggests that the "quality" of the features is a critical factor, as demonstrated by the 750 or 1500 threshold runs, where the quality of the 1500 features detected in the 512×288 images was significantly better than that of the 1500 features detected in the 256×144 images

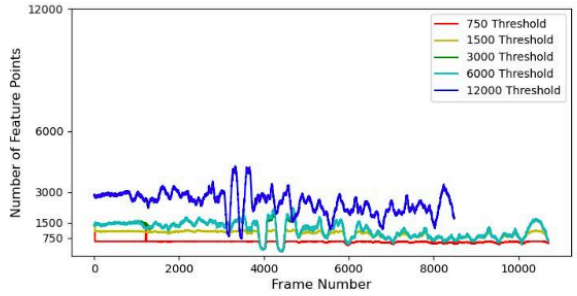

Fig. 10: Number of features detected per frame in ORBSLAM3 with images of resolution 256 × 144 in static environment. For the thresholds of 750 and 1500, ORB-SLAM3 consistently detects the maximum number of feature points throughout the entire trajectory.

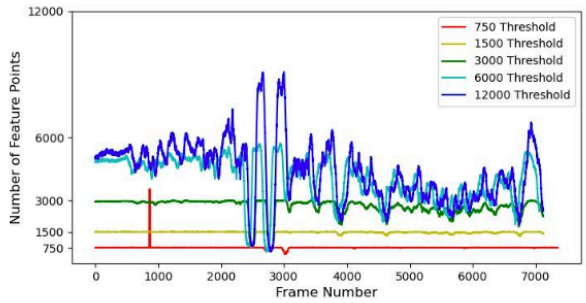

Fig. 11: Number of features detected per frame in ORBSLAM3 with images of resolution 512 × 288 in static environment. For the thresholds of 750 and 1500, ORB-SLAM3 consistently detects the maximum number of feature points throughout the entire trajectory. For higher thresholds, ORBSLAM3 detects significantly more feature points on the 512× 288 images than on the 256 × 144 images.

A visual graph in figure 12 is shown below to better compare the performance between the two resolutions, where the mean errors of each three runs are plotted, along with their sample standard deviation in the error bars. The graph shows that ORB-SLAM3 not only has significantly less error with higher resolution inputs, but the trajectory error remains very consistent throughout multiple runs. On the lower resolution inputs, however, ORB-SLAM3 was quite unstable in localization, generating significantly different trajectories per run, leading to a high standard deviation in the sample data.

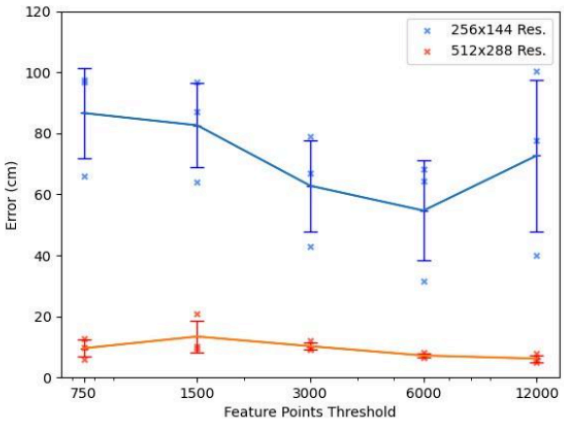

Fig. 12: Effects of resolution on ORB-SLAM3 performance under varying feature thresholds in static environment. These results indicate that the feature points detected by ORB-SLAM3 are of higher quality (for lower thresholds) and more numerous (for higher thresholds), both of which contribute to higher performance.

ORB-SLAM3 with extremely high feature points was able to construct a perceivable point-cloud map of the room. In figure 13, certain objects, like the walls, the lights, the table, and the rug, are discernible, though they are easier to identify directly in the interactive software outputting the point-cloud map.

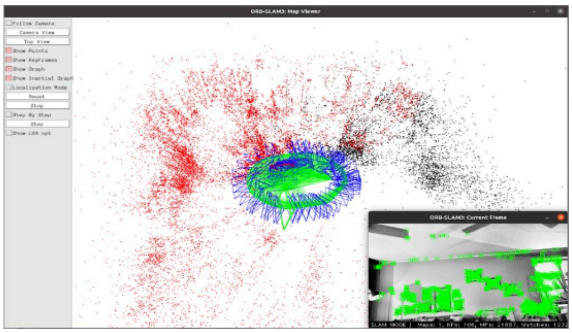

Fig. 13: Distinguishable objects are visible in the point-cloud map generated by ORB-SLAM3 with 512 × 288 resolution inputs and threshold of 12000 feature points.

B. Impacts of Resolution and Threshold in Dynamic Environment

The optimal performance of both resolutions seemed to lie within the 3000, 6000, and 12000 feature thresholds, and so under this range, I ran ORB-SLAM3 again within the dynamic environment. The results show that ORB-SLAM3 is significantly more robust to moving entities with the higher resolution images.

TABLE II: Absolute trajectory error of estimated trajectory in dynamic environment (cm)

		Feature Threshold		
		3000	6000	12000
Res.	256 × 144	104.524 87.443 58.399	63.135 60.367 101.922	99.287 104.449 99.836
	512 × 288	7.987 8.731 13.314	7.849 7.212 9.014	4.812 6.778 5.082

Since I was working with higher feature thresholds in the dynamic environment, there was a significant difference in the number of feature points detected between the 256×144 and 512 × 288 resolution images. Even though the figures below indicate that even at the 3000 threshold level, ORB-SLAM3 is detecting many more features in the 512 × 288 images, the difference in its performance is most likely due to the difference in quality of the feature points.

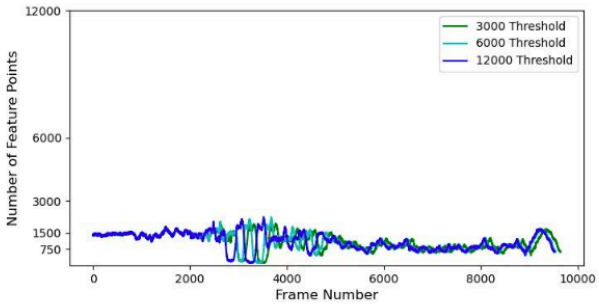

Fig. 14: Number of features detected per frame in ORBSLAM3 with images of resolution 256 × 144 in dynamic environment.

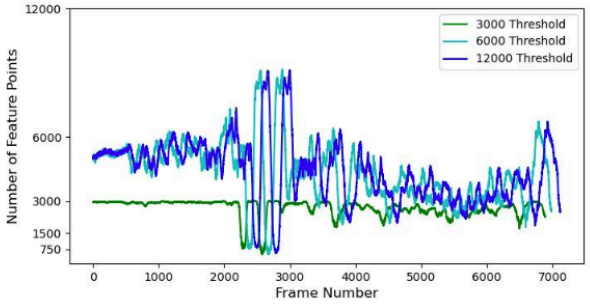

Fig. 15: Number of features detected per frame in ORBSLAM3 with images of resolution 512 × 288 in dynamic environment. For these higher thresholds, ORB-SLAM3 detects significantly more feature points on the 512×288 images than on the 288 × 144 images.

By superimposing the trajectory errors within the dynamic environment onto the those computed within the static, figure 16 shows that the performance of ORB-SLAM3 is barely affected when inputting 512 × 288 resolution images, while the absolute trajectory error increases by about 20 ~ 30cm with 256 × 144 resolution inputs.

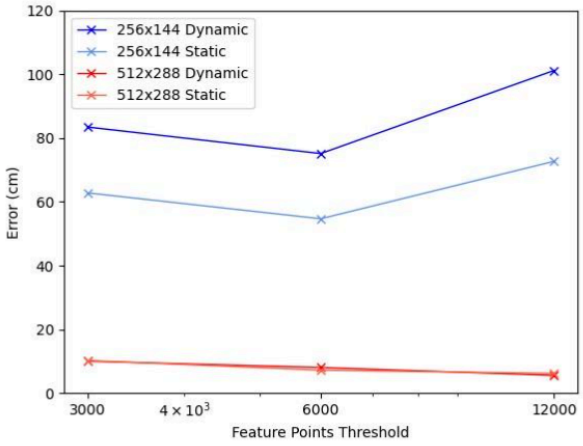

Fig. 16: Effects of resolution on ORB-SLAM3 performance under varying feature thresholds in both static and dynamic environments. This figure indicates that ORB-SLAM3 is much more robust in dynamic environments with 512×288 resolution inputs than with 256 × 144 resolution inputs.

I have organized the error difference below. Even though the presence of negative values indicates that there is a marginal improvement in tracking in the dynamic environment, this is most likely due to the stochasticity of ORB-SLAM3, and with subsequent runs, the average difference in the absolute trajectory error will converge to a positive value.

C. Necessity of Resolution Consistency

I want to emphasize a certain restriction on the resolution of the input images when working with AirSim and ORBSLAM3. It is extremely important that the resolution of the image and the resolution of the film have the same width-to-height ratio.

TABLE III: Increase in absolute trajectory error upon shift from static to dynamic environment (cm)

		Feature Threshold		
		3000	6000	12000
Res.	256×144	20.64	20.46	28.48
	512×288	-0.22	0.84	-0.62

During the experiment, I had initially worked with 256 × 256 and 512 × 512 resolution images. The respective focal lengths were computed to be $(f_x, f_y) = (128, 215, 227.939)$ for 256 × 256 and $(f_x, f_y) = (256.431, 455.877)$ for 512 × 512. However, running ORB-SLAM3 with these parameters had resulted in the 256 × 256 resolution inputs consistently outperforming the 512 × 512 resolution inputs.

TABLE IV: Absolute trajectory error of estimated trajectory in stationary environment with 1:1 ratio resolution (cm)

		Feature Threshold				
		750	1500	3000	6000	12000
Res.	256 × 256	22.702 25.030 20.705	36.570 31.278 30.555	26.764 33.358 27.503	20.625 21.965 25.265	23.856 23.846 22.253
	512 × 512	83.934 50.444 52.048	56.951 39.745 79.724	35.948 33.029 30.383	31.921 26.522 38.893	26.400 30.590 77.566

This was a very counter-intuitive result, as I would have expected that having more information of an image through higher resolutions would result in better tracking overall. I had hypothesized that 512 × 512 is too fine of a resolution, containing extremely large amounts of data that led ORB-SLAM3 to overfit the features in some way, but this contradicted the results of multiple other studies in the literature, where researchers would work with resolutions that went as high as 1920 × 1080 in very complex environments and still generated very accurate localization [12]. Even the TUM VI dataset consisted of images with a relatively high resolution of 1024 × 1024 pixels, and ORB-SLAM3 had still produced a consistently small ~ 7cm error.

I noticed that the parameters for ORB-SLAM3 tuned for the TUM VI Room 1 dataset had set the axes focal lengths to be approximately equal: $f_x \approx f_y$. I attempted to mimic this setting by modifying the resolution of my input images. If I keep the dimensions of the resolution $W:H$

the same as the dimensions of the film W_{sens}: H_{sens}, then the resulting calculations would lead to $f_x = f_y$. Since the sensor had a 16:9 ratio, I had modified my input resolutions to 256 × 144 and 512 × 288, which led to the axes focal lengths to be (128.215, 128.215) and (256.431, 256.431), respectively. This led to an error improvement up to a factor of 10 for the majority of simulations taking with the higher resolution cameras.

While I haven't found out exactly the reason why the image resolution must have the same dimensions as the film, this may simply be an intrinsic property of ORB-SLAM3. Regardless, this observation in its own right is very useful for future studies.

TABLE V: ORB-SLAM3 performance comparison between
1:1 ratio resolution and 16:9 ratio resolutions in static environment, averaged over 3 runs (cm)

		Feature Threshold				
		750	1500	3000	6000	12000
Res.	256 × 256	22.813	32.801	29.208	22.618	23.318
	256 × 144	86.629	82.648	62.811	54,676	72.712
	512 × 512	62.142	58.807	33.120	32.225	44.852
	512 × 288	9.566	9.791	10.235	7.185	6.173

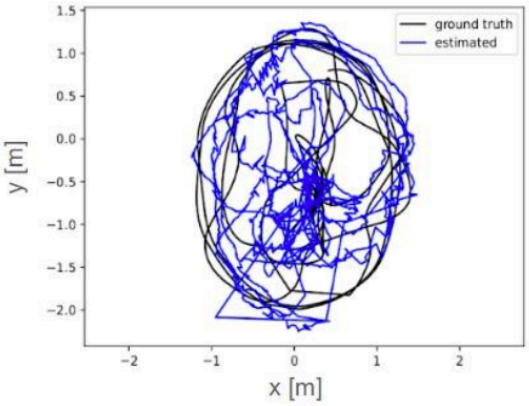

(a) Trajectories of 512 × 512 image frames with 1500 feature threshold.

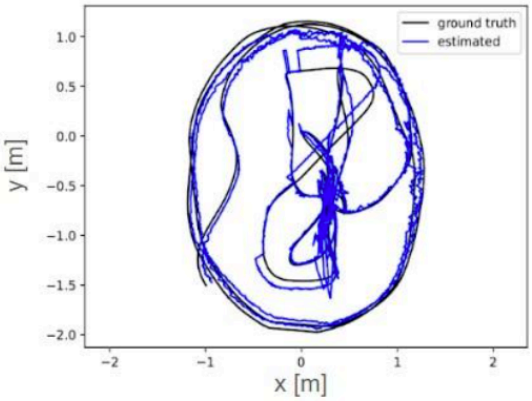

(b) Trajectories of 512 × 288 image frames with 1500 feature threshold.

Fig. 17: Upon modifying the resolutions to match the film dimensions, the ORB-SLAM3's tracking performance had greatly improved, from an error of 58.8cm to 9.8cm.

D. SLAM with iPhone Xr Camera in Physical Indoor Environment

Qualitatively, the localization of ORB-SLAM3 in a real-world environment appears to correspond reasonably well with the actual trajectory, as observed by comparing the video and localization module side-by-side. Moreover, the system generates a relatively dense point-cloud map of the environment, allowing for the identification of distinct features such as wall nooks.

Nonetheless, in both the graduate lounge and the common room, the localization exhibited considerable instability which was characterized by multiple instances of lost tracking. I attributed this phenomenon to two primary factors:

1) The substantial exposure to windows and transparent objects in the graduate lounge may have caused ORB-SLAM3 to lose tracking due to the glare and reflections of both the individual operating the system and the objects within the room.
2) The videos captured by the iPhone Xr displayed significant motion blur, even during relatively slow changes in pose. This factor could have potentially impeded ORB-SLAM3's capacity to detect features within each frame, consequently resulting in abrupt declines in performance.

V. FUTURE WORKS

This research has provided valuable insights and a foundation for further exploration and development in the

domain of visual SLAM. Based on our findings, I have identified three key areas for future works:

A. Visual-Inertial SLAM Integration

Expanding the scope of this research to include visual-inertial SLAM is essential, as the majority of real-world SLAM applications incorporate inertial data using gyroscopes. Integrating inertial measurement units (IMUs) with the visual ORB-SLAM3 framework could significantly improve the system's accuracy and robustness under various conditions. This integration would involve fusing IMU data with visual information, allowing for enhanced tracking and mapping in situations where visual data alone may not suffice, such as in low-light environments or during rapid motion. Furthermore, exploring various sensor fusion techniques and optimization methods could lead to even more accurate and reliable visual-inertial SLAM systems.

B. Diverse and Challenging Datasets

Creating diverse and challenging datasets is crucial for advancing the evaluation and development of SLAM algorithms, and many efforts have been made to add to the diversity of public datasets. The *RobotCar* dataset, collected through a consistent route in Oxford, UK, over the span of a year, contains large scale data in changing light and weather conditions for self-driving tasks [19]. Other researchers have taken advantage of emulators to efficiently navigate virtual environments to create diverse datasets such as TartanAir [8] and DISCOMAN [20]. Following this approach, by using emulators to generate complex datasets under different environments, weather conditions, and challenging trajectories, I can provide researchers with a wide range of test scenarios and foster the development of versatile SLAM systems. This endeavor could involve creating indoor and outdoor scenes, simulating varying lighting conditions, and incorporating challenging elements such as occlusions, dynamic objects, and complex motions. Ultimately, these comprehensive datasets would help assess the performance and robustness of SLAM algorithms under a broad array of real-world conditions.

C. Streamlining Camera Calibration Process

Streamlining the camera calibration process is a critical aspect of making SLAM systems more usable and accessible, since it may not be always the case that researchers have access to the relevant camera specifications. Certain calibration modules included in the OpenCV library allow one to extract an estimate of the camera intrinsic and extrinsic matrices, along with distortion parameters [21], but the integration of this process into SLAM and AirSim is still poor.

By using SLAM to initially approximate camera parameters, I believe that it is possible to develop a hierarchical model that adaptively tunes the hyperparameters of SLAM based on the range of parameters in which it performs optimally (i.e., exhibits the least trajectory error). This approach not only eases the calibration process but also allows for continuous adaptation and improvement of SLAM performance as the environment or operating conditions change. By refining this hierarchical model and exploring novel techniques for adaptive hyperparameter tuning, I cande enhance the accuracy and adaptability of SLAM systems, making them more suitable for a wide range of applications. This improvement in the calibration process could significantly enhance the usability and accessibility of SLAM systems for various researchers and developers.

VI. CONCLUSION

This study utilized the AirSim emulator to generate a challenging trajectory within the ArchViz Interior environment built within Unreal. Various modifications such as environment expansion and trajectory smoothing, paired with a careful calculation of the camera parameters, were applied to ensure stability of ORB-SLAM3's tracking module.

The results demonstrate that employing higher resolution images (256 × 144 and 512 × 288) at 30FPS significantly improves tracking performance in visual SLAM, specifically ORB-SLAM3. It also highlights the importance of environment selection, trajectory stability, and camera parameter tuning for maintaining consistent localization, allowing for a comprehensive evaluation of the visual ORB-SLAM3 performance. My results indicate that the optimal feature threshold is found to be between 3000 ~ 12000 feature points per frame, and ORB-SLAM3 shows enhanced robustness in dynamic environments with moving objects when using higher resolution inputs. These findings provide valuable insights and a streamlined workflow for virtual dataset generation, which can be used in the future development of not only visual SLAM systems, but for general computer vision algorithms.

Furthermore, qualitative testing in real-world indoor environments highlighted challenges faced by ORB-SLAM3, such as glare and motion blur, which offers

direction for future improvements in the SLAM system. Overall, the study's findings contribute to the growing body of knowledge in the field of visual SLAM and can potentially enhance the development and application of SLAM systems in computer vision.

ACKNOWLEDGMENTS

I would like to thank Ying Chen for her mentorship and Professor Maria Gorlatova for overseeing this Spring 2023 research independent study.

REFERENCES

1. X. Gao and T. Zhang, "Introduction to Visual SLAM From Theory to Practice," 2021.

2. A. Geiger, P. Lenz, C. Stiller, and R. Urtasun, "Vision Meets Robotics: The KITTI Dataset," in *IEEE Conference on Computer Vision and Pattern Recognition (CVPR)*, 2013, vol. 32, no. 11, pp. 1231-1237.

3. D. Schubert, T. Goll, N. Demmel, V. Usenko, J. Stuckler, and D. Cremers, "The TUM VI Benchmark for Evaluating Visual-Inertial Odometry," in *2018 IEEE International Conference on Robotics and Automation (ICRA)*, 2018, pp. 1696-1701.

4. S. Shah, D. Dey, C. Lovett, A. Kapoor, "AirSim: High-Fidelity Visual and Physical Simulation for Autonomous Vehicles," in *Proceedings of the 1st Annual Conference on Robot Learning*, 2017, vol. 78, pp. 1-16.

5. D. Detone, T. Malisiewicz, and A. Roabinovich, "SuperPoint: SelfSupervised Interest Point Detection and Description," in *IEEE Conference on Computer Vision and Pattern Recognition (CVPR)*, 2018, pp. 71227131.

6. P. H. Christiansen, M. F. Kragh, Y. Brodskiy, and H. Karstoft, "UnsuperPoint: End-to-end Unsupervised Interest Point Detector and Descriptor," in *European Conference on Computer Vision (ECCV)*, 2018, pp. 118-133.

7. J. Tang, H. Kim, V. Guizilini, S. Pillai, R. Ambrus, "Neural Outlier Rejection for Self-Supervised Keypoint Learning," in *Computing Research Repository (CoRR)*, 2019, vol. 43, no. 3, pp. 834-847.

8. W. Wang, D. Zhu, X. Wang, Y. Hu, W. Qiu, C. Wang, Y. Hu, A. Kapoor, S. Scherer, "TartanAir: A Dataset to Push the Limits of Visual SLAM" in *IEEE Robotics and Automation Letters*, 2020, vol. 5, no. 4, pp. 66736680.

9. J. Xu, H. Cao, D. Li, K. Huang, C. Quian, L. Shangguan, and Z. Yang, "Edge Assisted Mobile Semantic Visual SLAM," in *IEEE INFOCOM 2020 - IEEE Conference on Computer Communications*, 2020, pp. 18281837.

10. A. J. B. Ali, Z. S. Hashemifar, and K. Dantu, "Edge-SLAM: EdgeAssisted Visual Simultaneous Localization and Mapping," in *ACM Transactions on Embedded Computing Systems*, 2020, vol. 22, no. 1, pp. 1-31.

11. B. Ravani, B. Roth, "Motion Synthesis Using Kinematic Mappings," in *Journal of Mechanisms, Transmissions, and Automation in Design*, 1983, vol 105, no. 3, pp. 460-467.

12. C. Campos, R. Elvira, J. J. G. Rodriguez, J. M. M. Montiel, J. D. Tardos, "ORB-SLAM3: An Accurate Open-Source Library for Visual, VisualInertial and Multi-Map SLAM," in *IEEE Transactions on Robotics*, 2020, vol. 37, no. 6, pp. 1874-1890.

13. M. Burri, J. Nikolic, P. Gohl, T. Schneider, J. Rehder, S. Omari, M. Achtelik, and R. Siegwart, "The EuRoC micro aerial vehicle datasets" in *The International Journal of Robotics Research*, 2016, vol. 35, no. 10, pp. 1157-1163.

14. J. Li, B. Yang, D. Chen, N. Wang, G. Zhang, and H. Bao, "Survey and Evaluation of Monocular Visual-Inertial SLAM Algorithms for Augmented Reality" in *Journal of Virtual Reality & Intelligent Hardware*, 2019, pp. 386-410.

15. Epic Games, "Unreal Engine," Epic Games, March 2015, Available: *www.unrealengine.com*

16. R. Mur-Artal, J. M. M. Montiel, and J. D. Tardos, "Orb-slam: a versatile and accurate monocular slam system," in *IEEE Transactions on Robotics*, 2015, vol. 31, no. 5, pp. 1147–1163.

17. H. Qiu, F. Ahmad, F. Bai, M. Gruteser, and R. Govindan, "Avr: Augmented vehicular reality," in *MobiSys '18: Proceedings of the 16th Annual International Conference on Mobile Systems, Applications, and Services*, 2018, pp. 81-95.

18. T. Pire, T. Fischer, G. Castro, P. D. Cristoforis, J. Civera, and J. J.´ Berlles, "S-ptam: Stereo parallel

tracking and mapping," in *Robotics and Autonomous Systems*, 2017, vol. 93, pp. 27-42.

19. W. Maddern, G. Pascoe, C. Linegar, and P. Newman, "1 Year, 1000km: The Oxford RobotCar Dataset," in *The International Journal of Robotics Research (IJRR)*, 2017, vol. 36, no. 1, pp. 3–15.

20. P. Kirsanov, A. Gaskarov, F. Konokhov, K. Sofiiuk, A. Vorontsova, I. Slinko, D. Zhukov, S. Bykov, O. Barinova, and A. Konushin, "Discoman:

21. Dataset of indoor scenes for odometry, mapping and navigation," in *International Conference on Intelligent Robots and Systems (IROS)*, 2019, pp. 2470-2477.

22. Y. M. Wang, Y. Li and J. B. Zheng, "A camera calibration technique based on OpenCV," in *The 3rd International Conference on Information Sciences and Interaction Sciences*, 2010, pp. 403-406.

An Examination of Two Competing Interpretations of Quantum Mechanics with a Critique of the Kochen-Specker Theorem

Eliza Miller

Volume 2, Issue 2

Article Synopsis

The Kochen-Specker Theorem is a mathematical statement that is widely accepted as proof that deterministic interpretations of quantum mechanics must fail. By analyzing the definitions and logic underpinning Kochen and Specker's results, Miller finds that the axioms of the theorem are not applicable to quantum systems and thus that its results are inconsequential. This reintroduces the possibility of determinism, resolves what is often thought of as an inconsistency between quantum mechanics and classical physics, and highlights the need to better define several terms salient to effective physics discussion and communication.

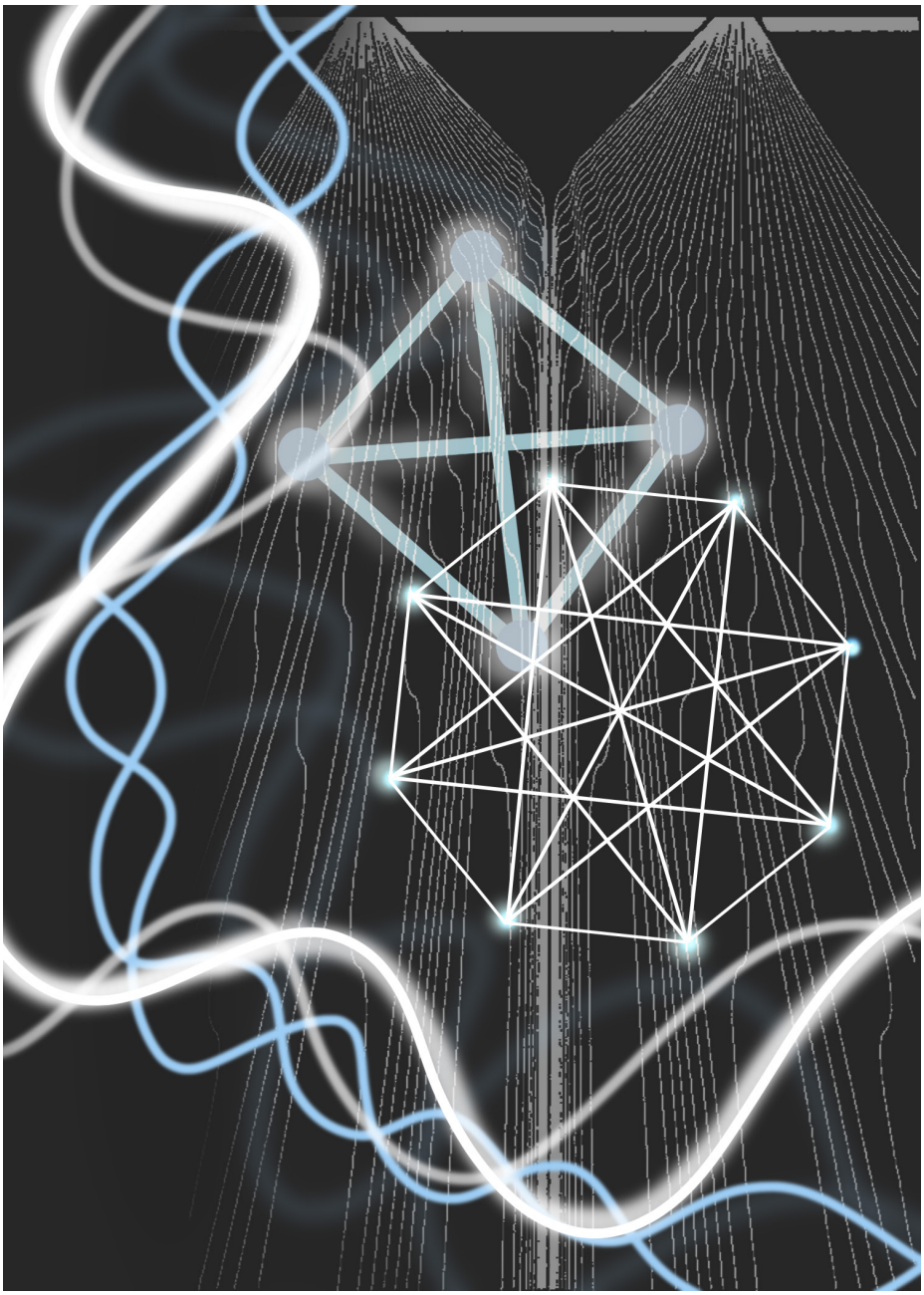

Graphic by Amanda Li

An Examination of Two Competing Interpretations of Quantum Mechanics with a Critique of the Kochen-Specker Theorem

Eliza Miller

Trinity College of Arts and Sciences, Duke University
https://doi.org/10.55894/dv2.23

ABSTRACT

There is ongoing discourse in philosophical and physics literature about whether the probabilistic essence of quantum mechanics indicates that deterministic interpretations of nature must be false. In 1967 two mathematicians, Simon Kochen and Ernst Specker, developed a mathematical theorem to the effect that particles do not have well-defined property values at a given time. A logical consequence of this is that there can be no well-defined hidden variables responsible for the outcomes of mysterious quantum behaviors. The theorem is thus fatal to the many deterministic interpretations of quantum mechanics that assume hidden variables, including pilot wave mechanics, a quantum theory developed by Louis de Broglie and David Bohm a few decades prior to the formulation of the Kochen-Specker Theorem. The purpose of this essay is to evaluate the legitimacy of the logical basis of Kochen's and Specker's argument considering its severe implications. It is concluded that Kochen and Specker do not provide sufficient evidence that deterministic theories must fail, due to their misinterpretation of the axioms on which hidden variable theories rely. This paper also finds that pilot wave mechanics is mathematically successful while remaining consistent with the deterministic understanding of broader physics and deserving of more serious consideration as a quantum theory. Above all it is emphasized that the nonsensicality of absolute randomness and indeterminism should be acknowledged, and theorems purporting to prove their existence should be critically examined, for such a discovery would undermine the legitimacy of logic itself.

Keywords: quantum mechanics, determinism, observables, hidden variables, pilot wave mechanics, Kochen-Specker Theorem

Introduction

Nearly a century after the invention of quantum mechanics (QM), even experts on the subject disagree about what it indicates about the fundamental nature of reality. QM, pioneered in 1925 by Austrian and German physicists Erwin Schrödinger and Werner Heisenberg, describes the behavior of particles by associating them with matter waves called wave functions, denoted by $|\Psi\rangle$. It is widely accepted that the square of the absolute value of some wave function ($|\Psi|^2$) integrated over a finite interval represents the probability of finding the function's associated particle on that interval at a given time, as first suggested by Max Born in 1925. However, even Schrödinger, the inventor of QM's signature wave equation, could not fully comprehend what he had created and famously misinterpreted the wave function multiplied by its complex conjugate ($|\Psi^*\Psi\rangle$) as electric charge density (Serway et al, 2005).

In the present day, many similar issues persist, with leading physicists, mathematicians, and philosophers tending to agree on the mathematical results of quantum calculations while disagreeing on how to interpret those outcomes (Schlosshauer et al., 2013).

QM has the peculiar characteristic that its equations define only probabilistic restrictions on the states of measured physical systems. One conclusion that can be drawn from this is that these states are incomplete descriptions of quantum systems, and there are certain unknown variables unaccounted for by wave functions. In these "hidden variables" (HV) theories, quantum-mechanical uncertainties are interpreted as epistemic probabilities of the sort that arise in ordinary statistical mechanics, such that QM could be supplemented with additional equations that would allow it to predict all observable information about a QM system. Such an HV description might not be practical given the impossibility of one perceiving the alleged variables, but its theoretical possibility is still meaningful to debates about determinism, decisions about which quantum theories to use, and questions about the fundamental nature of reality. However, there exist several theorems according to which any such HV theory must fail.

The following sections describe two competing interpretations of the incompleteness of QM as a predictive theory. The first section is an outline of a popular experiment that demonstrates the mystery of quantum-mechanical behaviors in the context of QM as it is currently understood. The second elaborates on one of the theorems that allegedly disproves the possibility of any HV theories sufficiently supplementing QM: the Kochen-Specker Theorem. Next, there is an overview of the HV interpretation of QM called pilot wave mechanics. Lastly, there is a discussion of whether this interpretation avoids the attacks of Kochen and Specker, including a consideration of the consequences of its doing so or not for HV theories and QM in general.

The Mystery

The root mystery of quantum mechanics is well-demonstrated by the famous "double-slit" experiment. Thomas Young originally conducted this experiment in 1801 with photons, but many variations of the experiment have since been carried out with electrons (Davisson and Germer), single electrons (Jonsson, 1961), and additional particle-detection methods (Thomson, 1927). In the version of the double-slit experiment involving electrons, particles are made to travel through two slits in a barrier toward a photographic screen (Figure 1).

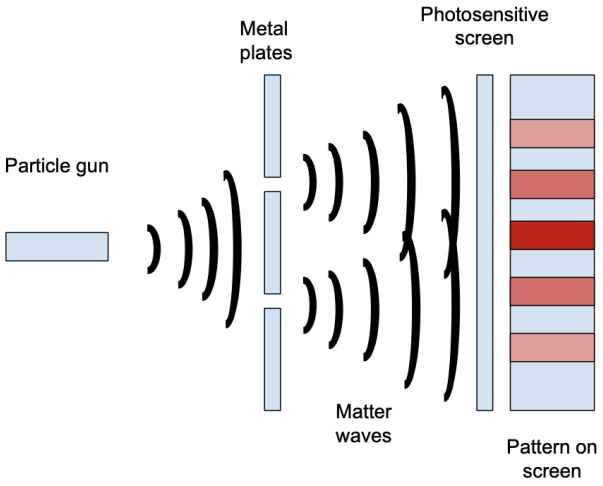

Figure 1: "Double slit" experiment. Darker coloring indicates a higher concentration of particle-detection-indicating light spots. The waves depicted are a metaphorical illustration of the abstract statistical properties of particles in spatial contexts, which give rise to the real striped interference pattern on the screen.

Specks of light appear as particles make contact with the screen, indicating their positions at the time the screen is reached. It has been empirically confirmed that a striped interference pattern—characteristic of wave behavior and, in this context, undefined electron positions—is observed whether many electrons are sent through the slits at once and allowed to interact with each other, or they are sent individually. Strangely, this indicates that the electron "particles" go through *both* slits, with some spread of position defined probabilistically by their wave equations, and subsequently interfere with themselves. Stranger still, if a camera is made to detect whether the individual electrons go through one of the slits, the result is positive about 50 percent

of the time, as is classically expected, but under these conditions, an interference pattern *no longer arises* on the screen. Rather, two Gaussian distributions directly behind each of the slits are observed, as if the experiment were done with any classical macroscopic objects (Moses et al, 2005). This bizarre ability of matter to behave like waves or particles depending on whether it is being observed has come to be known as the "wave-particle duality" of matter.

As it is currently understood, QM is capable of predicting the interference distributions that appear on the screen with Schrödinger's wave equation. It fails, however, to anticipate whether an electron goes through one slit or the other, or to explain why the particles' descriptive wave functions suddenly change when a camera is introduced. It has been said that observations of the incompletely-defined wave-like states force particles into fully-defined states, at which point the classical distributions are seen. However, the reasoning behind this remains unclear. The fact that the quantum wave function lacks this information about particular states seems to imply one of two things. One possibility is that there must be more unknown information that dictates the exact position of the particle at a given time such that it could theoretically be detected in a single slit (as suggested in HV theories). This state of affairs would be compatible with the classically-accepted idea of determinism, which is the notion that the laws of nature always have a unique solution for given initial conditions, such that all events could be completely described and predicted if one had enough information. Alternatively, the mysterious results could mean that particle behaviors are truly random and cannot be predicted, even if all existing information about their states and environments were known. Which is the accurate description of reality is a century-old debate that has divided history's greatest physicists. Einstein ("God does not play dice"), de Broglie, Bohm, and Bell, each supported the hidden variable, deterministic view, whereas Bohr, Feynmann, von Neumann, and Born, were all proponents of indeterministic randomness (Goldstein, 2001).

The Kochen-Specker Theorem

In the present day, there is waning support for HV interpretations of QM. In a 2013 poll of the positions of mathematicians, physicists, and philosophers at a conference on the foundations of quantum mechanics, 0% of 33 respondents answered that they attribute quantum randomness to hidden determinism, despite their being no consensus on what, then, randomness *can* be attributed to (Schlosshauer et al., 2013). This unique unanimity can be largely attributed to the publication and popularity of the Kochen-Specker Theorem (KST). The KST attacks HV theories in general by expressing their assumptions mathematically and proving their contradictory nature. Formulated in 1967, this was not the first theorem of its kind. John von Neumann in his 1932 publication *The Mathematical Foundations of Quantum Mechanics* was the first to claim that he had proved Einstein's dream of a deterministic, HV completion of quantum theory mathematically impossible. This view was quickly accepted by most mathematicians and physicists of the time, including Max Born, who formulated the statistical interpretation of QM mentioned earlier. In 1966, John Stewart Bell exposed Von Neumann's argument as fallacious, but the KST, being logically stronger, is still frequently cited in reference to the failure of HV interpretations (Goldstein, 2001).

The first assumption made by Kochen and Specker in the proof of their theorem is that all of a quantum system's observables have definite values at all times. QM does not reveal these exact values, but a complete HV theory would supposedly do so. This is called the assumption of *value definiteness*. The second assumption is of *noncontextuality* in quantum systems, which is the idea that if a quantum system possesses a property, i.e. if an observable Q has some value $v(Q)$, which the first assumption entails, then it does so independently of how the value is measured.

To illustrate their ultimate point, Kochen and Specker utilize an abstraction of a quantum-mechanical system called a Hilbert space, in which quantum states are represented as vectors. The space is defined such that there is a one-to-one correspondence between properties of a quantum system and projection operators in the space. An explicit statement of the theorem is as follows:

Let H be a Hilbert space of quantum-mechanical state vectors of dimension $x \geq 3$. There is a set *M* of observables on H, containing *y* elements, such that the following two assumptions are contradictory:

A1) All *y* elements of *M* simultaneously have definite values, i.e. are unambiguously mapped onto real numbers ($\forall Q \in M$, $v(Q)$ exists)

A2) Values of all observables in *M* conform to the following constraints:

(a) If *A*, *B*, *C* are all compatible and $C = A+B$, then $v(C) = v(A)+v(B)$

(b) if *A*, *B*, *C* are all compatible and $C = A \cdot B$, then $v(C) = v(A) \cdot v(B)$

Assumption 1 (A1) is trivially equivalent to an assumption of value definiteness. Less apparent is that Assumption 2 (A2) hinges on an assumption of noncontextuality. Two operators are said to be "compatible" if one can measure the first, then the second, then the first again and get the same result as for the initial measurement. Both (a) and (b) of A2 are consequences of a deeper, technical principle called the Functional Composition Principle, which is itself a consequence of noncontextuality. Effectively, the theorem states that in a Hilbert space with three or more dimensions, there must exist some set of observables that do not satisfy both value definiteness and noncontextuality. The proof of this will not be discussed in this paper, but further explanation can be found in section 4 of Carl Held's analysis of the Kochen-Specker Theorem (Held, 2022).

Kochen and Specker's original proof operates on a three-dimensional complex Hilbert space denoted by H_3. It requires that the basis of the observable's associated space be representable by a triple of vectors that are orthogonal in H_3, i.e. that the observable be three-dimensional. These bases vectors are analogous to the familiar unit vectors $\hat{\imath}$, $\hat{\jmath}$, and $\hat{k}$ that span the three spatial dimensions of the position observable. The spin degree of freedom of a one-particle spin-1 system is an example of a QM system that can be represented in H_3. This is because there are three possible states of the system, namely that the spin of the individual particle is +1, –1, or 0. Given an arbitrary direction *n* in physical space and an operator S_n representing the observable of a spin component in direction *n*, H_3 is spanned by the eigenvectors of S_n, which are $|S_n{=}1\rangle$, $|S_n{=}0\rangle$, and $S_n{=}{-}1\rangle$. These three vectors, corresponding to three possible results of measurement in *one* spatial direction, are mutually orthogonal in this context, which illustrates the different senses of orthogonality in H_3 and in physical space. For their proof, Kochen and Specker consider the eigenvectors of the squared components of orthogonal directions of spin in physical space S_x^2, S_y^2, S_z^2 as the basis of their space. This is because these are mutually compatible, as A2 requires, while the spin components themselves are not. A2 thus allows them to place the following constraint on the assignment of their measured values: $v(S_x^2) + v(S_y^2) + v(S_z^2) = 2$, where $v(S_i^2) = 1$ or 0 for $i = x, y, z$. A value of 1 indicates spin of either 1 or -1, and 0 of spin 0. This constraint, paired with A1 of value definiteness, becomes a requirement that for any triple of orthogonal vectors in H_3 $\{v(S_x^2), v(S_y^2), v(S_z^2)\}$, exactly one of its vectors must have a value of 0, and the others of 1.

If an assignment of values according to the prior constraints is possible on H_3, then it is possible on R_3, and vice versa. Thus, while H_3 is a complex space, the problem can be reduced to one on a real three-dimensional Hilbert space R_3. Kochen and Specker then proceed by establishing an analogy between this abstract framework and physical space. They merely fix their three orthogonal basis vectors to $\hat{\imath}$, $\hat{\jmath}$

, and $\hat{k}$, such that orthogonality in R_3 directly corresponds to orthogonality in physical space. Utilizing the accepted postulate that a vector in R_3 through the origin can be represented by a single point, Kochen and Specker then identify their spin operator eigenvectors as points on the unit sphere. This way there is no need to specify coordinates, and they can clearly display many vectors side by side, to form graphs that have come to be known as "KS diagrams." A representative KS diagram is displayed in Figure 2. In these diagrams, points joined by a straight line represent orthogonal vectors. The constraints of A2 on vector value ascriptions are then translated into constraints for coloring the vertices. Using white to indicate $v(S_i^2)$ equal to 1 and black for 0, Kochen and Specker transform their original numerical problem into a problem of coloring the vertices of their diagrams white or black such that joined vertices cannot both be white and triangles must have exactly one white vertex (Kochen and Specker, 1967).

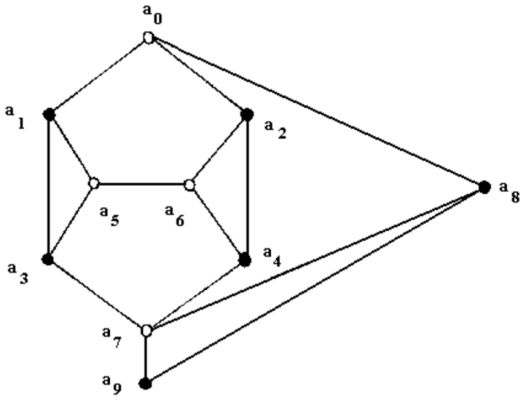

Figure 2: 10-point KS diagram. This example displays inconsistent coloring, in that two adjacent vertices both have white coloring (Held, 2000).

By way of this method, Kochen and Specker show that the rules just outlined must be violated for a specific set of triples, such that an assignment of numbers {1, 1, 0} to each realistic triple of eigenvectors is impossible. Thus, given the premises, a spin-1 particle cannot possess all the properties that it displays in different measurement arrangements at once, so value definiteness and noncontextuality are contradictory. Finally, because HV theories assume both value definiteness and noncontextuality, they must be false. This result led Kochen, Specker and many more to denounce HV interpretations of quantum mechanics and abandon determinism.

The de Broglie-Bohm Theory

In relation to a theory incorporating hidden variables, Einstein once remarked that "the statistical quantum theory would… take an approximately analogous position to the statistical mechanics within the framework of classical mechanics" (Einstein, 1949). This exactly describes the mathematical structures that Louis de Broglie and David Bohm independently invented decades apart for what is now known as the pilot wave model of QM, or pilot wave mechanics (PWM). Within the framework of this predominant HV theory, some system of *N* particles is described by its wave function $\psi = \psi(q_1, \ldots, q_N) = \psi(q)$, a complex function on the space of possible configurations *q* of the system, along with its actual configuration *Q* defined by the initial positions $\{Q_1, \ldots, Q_N\}$ of each particle. These positions evolve as usual according to Schrödinger's equation: $i\hbar\frac{\partial\psi}{\partial t} = H\psi$, where *H* is the Schrödinger Hamiltonian. This partial description is then completed by the specification of the actual configuration of the particles *Q*, according to the "guiding equation": $\frac{dQ_k}{dt} = \frac{\hbar}{m_k} Im\frac{\psi^*\partial_k\psi}{\psi^*\psi}(Q_1, \ldots, Q_N)$ for $k = 1, \ldots, N$, which expresses the velocities of the particles in terms of the wave function. Here m_k represents the *k*th particle's mass, *Im* indicates the imaginary part of the following term, and ∂_k is the gradient with respect to the usual coordinates $q_k = (x_k, y_k, z_k)$ for the *k*th particle (Held, 2022).

In PWM, the motion of a set of particles is deterministically choreographed by these two equations. For any quantum experiment, one must identify the relevant system as all particles being measured as well as the environment in which the experiment is performed, including all measuring

devices. Considering the importance of maintaining "closed systems" when predicting results in classical mechanics, the requirement of such a broad scope should not be surprising; ignoring this requirement one risks overlooking some nonnegligible variable. The PWM model is then determined by regarding the initial configuration of this bigger system as random in the usual statistical way, with distribution given by $|\Psi|^2$. The guiding equation for the whole system transforms the initial configuration into the final configuration at the conclusion of the experiment. In particular, when a particle is sent into a double-slit apparatus, the slit through which it passes and its location upon arrival at the photosensitive screen are completely determined by its initial position and wave function. Thus, the deterministic PWM model yields the usual quantum predictions for the results of the experiment, with an underlying deterministic model in which quantum randomness arises from averaging over ignorance.

Discussion

An assumption of the Kochen-Specker and similar theorems is that HV theories rely on the truth of both value definiteness and noncontextuality and are universally disproven by their contradiction. For PWM to escape such arguments, it must be proven not to depend on at least one of these premises.

Value definiteness was defined for the purposes of the Kochen-Specker argument such that spin valuation must be either 1, -1, or 0. Values being defined, however, means that the values are known, which requires that a measurement of the system has been taken. This necessitates that some property of the system has been affected in such a way that its equal and opposite reaction has manifested somehow in 3-dimensional position space so that it can ultimately be physically observed. Common examples of potential measurement results include changes in some pointer's orientations or flashes on a photographic plate. In this way, only literal spatial coordinates are truly "observables." When such a measurement process has not been undertaken, it does not make sense to say that some property has some specific value, because the value has not been compared to anything else. Without the interactions by which "observables" are compared to some other known value, particles cannot have "definite" properties. The same classical reasoning predicates that motion must be defined relative to the predefined motion of some other body or system in order to make sense. It is a widely-accepted concept that one cannot define the speed of an object that is the only object in the universe, in that measurements are dependent on the reference frame from which they are made. As such, it is a fallacy that particle spins must have definite values independent of any measurement process, and that spin is perfectly analogous to 3-dimensional position space. Thus, it is reasonable for a quantum theory to dictate that spin values need not be restricted to 1, -1, or 0 at all times, to which Kochen's and Specker's argument would not apply.

The ability of PWM to describe spin in contrast to the KS perspective is well-demonstrated by a consideration of a Stern-Gerlach experiment, and displays the superiority of PWM's treatment of the concept of value definiteness. Stern-Gerlach magnets are designed and oriented such that a wave packet (a localized wave function with reasonably well-defined velocity) directed towards the magnet will, by virtue of Schrödinger evolution, separate into distinct packets corresponding to the spin components of the wave function and move in a discrete set of directions. The "particle" itself, depending upon its initial position, ends up in one of the packets moving in one of the directions with some probability distribution (Gerlach and Stern, 1922). From a KS perspective, it is taken as a premise that the components of the spin observable must have definite values at all times. However, the components of spin in different directions are not always simultaneously measurable, in which cases the relationships between the vector components are not observable. Thus, the spin components cannot be said to have defined values, which the KS perspective is incapable of accounting for. On the other hand, it is known that spin can be represented by complex wave functions, which PWM can keep track of with its two constituent equations. The probability distribution for the directions of the particles can be conveniently expressed in terms of the quantum mechanical spin operators according to the theory's mathematical

framework. As such, PWM can predict and describe the outcomes of spin experiments without a reliance on the idea of value definiteness, and remains a viable HV theory despite the conclusions of Kochen and Specker.

While the independence of PWM from value definiteness is sufficient to restore its legitimacy, it is worth noting further the reason to doubt the importance of Kochen's and Specker's premise of noncontextuality as well. Noncontextuality was said to imply that "measurement of an observable must yield the same value independently of what other measurements may be made simultaneously" (Kochen and Specker, 1967). Their theorem depends on HV theories' reliance on this principle. However, the word "measurement" in this context quite strongly suggests the ascertaining of some preexisting value of some property, with any instrument involved playing a purely passive role (Bell, 1982). As represented by PWM, quantum experiments do not fit this description; any experimental results must be regarded as the joint product of the system being "measured" along with the apparatus. To illustrate this, consider an operator A that is compatible with operators B and C, which are mutually incompatible. What is said to be the value of A ($v(A)$) in an experiment measuring A with B usually disagrees with the value of A when measuring A with C. This is because these experiments differ, and different experiments have different results, an idea that is becoming increasingly acknowledged. A 2019 paper by Carnegie Mellon University professor Robert B. Griffiths on *Quantum Measurements and Contextuality* does well to clarify the varying meanings behind the words "contextuality" and "measurement," which he identifies as misused and often poorly defined in the field of quantum mechanics. It is worth reevaluating the implications of older theorems such as the in light of such updated awareness. The misleading reference to measurement for the purposes of the KST, which suggests that a preexisting value $v(A)$ remains the same and is being revealed in both cases, makes contextuality seem more than it is, and leads Kochen and Specker to implement constraints on their model that need not exist. Understood properly, contextuality amounts to little more than the unremarkable observation that results of experiments should depend upon how they are performed, even when the experiments are associated with the same observable (Griffiths, 2019). Rather than relying on noncontextuality as Kochen and Specker believed, HV theories actually rely on an opposite principle, and thus are unaffected by the results of the KST.

Conclusion

In the present day, claims are often made that quantum mechanics is incompatible with determinism, or about the existence of some quantum logic that deviates from or contradicts "typical" or "classical" logic. However, such claims are based on misunderstandings, among which are that the Kochen-Specker or a similar theorem proves outright that hidden variable, deterministic theories cannot work. De Broglie and Bohm's PWM accounts for all phenomena governed by nonrelativistic quantum mechanics. In particular, the usual measurement postulates of quantum theory, including wave-particle duality, and probabilities given by $|\Psi|^2$, emerge from an analysis of the theory's two constituent equations. No obscure status for human observation is required, as some imply by asserting that the wave functions of the particles in the double-slit experiment "collapse" when detection devices are instated. Further, the irrelevance of noncontextuality and the nonsensicality of value definiteness follow immediately from the theory's definitions.

As quantum experiments continue to show unusual behaviors, it becomes increasingly important that the physics community be precise in defining ideas both in everyday language and mathematical terms. In 1982, proponent of HV theories John Stewart Bell said, "I am convinced that the word "measurement" has now been so abused that the field [of quantum mechanics] would be significantly advanced by banning its use altogether, in favour for example of the word 'experiment.'" "Measurement" is not the only word that has been misunderstood in these contexts. In particular, the discussion here displays the importance of specifying what is meant by "value definiteness," "observables," and "contextuality." QM has confused humanity since its

creation, but to concede that it is incomprehensible is wholly unnecessary. Because no human can possess complete knowledge of the universe, anything is technically possible. The notion that inductive reasoning fails to extend to quantum scales, however, is much less plausible than that its patterns are not immediately apparent. If one is to achieve a true understanding of QM, and thus of the fundamental nature of the universe, then one must rely not only on its constituent mathematics and symbols, but on the coherence of the ideas that those symbols represent. Only then does it become possible to intuit the direction of the path toward more complete and more detailed descriptions of reality.

References

1. Bauer, M. (2023, January 26). *The Stern-Gerlach Experiment, Translation of: "Der experimentelle Nachweis der Richtungsquantelung im Magnetfeld."* ArXiv.org. https://doi.org/10.48550/arXiv.2301.11343

2. Bell, J. S. (1964). On the Einstein Podolsky Rosen paradox. *Physics Physique физика*, *1*(3), 195–200. https://doi.org/10.1103/physicsphysiquefizika.1.195

3. Bohm, D. (1952a). A Suggested Interpretation of the Quantum Theory in Terms of "Hidden" Variables. I. *Physical Review*, *85*(2), 166–179. https://doi.org/10.1103/physrev.85.166

4. Bohm, D. (1952b). A Suggested Interpretation of the Quantum Theory in Terms of "Hidden" Variables. II. *Physical Review*, *85*(2), 180–193. https://doi.org/10.1103/physrev.85.180

5. Born, M. (2021). On the Quantum Mechanics of Collision Processes [English Translation]. *Terry's Archive Online*, *2021*(08), 0828. https://doi.org/10.48034/20210828

6. Davisson, C., & Germer, L. H. (1927). The Scattering of Electrons by a Single Crystal of Nickel. *Nature*, *119*(2998), 558–560. https://doi.org/10.1038/119558a0

7. Gerlach, W., & Stern, O. (1922). Der experimentelle Nachweis des magnetischen Moments des Silberatoms. *Zeitschrift Für Physik*, *8*(1), 110–111. https://doi.org/10.1007/bf01329580

8. Goldstein, S. (2001). Bohmian Mechanics. *Plato.stanford.edu*. https://plato.stanford.edu/archives/fall2021/entries/qm-bohm/

9. Griffiths, R. B. (2019). Quantum measurements and contextuality. *Philosophical Transactions of the Royal Society A*, *377*(2157), 20190033–20190033. https://doi.org/10.1098/rsta.2019.0033

10. Heisenberg, Werner, (1955). The Development of the Interpretation of the Quantum Theory.W. Pauli (ed.), *Niels Bohr and the Development of Physics: Essays Dedicated to Niels Bohr on the Occasion of his Seventieth Birthday*, New York: McGraw-Hill, pp. 12–29

11. Held, C. (2000). The Kochen-Specker Theorem. *Plato.stanford.edu*. https://plato.stanford.edu/archives/fall2022/entries/kochen-specker/

12. Kochen, S., & Specker, E. (1967). The Problem of Hidden Variables in Quantum Mechanics. *Indiana University Mathematics Journal*, *17*(1), 59–87. https://doi.org/10.1512/iumj.1968.17.17004

13. Redhead, M. (1988). *Incompleteness, Nonlocality and Realism: A Prolegomenon to the Philosophy of Quantum Mechanics*. *Physics Today*, *41*(9), 104–105. https://doi.org/10.1063/1.2811563

14. Schlosshauer, M., Kofler, J., Zeilinger, A. (2013). A Snapshot of Fundamental Attitudes Towards Quantum Mechanics. *Studies in History and Philosophy of Modern Physics* 44, 222–238

15. Schrödinger, E. (1935). Die gegenwärtige Situation in der Quantenmechanik. *Die Naturwissenschaften*, *23*(50), 844–849. https://doi.org/10.1007/bf01491987

16. Serway, R. A., Moses, C. J., & Moyer, C. A. (2014). *Modern physics*. Cengage.

17. Thomson, G. P. (1927). The Diffraction of Cathode Rays by Thin Films of Platinum. *Nature*, *120*(3031), 802–802. https://doi.org/10.1038/120802a0

18. Young, T. (1800). The Bakerian Lecture. Experiments and Calculations Relative to Physical Optics. *Proceedings of the Royal Society of London*, *1*(0), 131–132. https://doi.org/10.1098/rspl.1800.0076

Effects on Status Striving: How Self-Perceived Value, Self-Esteem, and Personality Traits Impact Preferred Status

Sua Cho

Volume 2, Issue 2

Article Synopsis

Humans typically desire high status (i.e., leadership roles), but only when they believe they are useful to the group. In this paper, the author explores whether self-esteem and various personality traits influence the status people prefer when they believe they are useless to the group. Because self-esteem is correlated with socioeconomic status, the results of this study have implications for socioeconomic inequalities.

Graphic by Cindy Ju

Effects on Status Striving: How Self-Perceived Value, Self-Esteem, and Personality Traits Impact Preferred Status

Sua Cho

Department of Psychology and Neuroscience, Duke University
https://doi.org/10.55894/dv2.24

Abstract

Prior research shows that despite the belief that humans universally desire high status in group settings (i.e., leadership roles), individuals with low self-perceived value (SPV) perceive themselves as being unable to make meaningful contributions to the group's success. Thus, they prefer low status to conform to the external social pressure of other group members' expectations. Yet, internal factors such as self-esteem and personality traits may also shape individuals' preferred status by buffering the effects of external factors. To examine these hypotheses, two studies were conducted, in which the participants' self-perceived value and self-esteem were manipulated. The results from these studies were consistent with previous studies, showing that participants with higher SPV preferred and expected higher status than participants with lower SPV. Moreover, individuals' personality traits predicted the status they preferred and expected: more extroverted participants preferred and expected higher status than less extroverted participants, while participants with higher levels of neuroticism preferred and expected lower status than participants with lower levels of neuroticism. Participants with higher self-esteem were also more likely to prefer and expect higher status. Lastly, low self-esteem was associated with lower preferred status for participants with low SPV, but not high SPV. Because self-esteem is correlated with individuals' socioeconomic status (SES), this study further highlights the need to address the self-esteem gap between individuals in high and low SES to prevent pre-established social hierarchies from perpetuating

Introduction

Status is widely defined as the social standing and value others voluntarily give an individual based on respect, prestige, and deference (Anderson et al., 2020; Yu & Kilduff, 2020; Bendersky & Pai, 2018; Kilduff et al., 2016). High status is associated with interpersonal, material, physical, and psychological rewards, such as companion desirability (Henrich & Gil-White, 2001); access to scarce resources and information (Anderson & Kilduff, 2009; Savin-Williams, 1979); opportunities for further status advancement (Magee & Galinsky, 2008); attention from others (Lansu et al., 2013; Foulsham et al., 2010; Savin-Williams, 1979); better mental and physical health (Adler et al., 2000); and longer life span (Anderson & Kilduff, 2009). Given the benefits of high status, it is unsurprising that the desire for status in social groups is commonly assumed as a universal human motive (Anderson et al., 2012; Maslow, 1943). For instance, psychosocial need fulfillment (i.e., need for respect) is associated with well-being across a sample of 123 countries (Tay & Diener, 2011). Evolutionary psychologists likewise claim that humans have evolved to strive for social dominance, not only to gain access to resources but also to maintain their self-esteem (Barkow, 1975).

Despite the widespread notion that humans have a universal desire for high status, prior research has found that this is not necessarily the case (Schmid Mast et al., 2010; Smith et al., 2008; Josephs et al., 2006). Studies show that individuals have varied needs

for power (Schmid Mast et al., 2010; Smith et al., 2008), dominance (Josephs et al., 2006), and status (Anderson et al., 2020). Multiple studies replicated in real-life groups and laboratories showed that individuals' preferred status varies depending on their self-perceived value (SPV) to the group, defined as the skills they believe to possess that contributes to the group's success (Anderson et al., 2012). In other words, individuals who had low SPV, perceiving themselves to be unable to contribute to the group's success, preferred low status (i.e., non-leadership roles), whereas individuals who had high SPV, perceiving themselves to have the skills to contribute to the group, preferred high status.

The mechanism through which an individual's SPV influenced their preferred status was found to be the need to conform to the group's expectations, rather than the concern for the group's overall success, responsibility, or fairness (Anderson et al., 2012). Individuals with low SPV believed others expected them to remain in a low status and consequently avoided pursuing higher status than what was expected by the group (Anderson et al., 2012; Anderson et al., 2006). For example, the Anderson et al. (2012) study revealed that compared to the identified condition, participants with low SPV in the anonymous condition preferred higher status rank, since other group members could not have any expectations of their rank in the latter. This suggests that individuals with low SPV often resign themselves to a lower status rank due to the need to conform to others' expectations. These findings imply that individuals may be pressured by external constraints such as social expectations to accept low status even if internally they still prefer high status. Thus, once external constraints were removed from consideration, individuals expressed their desire for high status despite their low SPV (Anderson et al., 2012).

Literature on Self-Esteem

Self-esteem is an individual's confidence in or subjective evaluation of their own worth, independent from their objective abilities or others' evaluations (Orth & Robins, 2014; Donnellan et al., 2011). It reflects feelings of self-respect and contentment, rather than narcissism or excessive self-aggrandizement, which is the act of promoting oneself as being powerful or important (Orth & Robins, 2014; Ackerman et al., 2011). Prior studies show that high self-esteem reduces anxiety (Pyszczynski et al., 2004) and provides emotional stability in times of change through a process of self-verification of role identities in groups (Cast & Burke, 2002). Moreover, individuals' desire for self-esteem motivates them to maintain relationships in groups (Cast & Burke, 2002). Thus, while prior studies have pointed to external factors that may influence individuals' preferred status (Anderson et al., 2012), internal factors such as self-esteem may also play a role in determining who prefers high or low status by buffering the effects of such external factors. The effects of SPV on preferred status may be greater for participants with higher self-esteem and lower for participants with lower self-esteem. The study will examine whether self-esteem has a moderating effect of SPV on preferred status.

This has several implications for real-world scenarios, including the immediate concern about the group's success and effectiveness as an organization. For example, individuals with low SPV, lacking the necessary skills to contribute to the group's success, may obstruct the group by pursuing higher status regardless of their abilities, due to their high self-esteem. Likewise, individuals with high SPV might not pursue higher status despite their potential to contribute meaningfully to the group, due to their low self-esteem. Further, prior research shows that self-esteem is positively correlated with individuals' socioeconomic status (SES) (Twenge & Campbell, 2002; Zhang & Postiglione, 2001). Individuals with high SES report having higher self-esteem, which implies that individuals with high SES might be more likely to prefer high status despite having low SPV, and individuals with low SES might be more likely to prefer low status even with high SPV. Prior studies have also found that those already in a position of high status have more confidence in their abilities and thus a stronger status motive compared to those in a position of low status (Anderson et al., 2020; Donnelly et al., 2018). Although it may be helpful for the stability and coordination of group status hierarchies for some individuals to seek high status and some to seek low status, it becomes an issue of social and socioeconomic

equality when status motive starts to differ, as research shows, based on individuals' pre-established SES. If the following study finds that individuals' self-esteem does indeed moderate the effects of SPV on preferred status, it may encourage future studies to explore ways to motivate individuals with low SES to increasingly engage in status competition and pursue higher status. Thus, this study hypothesizes that self-esteem moderates the effect of SPV on preferred status, in that the positive effect of SPV on preferred status is greater for participants with higher self-esteem.

Literature on Extroversion

This study is also interested in examining individuals' personality traits that may affect their preferred status. One such trait is extroversion. Prior research shows that extroversion is highly correlated with incentive motivation, tendency to attract social attention, and stimulus-seeking behavior (Depue & Fu, 2013; Ashton et al., 2002; Farley & Farley, 1967). Thus, it is possible that individuals with greater extroversion have greater motivation to pursue higher status, due to the associated social benefits, such as greater attention from others (Lansu et al., 2013; Foulsham et al., 2010; Savin-Williams, 1979) and influence within the group (Fiske, 2010; Cheng et al., 2010; Savin-Williams, 1979; Berger et al., 1972). In fact, previous studies show that high extroversion predicts higher status among both men and women (Anderson et al. 2001), which prompts the study to examine whether greater extroversion rewards lead to a greater preference for high status. Prior research reveals that extroversion predicts general confidence levels, overconfidence, and positive emotions and expressions, including enthusiasm and activeness (Schaefer et al., 2004; Cheng & Furnham, 2002; Watson & Clark, 1997). Thus, this study will examine whether more extroverted participants not only prefer but also expect to gain higher status. This study hypothesizes that participants with greater extroversion will prefer and expect higher status due to the social benefits of high status and a higher level of confidence in their own abilities.

Literature on Neuroticism

Another potential personality trait that may affect an individual's preferred status independent of SPV is neuroticism, or how easily a person experiences anxiety or distress at perceived threats. Prior studies show that neuroticism is highly correlated with the fear of negative evaluation (FNE), the tendency to believe others are critical of the self (Naragon-Gainey & Watson, 2011), as well as a range of anxiety disorders, including social anxiety, social phobia, and generalized anxiety disorder (GAD) (Kotov et al., 2010; Bienvenu et al., 2007). Evolutionary psychologists suggest that this is because neuroticism has evolved as a part of the Behavioral Inhibition System, a withdrawal-oriented mechanism that inhibits undesirable or risky behavior (Naragon-Gainey & Watson, 2011; Tomarkenand & Keener, 1998). Literature also shows that individuals with higher status attract more blame than those with lower status in cases of organizational failure (i.e., financial mismanagement, cultural dysfunction, product failures), but do not attract more credit in cases of organizational success (Gibson & Schroeder, 2003). Thus, it is possible that individuals with higher levels of neuroticism prefer low-status positions, due to the social burdens associated with high status, including increased responsibility and attention from others (Anderson et al., 2012; Keltner et al., 2008; Savin-Williams, 1979). This study will examine whether greater neuroticism in individuals predicts a greater preference for low status.

Additionally, previous studies show that neuroticism is correlated with decreased levels of self-efficacy, or the belief in one's own ability to reach specific goals, lowering their confidence and beliefs about their own competence (Wang et al., 2018). Further, neuroticism levels were found to be a direct negative predictor of general self-confidence (Cheng & Furnham, 2002) while being a direct predictor of greater anxiety and shyness (Cheng & Furnham, 2002; Briggs, 1988). Thus, the study will also examine whether participants with higher levels of neuroticism also expect to receive lower status.

The study hypothesizes that participants with greater neuroticism will prefer lower status due to concerns about the increased responsibility of occupying a high status and expect lower status, as they have lower self-efficacy and confidence in their own abilities.

Hypotheses

The following hypotheses will be examined in this study:
Hypothesis 1a. Participants' SPV is positively correlated with their preferred status within that group. Participants with higher SPV, those who believe they have the necessary skills to contribute to the group's success, prefer higher status. As participants with high SPV on one task may have low SPV on another, the causal effect of SPV on preferred status is context-specific, occurring within a particular group. This is a replication of Study 3 from Anderson et al. (2012).

Hypothesis 1b. Participants with higher SPV naturally expect to receive higher status as they see themselves as deserving of it.

Hypothesis 2. Self-esteem moderates the effect of SPV on preferred status. The effects of high SPV on preferred status are greater for participants with higher self-esteem.

Hypothesis 3a. Participants with greater extroversion prefer higher status.

Hypothesis 3b. Participants with greater extroversion expect to receive higher status.

Hypothesis 4a. Participants with greater neuroticism prefer lower status.

Hypothesis 4b. Participants with greater neuroticism expect lower status.

Study 1 Methods

The following experimental design seeks to examine whether participants' SPV to the group is positively correlated with their preferred status and expected status within that group; whether participants' self-esteem moderates the effect of SPV on preferred status; whether participants with greater extroversion prefer and expect higher status; and whether participants with greater neuroticism prefer and expect lower status.

Participants. 51 individuals were recruited from CloudResearch, an online participant-sourcing platform, and another 65 individuals were recruited from a participant pool maintained by an interdisciplinary behavioral research center at a Southeastern university. This two-part recruitment procedure was conducted to ensure reliable data quality and eliminate suspicion for potential biases prior to conducting the study. The participant pool consisted of college students and non-student community members who were 18 years of age or older and residing in the United States. The participants were compensated $4.00 for completing an approximately 20-minute survey. Eleven participants stated they found a part of the research procedure difficult to believe during the suspicion check (i.e., questionnaire measuring how much participants suspect the use of deception in the study) or did not follow the study procedures as instructed and were thus excluded from the analyses, leaving a final sample of 105 participants for the analysis.

Procedure. The participants were told that the study had two components: an individual task and a group task. After first completing an online survey, they would be redirected to a separate platform in which they would interact with three other participants to complete the group task.

In the online survey, the participants completed the BFI-2-S personality measure, a 30-item questionnaire that measures 5 key personality traits: Extroversion, Agreeableness, Conscientiousness, Neuroticism, and Open-mindedness. (Soto & O. P., 2017). To manipulate the SPV, the participants then completed 10 trials of an individual "Contrast Sensitivity" perception task (Anderson et al., 2012; Troyer, 2001). Before proceeding, the participants read a note that their performance on this individual task will correlate to their ability to successfully contribute to the subsequent group task (Anderson et al., 2012).

In the "Contrast Sensitivity" task, the participants were told to decide which of two checkerboard photos of black and white squares had more white space. Although the participants were told that one alternative was correct over the other, both photos had equal spaces of black and white. Each trial lasted for 20 seconds.

Following the completion of the task, the participants underwent standard self-esteem manipulation (Riketa & Dauenheimer, 2003; Chartrand & Bargh, 1996). The participants were randomly assigned to the low self-esteem condition or high self-esteem condition. In each condition, the participants were told to focus their gaze on an asterisk placed in the center of the screen as a "flash" of the stimulus, the words described in the following paragraph, was presented in the participants' parafoveal visual field (i.e., between 2 to 5 cm around the asterisk). Prior research shows that the meaning of visual stimuli presented in this field is unconsciously encoded but not consciously processed (Chartrand & Bargh, 1996; Rayner, 1978), which allows for an effective manipulation of self-esteem.

The participants in the high self-esteem condition were presented with "flashes" of positive adjectives (i.e., "good," "important," "useful") paired with a self-referent word (i.e., "I"), while the participants in the low self-esteem condition were presented with negative adjectives (i.e. "bad," "lousy," "worthless") paired with a self-referent word (Riketa & Dauenheimer, 2003).

The participants were told this was a reaction task, rather than a self-esteem manipulation. Thus, the participants were told to place their index fingers on the E key and I key of the keyboard. They were told to hit the E key if the stimulus was presented on the left side of the screen and the I key if the stimulus was presented on the right side of the screen. There were 12 trials of affective adjectives. Each trial alternated with 500 milliseconds of a blank screen and 60 milliseconds of a screen that presented a random sequence of 8 letters paired with a self-referent word (e.g., "KHDFESWV"). All stimuli were presented as black capital letters on a white screen. To measure the effectiveness of the manipulation, the participants completed the Rosenberg Self-Esteem Scale (Rosenberg, 1979).

Upon completing the self-esteem manipulation, the participants received their scores and their teammates' scores on the Contrast Sensitivity task. These scores had initially been withheld from the participants to distinguish the self-perceived value manipulation from the self-esteem manipulation and to prevent participants from forming their self-esteem based on their Contrast Sensitivity scores rather than the self-esteem manipulation.

The participants were randomly assigned to the low self-perceived value condition or high self-perceived value condition. Participants in the low self-perceived value condition were told they scored 3 and would be assigned to a group wherein the other members scored 5, 6, and 8. The participants in the high self-perceived value condition were told they scored 8 and would be assigned to a group wherein the other members scored 3, 5, and 6. These scores were adjusted from the original Anderson et al. (2012) study, which involved 20 trials of the Contrast Sensitivity task instead of 10. To successfully manipulate their self-perceived values, participants in the high self-perceived value condition were the best performers in their group, and participants in the low self-perceived value condition were the worst performers in their group.

Finally, participants completed a brief survey asking how much value they perceive themselves to have in the group, which status they would prefer to have in the group, and which status they expected to have in the group. Afterwards, the participants completed a suspicion check and were debriefed.

Personality traits. The Big Five personality traits were assessed with the BFI-2-S personality measure (Soto & O. P., 2017). It includes 30 items such as "I am someone who tends to be quiet," and "I am someone who is outgoing, sociable," rated from 1 (disagree strongly) to 5 (agree strongly). The Domain Scales include Extroversion, Agreeableness, Conscientiousness, Neuroticism, and Open-Mindedness. The facet scales include Sociability, Assertiveness, Compassion, etc.

Self-Esteem. After the manipulation, participants' self-esteem was assessed with the 10-item Rosenberg Self-Esteem Scale (Rosenberg, 1979). Items include "On the whole, I am satisfied with myself," and "I feel that I'm a person of worth," rated from 1 (strongly agree) to 4 (strongly disagree). The RSE demonstrates high internal consistency, or the correlation between different items on the same test, with a test-retest correlation (i.e., consistency of results when same group of people receive the same test on two separate

time points) of 0.85 and 0.88 over a period of 2 weeks (Rosenberg, 1979).

Self-perceived Value. After completing the tasks, the participants were asked to rank on a scale of 1 (lowest value) to 7 (highest value): "How much value can you provide this group, relative to other group members?" "How much do you think you can contribute to the group task?" and "How much are you able to make important contributions to the group task?" The questions were adapted from the Anderson et al. (2012) study.

Preferred Status. The participants were asked to rank on a scale of 1 (lowest value) to 7 (highest value): "How motivated are you to achieve the leadership position?" "How much would you try to control the group's activities?" "How much would you try to act as the group leader?" "To what extent do you want to lead the group's activities?" and "To what extent do you want to have a high status and influence in the group?" In addition, the participants ranked on a scale of 1 (highest value) to 7 (lowest value): "In terms of your overall status in the group, which rank would you prefer?" and "In terms of your leadership standing in the group, which rank would you prefer?" The answers to the last two questions were reverse-coded. The questions were adapted from the Anderson et al. (2012) study.

Expected status. The participants were asked to rank on a scale of 1 (lowest value) to 7 (highest value): "To what extent do you believe you can lead the group's activities?" and "To what extent do you believe you can have a high status and influence in the group?" In addition, the participants ranked on a scale of 1 (highest value) to 7 (lowest value): "In terms of your overall status in the group, which rank do you expect to achieve in the following group activity?" "In terms of your leadership standing in the group, which rank do you expect to achieve in the following group activity?" and "Which rank do you expect you can realistically achieve in the following group activity?" The answers to the last three questions were reverse-coded. Although the Anderson et al. (2012) study did not include a direct measure for the status the participants realistically expected to occupy in the group, these questions were devised based on the measure for preferred status.

Results and Discussion

Initially, the manipulation of the participants' SPV was successful. Participants in the low SPV condition reported lower self-perceived value ($M = 3.978$, $SD = 1.483$) than the participants in the high SPV condition ($M = 5.689$, $SD = 0.815$), $t(103) = -6.931$, $p < 0.001$.

The study findings supported Hypothesis 1a, successfully replicating the original Anderson et al. (2012) study. Consistent with the hypothesis, there was a significant effect of participants' self-perceived value of the group on their preferred status within that group, $F(1, 103) = 18.870$, $p < 0.001$, $n2 = 0.155$. Participants' self-perceived value to the group accounts for about 18.9% of the variance in their preferred status. Participants with higher SPV were more likely to also prefer higher status (Figure 1). Further, Hypothesis 1b was also supported by this study. There was a significant effect of participants' self-perceived value of the group on their expected status within that group, $F(1, 103) = 4.439$, $p = 0.038$, $n2 = 0.041$. Participants with higher SPV were more likely to expect higher status (Figure 2). Thus, the participants' preferred status and expected status were both contingent upon the value they perceived themselves to provide to the group.

Figure 1: SPV on Preferred Status 1

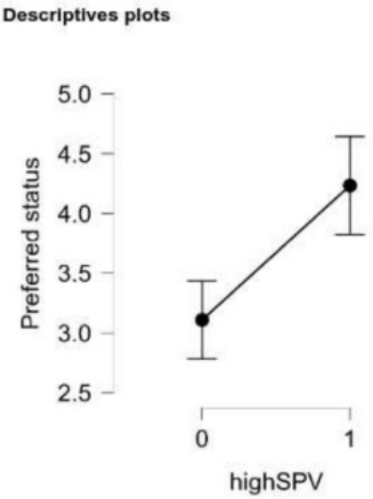

Figure 2: SPV on Expected Status 1

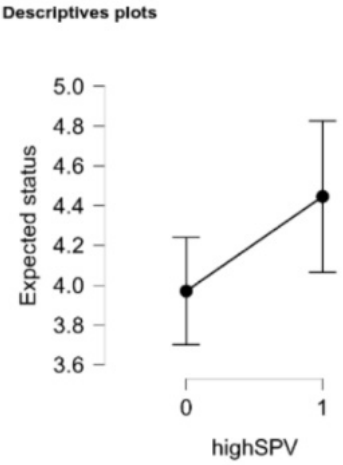

However, the manipulation of the participants' self-esteem was found to be ineffective, presenting difficulties for the researcher to analyze Hypothesis 2. Participants in the high self-esteem condition reported a similar level of self-esteem (M = 2.567, SD = 0.855) as the participants in the low self-esteem condition (M = 2.579, SD = 0.745), t(103) = 0.072, p = 0.943. There was a non-significant difference between the self-esteem of participants in the high self-esteem condition and the self-esteem of participants in the low self-esteem condition.

The primary difference between the use of visual stimuli for self-esteem manipulation in previous studies (Riketa & Dauenheimer, 2003) and that of this study is the latter's online nature. The study by Riketa and Dauenheimer (2003) was conducted in a laboratory where the experimenter could position the participants in front of a computer at a precise distance that enables parafoveal perception. The experimenter could also monitor the participants to make sure they stayed in their initial position and ensure they followed the instructions presented on the screen. However, due to its online nature, this study lacked such procedures, making it difficult to ensure the participants followed the instructions to look at the asterisk instead of the words presented around the asterisk or away from the screen entirely. Thus, a follow-up study was designed to better examine whether self-esteem moderates the effect of SPV on preferred status (see section Study 2 Methods).

The study findings supported Hypothesis 3a. Participants' levels of extroversion had a positive correlation with their preferred status within that group, r = 0.368, p < 0.001, 95% CI = [0.189, 0.523] (Table 1). Participants' levels of extroversion were calculated from their answers to the BFI-2-S personality measure on a scale of 1 (disagree strongly) to 5 (agree strongly; Soto & O. P., 2017). Questions on the Extroversion Domain Scale included, "I am someone who tends to be quiet," "I am someone who is dominant, acts as a leader," "I am someone who is full of energy," "I am someone who is outgoing, sociable," "I am someone who prefers to have others take charge," and "I am someone who is less active than other people" (Soto & O. P., 2017). The six items were averaged after reverse-coding three items to yield the final extroversion score. More extroverted participants were more likely to prefer higher status than less extroverted ones. Hypothesis 3b was also supported. Participants' levels of extroversion had a positive correlation with their expected status within that group, r = 0.277, p = 0.004, 95% CI = [0.090, 0.445] (Table 2). More extroverted participants were more likely to expect higher status than less extroverted ones.

The study findings supported Hypothesis 4a. Participants' levels of neuroticism had a negative correlation with their preferred status within that group, r = -0.250, p = 0.010, 95% CI = [-0.422, -0.062] (Table 1). Participants' levels of neuroticism were calculated using the same procedures as their extroversion score. Questions on the Neuroticism Domain Scale included, "I am someone who worries a lot," "I am someone who tends to feel depressed, blue," "I am someone who is emotionally stable, not easily upset," "I am someone who is relaxed, handles stress well," "I am someone who feels secure, comfortable with self," and "I am someone who is temperamental, gets emotional easily" (Soto & O. P., 2017). The six items were averaged after reverse-coding three items to yield the final neuroticism score. The Domain Scales for Agreeableness, Conscientiousness, and Open-Mindedness were likewise calculated from the BFI-2-S personality measure, by averaging the participants' answers to six items after reverse-coding three items. Participants with greater levels of neuroticism were more likely to prefer lower status than those with

lower levels of neuroticism. Further, Hypothesis 4b was supported. Participants' levels of neuroticism had a negative correlation with their expected status within that group, r = -0.304, p = 0.002, 95% CI = [-0.468, -0.119] (Table 2). Participants with greater levels of neuroticism were more likely to expect lower status than those with lower levels of neuroticism.

There was an unexpected finding that may be worth noting for future studies. Participants with higher levels of conscientiousness, or the likelihood to delay gratification and exert self-control, were more likely to prefer higher status, r = 0.202, p = 0.039, 95% CI = [0.011, 0.379] (Table 1). The finding is consistent with previous literature that revealed a negative correlation between conscientiousness and an avoidant leadership style (i.e., leaders who do not engage with others to accomplish goals), while revealing a positive correlation between conscientiousness and a transformational leadership style (Zopiatis & Constanti, 2012). In other words, individuals with greater conscientiousness have greater idealized influence, or charisma, which enables them to effectively motivate their group members' emotions to achieve results (Zopiatis & Constanti, 2012; Judge & Bono, 2000). Thus, this study suggests that individuals with greater conscientiousness would prefer higher status, a position of influence that allows such qualities to be useful.

Table 1: Personality Traits on Preferred Status

Pearson's Correlations

			Pearson's r	p	Lower 95% CI	Upper 95% CI
Preferred status	-	Extraversion	0.368	< .001	0.189	0.523
Preferred status	-	Agreeableness	0.174	0.076	−0.019	0.354
Preferred status	-	Conscientiousness	0.202	0.039	0.011	0.379
Preferred status	-	Neuroticism	−0.250	0.010	−0.422	−0.062
Preferred status	-	Open Mindedness	0.136	0.168	−0.057	0.319

In short, SPV to the group had a causal effect on preferred status and expected status. Participants with greater extroversion both preferred and expected to achieve higher status and participants with greater neuroticism preferred and expected to occupy a lower status within the group.

Study 2 Methods

As a follow-up of Study 1, the following experimental design seeks to better examine Hypothesis 2, whether participants' self-esteem moderates the effect of SPV on preferred status.

Participants. 154 individuals were recruited from CloudResearch. The participant pool consisted of college students and non-student community members who were 18 years of age or older and currently located in the United States. The participants were compensated $4.00 for completing an approximately 20-minute survey. 27 participants raised suspicions about the feedback they received or did not follow the study procedures as instructed and were thus excluded from the analyses, leaving a final sample of 127 participants for the analysis.

Procedure. The participants were told they would first complete an online survey individually, and then interact with three other participants to complete the group task on a separate platform. The procedure was identical to that of Study 1 except for two changes. First, this study excluded the BFI-2-S personality measure (Soto & O. P., 2017) to increase brevity, as Hypotheses 3 and 4 were already supported in the previous study.

Additionally, different self-esteem manipulations and measures were used. Instead of manipulating self-esteem with subliminally presented words (Riketa & Dauenheimer, 2003; Chartrand & Bargh, 1996), a recollection exercise addressing both the moral and competence aspects of oneself was used to manipulate the participants' self-esteem (Harber, 2005). The participants randomly assigned to the high self-esteem

Table 2: Personality Traits on Expected Status

Pearson's Correlations

			Pearson's r	p	Lower 95% CI	Upper 95% CI
Expected status	-	Extraversion	0.277	0.004	0.090	0.445
Expected status	-	Agreeableness	0.188	0.055	−0.004	0.366
Expected status	-	Conscientiousness	0.156	0.113	−0.037	0.337
Expected status	-	Neuroticism	−0.304	0.002	−0.468	−0.119
Expected status	-	Open Mindedness	0.229	0.019	0.039	0.403

condition were asked to recall a time when they provided substantial help to someone of great importance to them. Then the participants were asked to provide a detailed description (minimum of 30 words) about a) the person they helped and how they feel about this person; b) the situation in which this person needed help; c) their own actions on this person's behalf; d) how their actions made this person feel about his or her problem and about them; and e) how they feel about themselves in regard to this situation (Harber, 2005). The participants randomly assigned to the low self-esteem condition responded to the same questions for a time when they failed to help someone of great importance to them or betrayed that person's trust (Harber, 2005). The participants randomly assigned to the control condition were asked to recall a time they did the laundry, a household chore unrelated to this study, and provide a detailed description about a) where they did the task; b) the steps involved in the wash phase; c) the steps involved in the drying phase; d) the steps involved in folding the laundry; and e) how they feel about doing the laundry (Harber, 2005).

Lastly, rather than using the Rosenberg Self-Esteem Scale (Rosenberg, 1979), the State Self-Esteem Scale (SSES; Heatherton & Polivy, 1991) was used to measure the temporary changes in self-esteem due to experimental manipulation.

Results and Discussion 2

The manipulation of the participants' SPV was again successful. Participants in the low SPV condition reported lower self-perceived value than the participants in the high SPV condition, $F(1, 126) = 90.819$, $p < 0.001$. Hypotheses 1a and 1b were both successfully replicated a second time. Participants' self-perceived value to the group had a significant effect on their preferred status within that group, $F(1, 126) = 100.091$, $p < 0.001$. Participants' self-perceived value of the group had a significant effect on their expected status within that group, $F(1, 126) = 222.791$, $p < 0.001$. Participants with higher SPV were more likely to prefer and expect higher status.

The manipulation of the participants' self-esteem was found to be ineffective. Participants in the high self-esteem, low self-esteem, and control conditions reported a statistically non-significant difference in their State Self-Esteem Scale scores, $F(2, 124) = 1.598$, $p = 0.206$, $n^2 = 0.025$. The participants in the low self-esteem condition did, however, report a marginally significant decrease in their State Self-Esteem Scale scores compared to the participants in the high self-esteem and control conditions, $F(1, 126) = 2.991$, $p < 0.086$.

Further analyses revealed that the participants' self-esteem was correlated with their SPV, $F(1, 126) = 11.773$, $p < 0.001$ (Figure 3), but not with the SPV manipulation condition (i.e. low, high), $F(1, 126) = 0.002$, $p = 0.963$, which suggests that the measures of SPV and self-esteem were indistinct, rather than the SPV manipulation having an effect on both the participants' SPV and self-esteem.

Figure 3: Self-esteem and SPV

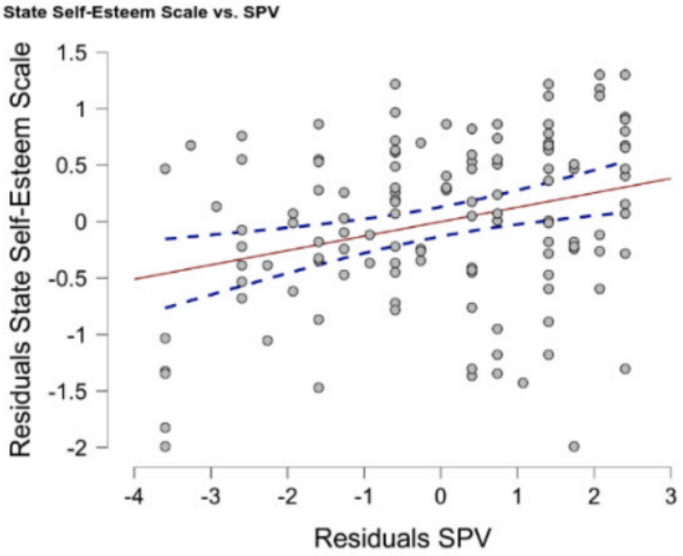

Although the participants' self-esteem could not be manipulated, analysis revealed that the participants' self-esteem correlated with their preferred status within that group, $F(1, 126) = 16.850$, $p < 0.001$ (Figure 4). Participants' self-esteem to the group also correlated with their expected status within that group, $F(1, 126) = 18.247$, $p < 0.001$ (Figure 5). In short, participants with higher self-esteem were more likely to prefer and expect higher status within the group.

Figure 4: Self-esteem and Preferred Status

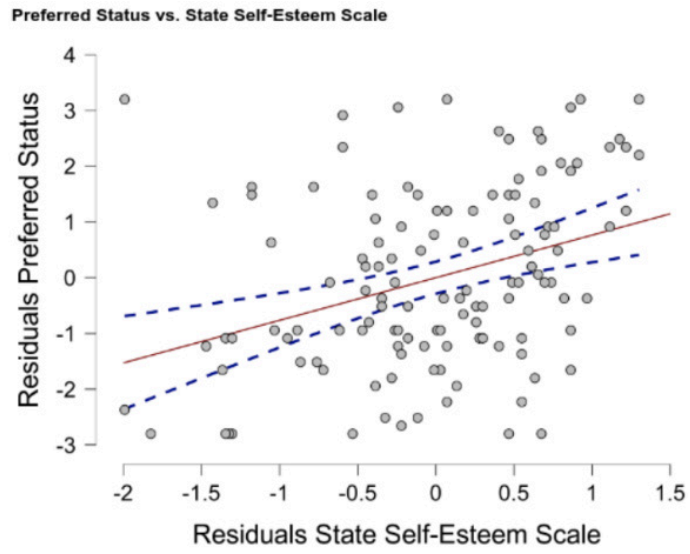

Figure 5: Self-esteem and Expected Status

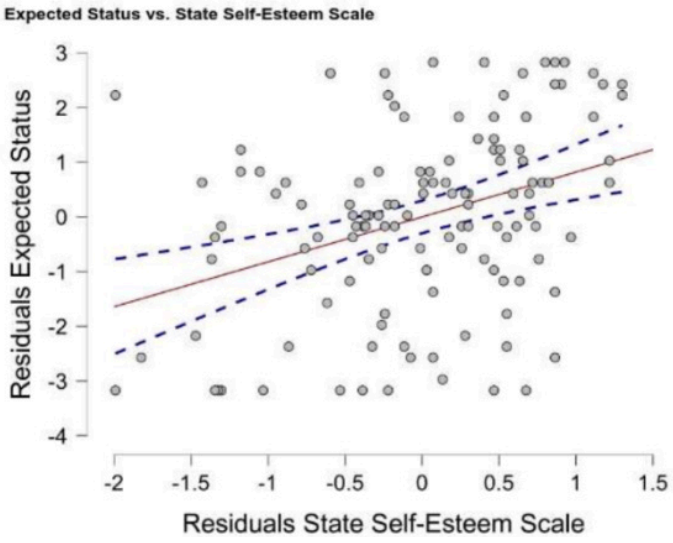

Further, a linear multiple regression analysis on whether the participants' self-esteem moderates the effect of SPV on preferred status was conducted. The interaction between self-esteem and SPV was marginally significant, in that having low self-esteem decreased preferred status within the group for participants with low SPV, $F(1, 123) = 3.264$, $p = 0.073$ (Figure 6), but not high SPV.

Figure 6: Self-esteem by SPV Interaction on Preferred Status

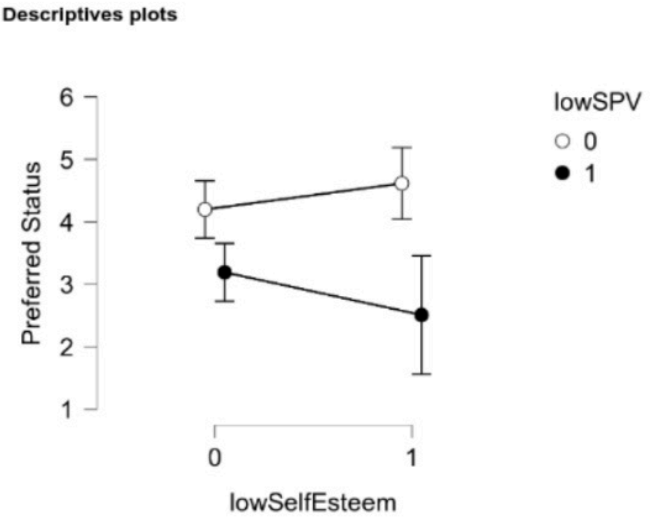

Note. Reference category is the low self-esteem condition compared to the two other conditions (combined).

However, the self-esteem by SPV interaction was not significant for expected status, in that having low self-esteem did not influence the expected status within the group for participants with low SPV, $F(1, 123) = 0.331$, $p = 0.566$, nor high SPV.

Conclusion

The two studies provided consistent support for the hypothesis that participants with higher SPV are not only more likely to prefer higher status but also expect higher status. The participants' personality traits were also found to be an important factor in predicting the status they preferred and expected. More extroverted participants preferred and expected higher status than their less extroverted counterparts, and participants with higher levels of neuroticism preferred and expected lower status than their counterparts with lower levels of neuroticism. The second study revealed that higher self-esteem was associated with higher preferred and expected status within the group, while low self-esteem was associated with lower preferred and expected status within the group for participants with low SPV.

Implications for Study

Individuals with low self-esteem are more likely to be discouraged by their low SPV and opt out of pursuing status, compared to those with similar SPV but higher self-esteem. Because self-esteem is correlated with individuals' socioeconomic status (SES; Twenge & Campbell, 2002; Zhang & Postiglione, 2001), individuals with high SES and consequently higher self-esteem may be more likely to prefer high status despite having low SPV. Conversely, individuals with low SES and consequently lower self-esteem may be more likely to prefer low status despite having high SPV. This tendency, in addition to the greater confidence level and status motive of those already in a position of high status (Anderson et al., 2020; Donnelly et al., 2018), may contribute to the perpetuation of the existing social hierarchies and socioeconomic inequality, which indicates a potential direction for future research.

Studies document the negative effects of socioeconomic inequality on the health and happiness of a population. Individuals with lower SES suffer disproportionately from various health issues and have higher mortality, psychiatric morbidity, and disabilities than individuals with higher SES (Mackenbach et al., 2008; Lorant, 2003; Adler, 1993). Further, individuals in a society with greater inequality report lower levels of happiness (Alesina et al., 2004). As such, the effect of pre-established SES on individuals' self-esteem and resulting status motive may, as a whole, harm society by perpetuating its social ills.

In addition, the findings on the moderating relationship between self-esteem and SPV on preferred status have implications for the effectiveness of organizations. When individuals who lack the ability to make meaningful contributions to the group pursue higher status regardless of their competence, they may decrease the overall productiveness of the group by competing with the more competent members and decreasing their chances of playing a role. Conversely, individuals who possess the ability to lead the group to success may not pursue higher status, depriving the group of valuable skills and knowledge. Hence, the findings of this study point to the need to address the self-esteem gap between individuals in high and low SES, in order to decrease the harmful effects of socioeconomic inequality and maximize the productivity of corporate organizations.

Limitations & Future Research

The manipulation of the participants' self-esteem was ineffective in this study, preventing it from establishing causation. It would thus be interesting for future researchers to examine whether self-esteem moderates the effect of SPV on preferred status by using a different self-esteem manipulation or a more distinct measure of SPV and self-esteem to avoid potential overlap between the participants' SPV and self-esteem scores. Furthermore, a potential direction for future studies is to examine ways to motivate individuals with low SES to engage in status competition to a greater extent. Given that self-esteem is directly correlated with both greater status pursuit and SES, developing intervention strategies such as Cognitive Behavioral Therapy, a widely used treatment for a range of mental

health disorders (Niveau et al., 2021), to promote higher self-esteem in individuals with low SES may be a constructive way to counter the effects of inequality present in society.

References

1. Ackerman, R. A., Witt, E. A., Donnellan, M. B., Trzesniewski, K. H., Robins, R. W., & Kashy, D. A. (2011). What Does the Narcissistic Personality Inventory Really Measure? Assessment, 18(1), 67–87. https://doi.org/10.1177/1073191110382845.

2. Adler, N. E. (1993). Socioeconomic inequalities in health. JAMA, 269(24), 3140. https://doi.org/10.1001/jama.1993.03500240084031.

3. Adler, N. E., Epel, E. S., Castellazzo, G., & Ickovics, J. R. (2000). Relationship of subjective and objective social status with psychological and physiological functioning: Preliminary data in healthy, White women. Health Psychology, 19(6), 586–592. https://doi.org/10.1037/0278-6133.19.6.586.

4. Alesina, A., Di Tella, R., & MacCulloch, R. (2004). Inequality and happiness: Are Europeans and Americans different? Journal of Public Economics, 88(9-10), 2009–2042. https://doi.org/10.1016/j.jpubeco.2003.07.006.

5. Anderson, C., Hildreth, J. A. D., & Sharps, D. L. (2020). The Possession of High Status Strengthens the Status Motive. Personality and Social Psychology Bulletin, 46(12), 1712–1723. https://doi.org/10.1177/0146167220937544.

6. Anderson C, John OP, Keltner D, Kring AM. 2001. Who attains social status? Effects of personality and physical attractiveness in social groups. J. Pers. Soc. Psychol. 81:116–32. https://doi.org/10.1037/0022-3514.81.1.116.

7. Anderson, C., & Kilduff, G. J. (2009). The Pursuit of Status in Social Groups. Current Directions in Psychological Science, 18(5), 295–298. https://doi.org/10.1111/j.1467-8721.2009.01655.x.

8. Anderson, C., Srivastava, S., Beer, J. S., Spataro, S. E., & Chatman, J. A. (2006). Knowing your place: Self-perceptions of status in face-to-face groups. Journal of Personality and Social Psychology, 91(6), 1094–1110. https://doi.org/10.1037/0022-3514.91.6.1094.

9. Anderson, C., Willer, R., Kilduff, G. J., & Brown, C. E. (2012). The origins of deference: When do people prefer lower status? Journal of Personality and Social Psychology, 102(5), 1077–1088. https://doi.org/10.1037/a0027409.

10. Aronson, E., & Mettee, D. R. (1968). Dishonest behavior as a function of differential levels of induced self-esteem. Journal of Personality and Social Psychology, 9(2, Pt.1), 121–127. https://doi.org/10.1037/h0025853.

11. Ashton, M. C., Lee, K., & Paunonen, S. V. (2002). What is the central feature of extraversion? Social attention versus reward sensitivity. Journal of Personality and Social Psychology, 83(1), 245–252. https://doi.org/10.1037/0022-3514.83.1.245.

12. Barkow, J. H. (1975). Prestige and culture: A biosocial interpretation. Current Anthropology, 16, 553–572. https://doi.org/10.1086/201619.

13. Bendersky, C., & Pai, J. (2018). Status Dynamics. Annual Review of Organizational Psychology and Organizational Behavior, 5(1), 183–199. https://doi.org/10.1146/annurev-orgpsych-032117-104602.

14. Berger, J., Cohen, B. P., & Zelditch, M. (1972). Status characteristics and social interaction. American Sociological Review, 37(3), 241. https://doi.org/10.2307/2093465.

15. Bienvenu, O. J., Hettema, J. M., Neale, M. C., Prescott, C. A., & Kendler, K. S. (2007). Low extraversion and high neuroticism as indices of genetic and environmental risk for social phobia, agoraphobia, and animal phobia. American Journal of Psychiatry, 164(11), 1714–1721. https://doi.org/10.1176/appi.ajp.2007.06101667.

16. Briggs, S. R. (1988). Shyness: Introversion or

neuroticism? Journal of Research in Personality, 22(3), 290–307. https://doi.org/10.1016/0092-6566(88)90031-1.

17. Cast, A. D., & Burke, P. J. (2002). A theory of self-esteem. Social Forces, 80(3), 1041–1068. https://doi.org/10.1353/sof.2002.0003.

18. Chartrand, T. L., & Bargh, J. A. (1996). Automatic activation of impression formation and memorization goals. Journal of Personality and Social Psychology, 71, 464–478.

19. Cheng, Helen, & Furnham, Adrian. (2002). Personality, peer relations, and self-confidence as predictors of happiness and loneliness. Journal of Adolescence, 25(3), 327–339. https://doi.org/10.1006/jado.2002.0475.

20. Cheng, J. T., Tracy, J. L., & Henrich, J. (2010). Pride, personality, and the Evolutionary Foundations of human social status. Evolution and Human Behavior, 31(5), 334–347. https://doi.org/10.1016/j.evolhumbehav.2010.02.004.

21. Depue, R. A., & Fu, Y. (2013). On the nature of extraversion: Variation in conditioned contextual activation of dopamine-facilitated affective, cognitive, and Motor Processes. Frontiers in Human Neuroscience, 7. https://doi.org/10.3389/fnhum.2013.00288.

22. Donnellan, M. B., Trzesniewski, K. H., & Robins, R. W. (2011). Self-esteem: Enduring issues and controversies. In T. Chamorro-Premuzic, S. von Stumm, & A. Furnham (Eds.), The Wiley-Blackwell handbook of individual differences (pp. 718–746). Wiley Blackwell.

23. Farley, F., & Farley, S. V. (1967). extraversion and stimulus-seeking motivation. Journal of Consulting Psychology, 31(2), 215–216. https://doi.org/10.1037/h0024418.

24. Fiske, S. T. (2010). Interpersonal stratification: Status, power, and subordination. Handbook of Social Psychology. https://doi.org/10.1002/9780470561119.socpsy002026.

25. Gibson, D. E., & Schroeder, S. J. (2003). Who ought to be blamed? the effect of organizational roles on blame and credit attributions. International Journal of Conflict Management, 14(2), 95–117. https://doi.org/10.1108/eb022893.

26. Foulsham, T., Cheng, J. T., Tracy, J. L., Henrich, J., & Kingstone, A. (2010). Gaze allocation in a dynamic situation: Effects of social status and speaking. Cognition, 117(3), 319–331. https://doi.org/10.1016/j.cognition.2010.09.003.

27. Goubin, S., & Hooghe, M. (2020). The effect of inequality on the relation between socioeconomic stratification and political trust in Europe. Social Justice Research, 33(2), 219–247. https://doi.org/10.1007/s11211-020-00350-z.

28. Harber, K. D. (2005). Self-esteem and affect as information. Personality and Social Psychology Bulletin, 31(2), 276–288. https://doi.org/10.1177/0146167204271323.

29. Heatherton, T. F., & Polivy, J. (1991). Development and validation of a scale for measuring state self-esteem. Journal of Personality and Social Psychology, 60(6), 895–910. https://doi.org/10.1037/0022-3514.60.6.895.

30. Henrich, J., & Gil-White, F. J. (2001). The evolution of prestige: Freely conferred deference as a mechanism for enhancing the benefits of cultural transmission. Evolution and Human Behavior, 22(3), 165–196. https://doi.org/10.1016/s1090-5138(00)00071-4.

31. Hollenbaugh, E. E., & Ferris, A. L. (2015). Predictors of honesty, intent, and valence of facebook self-disclosure. Computers in Human Behavior, 50, 456–464. https://doi.org/10.1016/j.chb.2015.04.030.

32. Josephs, R. A., Sellers, J. G., Newman, M. L., & Mehta, P. H. (2006). The mismatch effect: When testosterone and status are at odds. Journal of Personality and Social Psychology, 90(6), 999–1013. https://doi.org/10.1037/0022-3514.90.6.999.

33. Judge, T. A., & Bono, J. E. (2000). Five-Factor Model of personality and transformational leadership. Journal of Applied Psychology, 85(5), 751–765. https://doi.org/10.1037/0021-9010.85.5.751.

34. Keltner, D., Van Kleef, G. A., Chen, S., & Kraus, M. W. (2008). A reciprocal influence model of social power: Emerging principles and lines of inquiry. Advances in Experimental Social Psychology, 151–192. https://doi.org/10.1016/s0065-2601(07)00003-2.

35. Kilduff, G. J., Willer, R., & Anderson, C. (2016). Hierarchy and Its Discontents: Status Disagreement Leads to Withdrawal of Contribution and Lower Group Performance. Organization Science, 27(2), 373-390. https://doi.org/10.1287/orsc.2016.1058.

36. Kotov, R., Gamez, W., Schmidt, F., & Watson, D. (2010). Linking "big" personality traits to anxiety, depressive, and substance use disorders: A meta-analysis. Psychological Bulletin, 136(5), 768–821. https://doi.org/10.1037/a0020327.

37. Lansu, T. A., Cillessen, A. H., & Karremans, J. C. (2013). Adolescents' selective visual attention for high-status peers: The role of Perceiver Status and gender. Child Development, 85(2), 421–428. https://doi.org/10.1111/cdev.12139.

38. Lorant, V. (2003). Socioeconomic inequalities in depression: A meta-analysis. American Journal of Epidemiology, 157(2), 98–112. https://doi.org/10.1093/aje/kwf182.

39. Mackenbach, J. P., Stirbu, I., Roskam, A.-J. R., Schaap, M. M., Menvielle, G., Leinsalu, M., & Kunst, A. E. (2008). Socioeconomic inequalities in health in 22 European countries. New England Journal of Medicine, 358(23), 2468–2481. https://doi.org/10.1056/nejmsa0707519.

40. Magee, J. C., & Galinsky, A. D. (2008). 8 social hierarchy: The Self□reinforcing nature of power and status. Academy of Management Annals, 2(1), 351–398. https://doi.org/10.5465/19416520802211628.

41. Maslow, A. H. (1943). A theory of human motivation. Psychological Review, 50, 370–396. https://doi.org/10.1037/h0054346.

42. Naragon-Gainey, K., & Watson, D. (2011). Clarifying the dispositional basis of social anxiety: A hierarchical perspective. Personality and Individual Differences, 50(7), 926–934. https://doi.org/10.1016/j.paid.2010.07.012.

43. Niveau, N., New, B., & Beaudoin, M. (2021). Self-esteem interventions in adults – a systematic review and meta-analysis. Journal of Research in Personality, 94, 104131. https://doi.org/10.1016/j.jrp.2021.104131.

44. Orth, U., & Robins, R. W. (2014). The Development of Self-Esteem. Current Directions in Psychological Science, 23(5), 381–387. https://doi.org/10.1177/0963721414547414.

45. Pyszczynski, T., Greenberg, J., Solomon, S., Arndt, J., & Schimel, J. (2004). Why Do People Need Self-Esteem? A Theoretical and Empirical Review. Psychological Bulletin, 130(3), 435–468. https://doi.org/10.1037/0033-2909.130.3.435.

46. Rayner, K. (1978). Foveal and parafoveal cues in reading. Attention and Performance, 8, 149–161.

47. Riketta, M., & Dauenheimer, D. (2003). Manipulating self-esteem with subliminally presented words. European Journal of Social Psychology, 33(5), 679–699. https://doi.org/10.1002/ejsp.179.

48. Rosenberg, M. (1979). Conceiving the Self. New York: Basic Books.

49. Savin-Williams, R. C. (1979). Dominance hierarchies in groups of early adolescents. Child Development, 50, 923–935. https://doi.org/10.2307/1129316.

50. Schaefer, P. S., Williams, C. C., Goodie, A. S., & Campbell, W. K. (2004). Overconfidence and the big five. Journal of Research in Personality, 38(5), 473–480. https://doi.org/10.1016/j.

jrp.2003.09.010.

51. Schmid Mast, M., Hall, J. A., & Schmid, P. C. (2010). Wanting to be boss and wanting to be subordinate: Effects on performance motivation. Journal of Applied Social Psychology, 40, 458–472. doi:10.1111/ j.1559-1816.2009.00582.x.

52. Smith, P. K., Wigboldus, D. H. J., & Dijksterhuis, A. (2008). Abstract thinking increases one's sense of power. Journal of Experimental Social Psychology, 44, 378–385. https://doi.org/10.1016/j.jesp.2006.12.005.

53. Soto, C. J., & John, O. P. (2017). Short and extra-short forms of the big five inventory–2: The BFI-2-S and BFI-2-XS. Journal of Research in Personality, 68, 69–81. https://doi.org/10.1016/j.jrp.2017.02.004

54. Tay, L., & Diener, E. (2011). Needs and subjective well-being around the world. Journal of Personality and Social Psychology, 101, 354–365.

55. Tomarkenand, A. J., & Keener, A. D. (1998). Frontal brain asymmetry and depression: A self-regulatory perspective. Cognition & Emotion, 12(3), 387–420. https://doi.org/10.1080/026999398379655.

56. Troyer, L. (2001). Effects of protocol differences on the study of status and social influence. Current Research in Social Psychology, 6, 182–205.

57. Twenge, J. M., & Campbell, W. K. (2002). Self-esteem and socioeconomic status: A meta-analytic review. Personality and Social Psychology Review, 6(1), 59–71. https://doi.org/10.1207/s15327957pspr0601_3.

58. Wang, W., Han, R., Luo, Y., Wu, Z., Jin, Y., Li, Q., & Li, B. (2018). The mediating role of self-efficacy between neuroticism and procrastination among undergraduates. 2018 IEEE International Conference on Mechatronics and Automation (ICMA). https://doi.org/10.1109/icma.2018.8484534.

59. Ward, D. A. (1986). Self-esteem and dishonest behavior revisited. The Journal of Social Psychology, 126(6), 709–713. https://doi.org/10.1080/00224545.1986.9713652.

60. Watson, D., & Clark, L. A. (1997). Extraversion and its positive emotional core. Handbook of Personality Psychology, 767–793. https://doi.org/10.1016/b978-012134645-4/50030-5.

61. Yu, S., & Kilduff, G. J. (2020). Knowing where others stand: Accuracy and performance effects of individuals' perceived status hierarchies. Journal of Personality and Social Psychology, 119(1), 159–184. https://doi.org/10.1037/pspi0000216.

62. Zhang, L.-fang, & Postiglione, G. A. (2001). Thinking styles, self-esteem, and socio-economic status. Personality and Individual Differences, 31(8), 1333–1346. https://doi.org/10.1016/s0191-8869(00)00227-0.

63. Zopiatis, A., & Constanti, P. (2012). Extraversion, openness and conscientiousness. Leadership & Organization Development Journal, 33(1), 86–104. https://doi.org/10.1108/01437731211193133.

Meet Our Editing Team

EDITORIAL BOARD

Julia Davis,
President & Editor-in-Chief

Julia Davis (Trinity ‘24) is majoring in Neuroscience and pursuing a certificate in Science and Society from Boston, MA. She is also the Editor-in-Chief of Vertices’ Academic Research Journal, and she has been involved with Vertices since her freshman year. Upon graduation, Julia hopes to go to medical school with the intention of becoming an OBGYN. Julia also dances in Duke’s ballet Company (Devils en Pointe) and loves to play 70s and 80s blues songs on the electric guitar.

Sasha Bacot,
Senior Editor

Sasha (Trinity ‘25) is from South Carolina and is a double major in Biology and Computer Science. She loves being a Vertices peer reviewer because it allows her to delve deeper into what she’s most passionate about: scientific research! Outside of her work with Vertices, Sasha loves to figure skate, listen to music, and try out all the cool restaurants in Durham (especially for boba)!

Kaeden Hill,
Senior Editor

Kaeden (Trinity ‘25) is a Vertices Senior Editor from Atlanta, Georgia, double majoring in biology with a concentration in molecular and cell biology, and evolutionary anthropology with a minor in chemistry. After graduating, he plans to pursue a Ph.D. and a career in research. He is specifically interested in DNA tumor viruses and how their “cellular hijacking” can drive cells towards cancer, and he is a member of the Luftig Lab, studying Epstein-Barr virus and the cancers that it causes. Outside of academics, he loves to hike, travel, ski, scuba dive, collect minerals, and make jewelry.

PEER REVIEW TEAM

Aditya Raj

Aditya is a sophomore studying a combination of Biology, Information Technology, and Policy. He is passionate about regenerative medicine and scientific communication. He enjoys playing squash, walking in forests, and listening to jazz.

Angela Xiong

Angela Xiong is a first-year undergraduate student at Duke University, intending to major in Medical Sociology and minor in Chemistry. She is particularly drawn to the social determinants of health and addressing health disparities in minority and marginalized populations. Outside of Vertices, Angela also serves as a first-year senator on Duke Student Government, and volunteers at the puppy kindergarten!

Anya Milberg

Anya Milberg is a sophomore from New York City majoring in Neuroscience with a minor in Sociology. She is interested in exploring the intersection of science and law, currently researching trauma-informed court practices. Outside of Vertices, she can be found leading tours of campus, volunteering with the Duke Justice Project, baking, and spending time with friends.

Arielle Kim

Arielle Kim (Trinity ‘26) is a Duke University undergraduate majoring in Biology with minors in Computer Science and Computational Biology and Bioinformatics! She is particularly drawn to the intersection of microbiology and ecology, and she is currently exploring symbiotic systems involving fungi and their photobionts as a member of the Lutzoni Lab.

Arnav Singh

Arnav is a third-year undergraduate student in the Department of Biomedical Engineering. His passion lies at the intersection of AI and Medicine, and is currently working with Dr. Amanda Randles, on developing a Deep Learning Computational Fluid Dynamics (CFD) model for the noninvasive diagnosis of Coronary Artery Disease (CAD). Outside of Vertices, he serves as the Head of Duke Applied Recycling Center (DARC), the first on-campus plastic recycling center on a university campus in the United States.

Caleb Lian

Caleb Lian is a freshman from San Marino, California majoring in Neurobiology and Psychology with a particular interest in psychopathology. He is currently exploring the role of epigenetic histone modifications on astrocyte maturation in the Eroglu Lab, and is also a part of the CAPER research program at the Duke Hospital. In his free time, Caleb enjoys running with DCR and playing intramural soccer.

Colby Cheshire

Colby is a senior studying Biology and French. He has previously worked with the Alberts Lab at Duke, the Speliotes Lab at the University of Michigan, and the Turnbaugh Lab at UCSF. Outside of lab and class, Colby enjoys volunteering with Crisis Text Line, reading books, and discovering new coffee shops in Durham.

Cooper Ruffing

Cooper is a Biology and Statistics Major from Raleigh, North Carolina. In addition to exploring his love for all sorts of sciences, he plays golf, volunteers with Duke STEM Connect, and tutors math!

Daliya Rizvi

Daliya Rizvi is a first-year student studying biochemistry and ethics. She loves research and the research process, and is passionate about making scientific knowledge and news accessible to everyone.

Daniel Levin

Daniel is a first-year undergraduate from Pittsburgh, PA, studying biology and human rights. His research at Duke focuses on understanding the role of noncoding RNA during immune responses. After graduating, he aspires to pursue a Ph.D. to further investigate the mechanisms behind microbial pathogenesis and advance treatments for infectious diseases. Outside of the lab, Daniel enjoys biking and gardening.

Daniel Sul

I am a biology major with a chemistry minor on the premed track. On campus, I am involved in vision health research, clinical volunteering, and science journalism

Dennis Wu

Dennis Wu is a future astrophysicist working on research and fiction writing. He enjoys mountains as his refuge when he hikes and stargazes. As a peer reviewer at Vertices, he is dedicated to help students to bring forth quality research.

Eliza Goldstein

Eliza Goldstein is a second-year undergraduate student majoring in Psychology with a minor in Global Health. She is interested in clinical and social psychology, specifically the intersections and variance of psychopathology among differing backgrounds and experiences. After completing her undergraduate degree, she plans to pursue a Ph.D. in Clinical Psychology. At Duke, she is the Lab Manager for the Culture Lab and a Research Assistant for the Zucker Lab. Outside of research, she enjoys biking, reading, and spending time with her friends.

Grace Wang

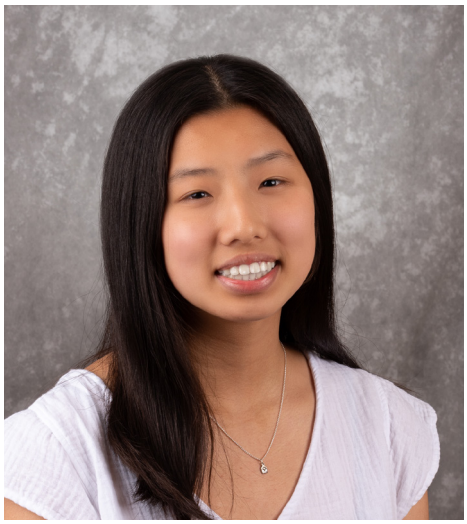

Grace Wang is an undergraduate student intending to major in Chemistry or Evolutionary Anthropology. She is drawn to the puzzle-solving nature of scientific research and is currently exploring the organic synthesis of medicinal compounds in the Hong Lab.

Jane Lee

I am a sophomore majoring in biology with a neurobiology concentration with minors in psychology and chemistry. I'm originally from Southern California but now live in Cary, NC! My research interests include neurodegenerative disorders and developmental disabilities.

Jeffrey Bohrer

I am freshman from Guayaquil, Ecuador majoring in Chemistry with a concentration in chemical biology. I am currently working as a research assistant in Varghese Lab studying organ-on-chip platforms. Outside of academics, I am a huge fan of rock music!

Jeremy Yarden

Jeremy is a senior majoring in Biology with minors in Chemistry and Classical Civilizations. He currently works in the Kwatra Lab studying potential therapies for glioblastoma and is interested in pursuing a career in medicine.

Kate Lee

Kate Lee is a Duke undergraduate student from South Korea intending to major in either chemistry or biology. She is passionate about medicine and science and loves reading and writing scientific papers. She is currently studying cancer and immunotherapy, utilizing both germ free and SPF mice as a researcher in Conejo-Garcia Lab.

Katherine Long

Katherine Long (Trinity ‘24) is a Biology and Chemistry student with a passion for research and scientific communication. Outside of science, she enjoys painting, cooking, and reading.

Lizaveta Slootskaya

I am a current freshman studying Biomedical Engineering and Electrical Computer Engineering. I am very interested in cancer biology research and medical devices.

Nathanael Ren

Nathanael Ren is a student at Duke studying Computer Science, Electrical and Computer Engineering, and Mathematics. His previous work includes applications of the aforementioned fields to the financial services and healthcare fields. He is also involved in the Duke University Debate Society and Duke Robotics Team.

Nitya Chadha

Nitya (Trinity ‘27) is a freshmen who is currently thinking of majoring in neuroscience with a minor in economics. She is extremely passionate about science and is interested in pursuing a career in research. Outside of academics, Nitya enjoys singing and playing tennis.

Sai Gayathri Kurup

I am a freshman in the Trinity College of Arts and Sciences, and I am a prospective biology major with a certificate in health policy. I am passionate about translational research, especially related to the life sciences, through the lens of science communication.

Will Sun

Will (Trinity ‘27) is an undergraduate student who intends to major in biology with a concentration in ecology, marine science and conservation from San Jose, CA. Outside of working in the Miao Lab on integrative immunology, he also enjoys playing basketball, watching sunsets, and eating ramen.

Zishen Li

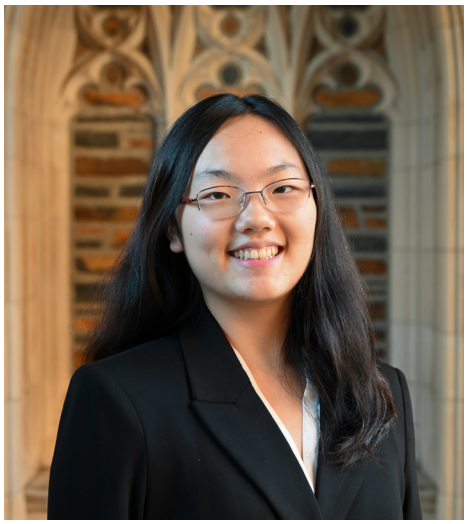

Zishen is an undergraduate student at Duke. She is interested in medicine as well as the intersection between science and art. Outside of Vertices, she enjoys playing ping pong and trying out new things!

Darsh Mandera

Darsh is a first-year undergraduate with interests in AI, biology, and linguistics. His research experiences include work in precision oncology as well as computational modeling of stem cell differentiation. Beyond Vertices, he likes reading about language and current affairs.

Meet Our Design Team

AJ Kochuba,
Artistic Director

AJ (Trinity ‘25) is from Cary, North Carolina, studying neuroscience, psychology, and visual arts on the pre-med track. AJ is particularly interested in humanities-based approaches to medical practice and research and hopes to enrich the symbiotic relationship between the fields of science and arts. Outside of Vertices, AJ can be found hosting arts- and identity-focused events and competing on the pickleball courts.

Sage Cooley
Website Director

Sage (Pratt ‘25) is from Raleigh, North Carolina and is majoring in mechanical / aerospace engineering. Outside of Vertices, you’ll find her working on rocketry with Duke’s AERO society, spending time with friends, or going on a nature walk!

Amanda Li

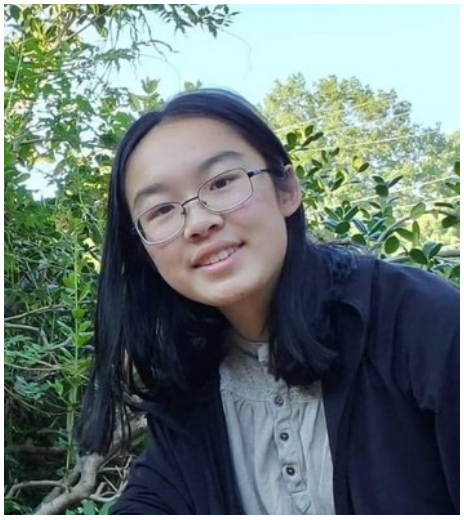

Amanda (Pratt ‘27) is from Charlotte, North Carolina and is majoring in biomedical engineering. She loves learning about anything and everything, doodling in her spare time, and exploring new things.

Cindy Ju

Cindy is a sophomore from South Carolina planning to major in economics. She enjoys arts and crafts, walking in the Duke Gardens, and trying out different boba shops around Durham.

Erin Heyeck

Erin (Trinity ‘24) is a Senior from Princeton, New Jersey, studying biology and computational biology. She is passionate about the intersections of science and art. Outside of academics, Erin can be found on the water with Duke Women’s Rowing and exploring new restaurants in the Triangle.

Gaby Dunn

Gaby is a sophomore from South Florida with too many interests that she is trying to find a major for. She is fascinated by the intersections of education, art, & STEM. When procrastinating, she enjoys rock climbing, critiquing movies, and spending time outdoors.

Jessica Pham

Jessica is a first year from Monroe, LA, planning to major in biomedical engineering and pursue the pre-med track. She's passionate about intellectual exploration, creative writing, and the intersection between science and the humanities. She may be found wandering various places, lost inside her head.

Monet Shum

Monet (Trinity '27) is a freshman from Aldie, Virginia planning to study linguistics, computer science, and classical civilizations. Outside of Vertices, she also works with Duke's Digital Art History and Visual Culture Lab and enjoys beading and walking in the Duke Gardens.

Acknowledgements

VERTICES EXECUTIVE BOARD

Editor in Chief
Julia Davis

Senior Editors
Sasha Bacot
Kaeden Hill

Artistic Director
AJ Kochuba

PEER REVIEW TEAM

Julian Burbano
Nitya Chadha
Colby Cheshire
Ahilan Eraniyan
Amrita Ganeriwa
Sai Gayathri-Kurup
Eliza Goldstein
Jerffrey Guerra
Selena Halabi
Imani Hall
Vishruth Hanumaihgari
Arielle Kim
Katie Lam
Eric Lee
Kate Lee
Jane Lee
Daniel Levin
Zishen Li
Caleb Lian
Katherine Long
Darsh Mandera
Anya Milberg
Justine Prophete
Winston Qian
Aditya Raj
Aditi Ramesh Iyer
Nathanael Ren
Daliya Rizvi
Cooper Ruffing
Canaan Salles-Spar
Arnav Singh
Lizaveta Slootskaya
Daniel Sul
William Sun
Ashwer Wallen
Grace Wang
Dennis Wu
Angela Xiong
Jeremy Yarden

DESIGN

Spring 2023 Issue & Layout Design
AJ Kochuba

Cover & Article Graphics
Jessica Pham
Erin Heyeck
Gaby Dunn
Amanda Li
Cindy Ju

Website Design
Sage Cooley

FACULTY/EXPERT REVIEWERS

Harold Baranger, Ph.D. | Professor of Physics
Thomas Barthel, Ph.D. | Assistant Professor of Physics
Billy Carson | Ph.D. Student - Biomedical Engineering
Sarah Eom | Ph.D. Student - Duke Pratt School of Engineering
Easop Lee | Ph.D. Student - Duke Pratt School of Engineering
Esha Naidu, Ph.D. | Postdoctoral Researcher - Duke Psychology & Neuroscience
Anna Nelson, Ph.D. | Assistant Professor of Mathematics
Carlo Tomasi, Ph.D. | Professor of Computer Science
Laurie Sanders, Ph.D. | Associate Professor in Neurology
Linmarie Sikich, MD. | Investigator in the Duke Institute for Brain Sciences
Carla Wall, Ph.D. | Postdoctoral Associate - Duke Psychiatry for Brain Sciences

A special thank you to:
Reviewers from Georgetown's Scientific Research Journal